SEISMIC INVERSION AND UNCERTAINTY ANALYSIS USING

TRANSDIMENSIONAL MARKOV CHAIN MONTE CARLO METHOD

A Dissertation

by

DEHAN ZHU

Submitted to the Office of Graduate and Professional Studies of
Texas A&M University
in partial fulfillment of the requirements for the degree of

DOCTOR OF PHILOSOPHY

Chair of Committee,	Richard L. Gibson
Committee Members,	Benchun Duan
	Mark E. Everett
	Michael J. King
	Yuefeng Sun
Head of Department,	Mike Pope

August 2016

Major Subject: Geophysics

ABSTRACT

We use a transdimensional inversion algorithm, reversible jump MCMC (rjMCMC), in the seismic waveform inversion of post-stack and prestack data to characterize reservoir properties such as seismic wave velocity, density as well as impedance and then estimate uncertainty. Each seismic trace is inverted independently based on a layered earth model. The model dimensionality is defined as the number of the layers multiplied with the number of model parameters per layer. The rjMCMC is able to infer the number of model parameters from data itself by allowing it to vary in the iterative inversion process, converge to proper parameterization and prevent underparameterization and overparameterization. We also use rjMCMC to enhance uncertainty estimation since it can transdimensionally sample different model spaces of different dimensionalities and can prevent a biased sampling in only one space which may have a different dimensionality than that of the true model space. An ensemble of solutions from difference spaces can statistically reduce the bias for parameter estimation and uncertainty quantification. Inversion uncertainty is comprised of property uncertainty and location uncertainty. Our study revealed that the inversion uncertainty is correlated with the discontinuity of property in such a way that 1) a smaller discontinuity will induce a lower uncertainty in property at the discontinuity but also a higher uncertainty of the location of that discontinuity and 2) a larger discontinuity will induce a higher uncertainty in property at the discontinuity but also a higher "certainty" of the location of that discontinuity. Therefore, there is a trade-off between the property uncertainty and the location uncertainty. To our surprise, there is a lot of hidden information in the uncertainty result that we can actually take advantage of due to this trade-off effect. On the basis of our study

using rjMCMC, we propose to use the inversion uncertainty as a novel attribute in an optimistic way to characterize the magnitude and the location of subsurface discontinuities and reflectors.

To my Lord and God Jesus Christ and parents

ACKNOWLEDGEMENTS

TABLE OF CONTENTS

LIST OF FIGURES

1.   INTRODUCTION

1.1   Research Question and Motivation

In the geophysical studies, what we know is the data collected via a variety of ways and what we don't know is the model that can honor the real earth and explain the data. Inversion is the mapping process from data space to model space, which is an informational conversion from the data to the model. A successful inversion should answer these three critical questions for most geophysical inverse problems, that is, how to parameterize the earth model with appropriate parameters, how to estimate these parameters from the data available and how to assess the uncertainty. Most geophysical inversion studies in the past century focused on answering the second question and didn't put emphasis on the first and the third questions. Only in the recent couple of decades, geophysicists started to study more on answering these two questions. On the one hand, an proper parameterization prior to inversion is a prerequisite rather than an option for a good inversion. On the other, a complete inversion result should include the parameter estimation as well as the uncertainty quantification for these parameters since the non-uniqueness of inversion results is almost inevitable for most inverse problems. This PhD dissertation aims at tackling all these three crucial questions at the same time with one approach, and in order to make this research outstanding and distinct from other people's work, we put more emphasis on answering the first and the third questions using a modern inversion algorithm, transdimensional Markov chain Monte Carlo method which will be explained later on. Although we conducted this research using seismic waveform data to build the earth model through seismic inversion, the inversion method and the uncertainty analysis in this dissertation can be generalized to be applied in other

geophysical inverse problems as well as those in other scientific areas.

Seismic inversion is a quantitative inference of the interior physical properties of the earth from seismic data. However, the complexity of the earth properties is barely well known or even unknown, so a proper parameterization of the earth model is accordingly unknown and cannot be presumed. Most inversion algorithms, either deterministic or stochastic, presume a certain parameterization and fix the model dimensionality (number of model parameters), which may lead to underparameterization or overparameterization. Underparameterization and overparameterization may force the inversion to search in a wrong model space of a wrong dimensionality. To deal with this issue, the inversion method should be able to allow the model dimensionality to vary and let the data itself to infer it which means that the model dimensionality is treated as an unknown parameter that needs to be inverted. Therefore, we decided to use a transdimensional inversion approach.

In the meanwhile, the transdimensional approach can also enhance the uncertainty estimation on the grounds that it conducts sampling in different spaces with different dimensionalities and forces the inversion to favor those spaces which include or are close to the space of the true model. Hence, the average solution can serve as an optimal representation of the true model. In a statistical sense, the transdimensional implementation exerts a less bias for both parameter estimation and uncertainty quantification compared to the traditional scenario that the inversion is only allowed to search in a predefined single space which may be distinct from the true model space. Obviously, if using the traditional inversion methods with an improper parameterization, the solution or the ensemble of solutions will be biased and consequently the uncertainty estimation will also be biased due to the searching in the wrong model space. Therefore we promoted to utilize the transdimensional approach to facilitate uncertainty analysis. But before we go deeper into this method, let us first

have an overview of traditional non-transdimensional algorithms which are widely used in geophysics.

1.2   Brief Overview of Conventional Algorithms

Many inversion algorithms and their applications in geophysical inverse problems are well documented. Inversion algorithms are comprised of two major categories, deterministic and stochastic. Deterministic algorithms have been widely used in geophysics since a few decades ago in that they generally don't need many iterations and are fast to implement. A commonly used deterministic method is the generalized linear inversion (GLI) (Tarantola and Valette, 1982a; Cooke and Schneider, 1983). GLI is an iterative process which requires derivative information of an objective function and a good initial model which can be built based on prior information such as well logs. The application of GLI in seismic inversion is referred to Hampson et al. (1984), Tarantola (1986), Mora (1987), Demirbag et al. (1993) and Pan et al. (1994).

Unlike deterministic algorithms which needs a good initial model and produces one single model as the final solution, stochastic algorithms generally don't require a good initial model and they are able to search the entire model space and produce a set of models which can fit the data within a certain predefined tolerance, and therefore they can enhance inversion process and uncertainty estimation. However, they need more computational iterations than deterministic methods in order to search the model space globally instead of locally. Due to this reason, stochastic approaches may require a fast forward calculation. Common stochastic methods include Monte Carlo methods such as Markov chain Monte Carlo (MCMC), Simulated Annealing (SA), Genetic Algorithm (GA), Neural Network (NN), Swarm Intelligence methods such as Particle Swarm Optimization (PSO), and Neighborhood Algorithm (NA), etc.

MCMC usually adopts the Metropolis-Hastings algorithm which generates a random walk using a proposal probability distribution. This random walk proposes a new model based on the current model and also rejects some of the proposed models. Early introduction is given by Metropolis et al. (1953) and Hastings (1970). MCMC is generally cast in a Bayesian framework and is widely used in geophysical inversion (Mosegaard and Tarantola, 1995; Sen and Stoffa, 1995, 1996; Curtis and Lomax, 2001; Mosegaard and Sambridge, 2002; Sambridge and Mosegaard, 2002; Malinverno and Briggs, 2004; Malinverno and Leaney, 2005) and particularly in seismic inversion (Godfrey et al., 1980; Mosegaard et al., 1997; Eidsvik et al., 2004; Hong and Sen, 2009; van der Burg et al., 2009; Martin et al., 2012; Chen and Glinsky, 2014).

SA is an optimization process that simulates the evolution of a physical system as it cools and anneals into a state of minimum energy (Sen and Stoffa, 2013). This method is an adaptation of the Metropolis?Hastings algorithm, that is, a Monte Carlo method to generate sample states of a thermodynamic system. The SA was early introduced by Kirkpatrick et al. (1983) and then further described by Geman and Geman (1984), Mitra et al. (1986), Anily and Federgruen (1987a,b), van Laarhoven and Aarts (1987) and Aarts and Korst (1988). It has been successfully applied in many geophysical inverse problems (Rothman, 1985, 1986; Basu and Frazer, 1990; Scales et al., 1992) and especially in the seismic inversion (Sen and Stoffa, 1991; Scales et al., 1991, 1992; Vestergaard and Mosegaard, 1991; Ma, 2001a,b, 2002; Srivastava and Sen, 2009, 2010; Tran and Hiltunen, 2012b).

GA, first proposed by Holland (1975), is based on the analogies with genetic processes of selection, crossover and mutation. Detailed description is referred to Davis (1987), Goldberg (1989), Buckles and Petry (1992) and Forrest (1993). GA was first used by geophysicists in the early 1990s (Stoffa and Sen, 1991; Gallagher et al., 1991; Smith et al., 1992; Scales et al., 1992) and has been used mainly in the

area of seismic inversion (Stoffa and Sen, 1991; Sen and Stoffa, 1992; Sambridge and Drijkoningen, 1992; Gallagher and Sambridge, 1994; Mallick, 1995, 1999; Boschetti et al., 1995, 1996; Morgan et al., 2012; Tran and Hiltunen, 2012a; Padhi and Mallick, 2013, 2014; Li and Mallick, 2015; Fang and Yang, 2015).

NN simulates systems of interconnected ''neurons'' which exchange messages between each other. These connections have numeric weights which can be tuned based on experience so that the neural network is adaptive to inputs and capable of learning. Its applications in geophysics are described by Calderón-Macías et al. (2000), van der Baan and Jutten (2000) and Poulton (2002). It is both implemented in seismic inversion (Röth and Tarantola, 1994; Langer et al., 1996; Baddari et al., 2010) and reservoir chacterization (An et al., 2001; Saggaf et al., 2003; Leite and Vidal, 2011; Ahmadi et al., 2013; Mohamed et al., 2015).

PSO is a stochastic evolutionary inversion and optimization algorithm originally inspired by the social behavior of individuals (called particles) in nature such as bird flocking and fish schooling (Kennedy and Eberhart, 1995). In the PSO, the models, called particles, are navigated in the model space by following the current optimal model as well as their individual best location in the moving history. This method is relatively newer than the above methods, and it is now used to invert geophysical data and characterize reservoir (Shaw and Srivastava, 2007; Fernández-Martínez et al., 2008, 2012; Zhe and Gu, 2013).

NA was introduced by Sambridge (1999a,b) for geophysical inverse problems. NA divides the model space using *Voronoi* cells and facilitates the global inversion. A seismic inversion example can be referred to Fliedner et al. (2012).

1.3   Overview of the Transdimensional Approach, rjMCMC

All the abovementioned conventional methods generally presume a certain parameterization and fix the model dimensionality in the inversion process. This will give rise to issues such as underparameterization and overparameterization. Using too few parameters will lead to data underfitting and biased solutions. Using more parameters than necessary can lead to the overfitting of data noise and under-determined parameters with excessive uncertainty (Dosso et al., 2014), not to mention the low computation efficiency due to the "curse of dimensionality". Therefore, the transdimensional approach can solve this challenge since it treats the model dimensionality as an unknown to be inverted and uses the data to infer the dimensionality. The transdimensional approach in our research, rjMCMC, originates from Geyer and Moller (1994) and Green (1995, 2003). This method has been termed transdimensional Markov chain by Sisson (2005). Sambridge et al. (2006) and Gallagher et al. (2009) presented an overview of this algorithm and its applications in Earth science. The rjMCMC was first applied in geophysics in 2000 in an inversion study of zero-offset vertical seismic profiles (Malinverno, 2000; Malinverno and Leaney, 2000). Since then, it has been utilized in a variety of geophysical inverse problems, including earthquake seismology and tomography (Bodin et al., 2009; Bodin and Sambridge, 2009; Agostinetti and Malinverno, 2010; Bodin et al., 2012a,b; Young et al., 2013; Zulfakriza et al., 2014; Kolb and Lekić, 2014; Galetti et al., 2015), geoacoustic inversion (Dettmer et al., 2010; Dettmer and Dosso, 2012; Steininger et al., 2013; Dettmer et al., 2013; Dosso et al., 2014), and electrical and magnetotelluric geophysics (Malinverno, 2002; Minsley, 2011; Brodie and Sambridge, 2012; Ray and Key, 2012; JafarGandomi and Binley, 2013; Ray et al., 2014; Gehrmann et al., 2015). Dadi (2014) and Dadi et al. (2015) used rjMCMC for seismic impedance inversion, uncertainty estimation

and well log upscaling. Biswas and Sen (2015) applied it to seismic inversion by using a synthetic model. In our research, we firstly applied the rjMCMC by using oilfield data to characterize the petroleum reservoir and assess uncertainty.

1.4   Outline of This Dissertation and Scientific Contributions

In this dissertation, section 1 covers an introduction and literature overview of conventional inversion methods and the transdimensional approach. In section 2, we implement the trandimensional method in seismic inversion and uncertainty estimation, and explain how we apply the method in detail. The research work in section 3 is a more advanced topic compared to section 2, and we use prestack data to simultaneously invert acoustic/shear impedance and density and conduct uncertainty quantification since prestack seismic inversion can provide more insights to understand reservoir's fluids and lithology which are the important aspects in the petroleum exploration. In section 4, we concentrate on uncertainty analysis in the seismic inversion and we find out that the inversion uncertainty (including property uncertainty and location uncertainty) is correlated with the discontinuity of property. And we firstly discover that there is a trade-off between the property uncertainty and the location uncertainty in the inversion. Therefore, we propose to use the inversion uncertainty as a new attribute to facilitate delineation of subsurface reflectors and quantify the magnitude of subsurface discontinuities.

2. SEISMIC WAVEFORM INVERSION AND UNCERTAINTY ESTIMATION USING TRANSDIMENSIONAL MARKOV CHAIN MONTE CARLO METHOD

2.1 Introduction

Inversion is the mapping process from data space to model space. Seismic inversion is a quantitative inference of the interior physical properties of the earth from seismic data. For most geophysical inverse problems, a successful inversion method should be able to answer these 3 critical questions altogether. They are 1) how to parameterize the model with proper parameters, 2) how to estimate these parameters and 3) how to quantify the uncertainty of parameter estimation. Scientific approaches that answer the second question have been well documented in geophysical literatures, but most of them don't put too much emphasis on solving the first and third questions. The purpose of this research is to answer all these three questions together by using a modern inversion algorithm and put more emphasis on tackling the first and third questions.

As for the first question, the complexity of the earth properties is not well known or even unknown, so a proper parameterization of the earth model is a necessary process for a successful and efficient inversion. The model dimensionality is defined as the number of model parameters to depict the model. Most inversion algorithms, either deterministic or stochastic, presume a certain parameterization and fix the model dimensionality, which may lead to underparameterization or overparameterization. Our objective of seismic inversion is not only to find good models that fit the data but also to appraise the uncertainty in the inversion results from a sampling procedure. But the challenge is that if the sampling takes place in a model space which may have

a very different dimensionality from the true model's dimensionality, the solution ensemble may be biased and give rise to biased uncertainty estimation. Therefore, we used a modern stochastic transdimensional approach known as the reversible jump Markov chain Monte Carlo (rjMCMC) method (Green, 1995, 2003). This approach is able to allow the number of parameters to vary and search the model spaces of different dimensionalities to achieve appropriate parameterizations. It also enhances the uncertainty quantification by obtaining a set of solutions from these different spaces. The term reversible jump means the Markov chain is able to jump back and forth between the different spaces corresponding to different numbers of model parameters. For a layered model example, this transdimensional process is accomplished by occasionally proposing to split a layer by adding a layer interface or merge two adjacent layers by deleting their interface (Malinverno, 2002).

As for the third question, the uncertainty estimation in stochastic inversion is mainly contingent on the model ensemble collected via a global searching in the model space. If the above first question were not well addressed, or in other words, the model were not properly parameterized, the inversion sampler would search in the wrong model space, and the following consequence would be a biased uncertainty estimation when assessing the model ensemble. Therefore, the transdimensional algorithm is promoted to facilitate uncertainty quantification as will be mentioned later.

The advantage of rjMCMC over other conventional non-transdimensional approaches is the main motivation of this research, and we introduce the rjMCMC in the seismic waveform inversion to characterize reservoir properties and assess the uncertainty. The overview of the rjMCMC and its advantages over other conventional inversion methods are referred to Section 1.3. In this dissertation, the data refers to the seismic data including amplitudes, travel times and waveforms so our inversion is

9

waveform-based instead of amplitude-based.

2.1.1 Uncertainty Estimation

The knowledge of any object can be subdivided into what we know we know and what we know we do not know (Ma, 2011; Osypov et al., 2013). The goal of the uncertainty quantification is to answer what we know we do not know. For clarification, the uncertainty should not be treated as something we don't know, but it is defined as the range of possible outcomes. In the recent years, geophysicists started to put more emphasis on uncertainty estimation. Uncertainty includes measurement uncertainty (or data uncertainty) and inference uncertainty (or model uncertainty). In this study, we focus on inversion inference and model uncertainty so the uncertainty in this dissertation refers to model uncertainty. Sen and Stoffa (1996) and Scales and Tenorio (2001) presented overviews of uncertainty quantification in geophysics, and Duijndam (1988b) in seismic inversion. The uncertainty in geophysical inverse problems was estimated by various stochastic inversion algorithms, such as MCMC (Liu and Stock, 1993; Malinverno and Briggs, 2004; Chen and Dickens, 2009; Gunning et al., 2010; Kwon and Snieder, 2011), SA (Dosso, 2002; Dosso and Nielsen, 2002; Bhattacharya et al., 2003; Roy et al., 2005; Varela et al., 2006), PSO (Fernández-Martínez et al., 2012; Rumpf and Tronicke, 2015), and rjMCMC (Dettmer et al., 2013; Reading and Gallagher, 2013; Dadi, 2014; Galetti et al., 2015; Dadi et al., 2015). In most of these works, the uncertainty analysis is cast in a Bayesian framework.

2.1.2 Outline of This Section and Scientific Contributions

In this section, we will illustrate the methodology (Section 2.2), apply rjMCMC using synthetic seismic data (Section 2.3), and then apply it using an oilfield seismic data to characterize the petroleum reservoir in Norne field, North Sea (Section 2.4).

We will show these following benefits of using rjMCMC in seismic waveform

inversion.

1. The rjMCMC can infer the model dimensionality from the data itself, achieve proper parameterizations to prevent underparameterization and overparameterization. This approach is able to obtain a family of inverted solutions with different parameterizations.

2. The inversion uncertainty, which includes property uncertainty and location uncertainty, is correlated with the discontinuity of property. Larger discontinuity will cause more uncertainty in model property but also more certainty in location. Hence, the inversion uncertainty caused by major discontinuities will, however, assist in delineation of layer interfaces or boundary surfaces. This means that we can use the inversion uncertainty from a positive perspective to pinpoint the layer interfaces and quantify the magnitude of subsurface discontinuities such as a transition of lithology, which enhances the drilling management.

2.2   Methodology

The inverse problem in this section includes seismic waveform inversion of a 2-D post-stack data to build a 2-D earth model and uncertainty analysis. The inversion involves these general steps: 1) stochastically generate an initial model based on prior information, 2) update the model using rjMCMC iteratively via a data fitting process that compares the observed data with the modeled data and 3) collect an ensemble of all the models with good fitness, obtain the average model and estimate the uncertainty. Each seismic trace is inverted independently based on 1-D layered model, and then all the inverted 1-D models are combined to make the 2-D earth model. The model properties to be inverted are comprised of P-wave velocity V_p and

11

density ρ of each layer. The inverted P-wave impedance Z_p is calculated by $V_p\rho$. The number of layers is also treated as an unknown, and it will be inferred from the data through the transdimensional inversion.

2.2.1   Model Parameterization

Our model is represented by $\mathbf{m} = [\mathbf{V_p}, \rho, \mathbf{L}, n]$, where n is the number of layers, $\mathbf{L} = [L_1, L_2, ..., L_{n-1}]$ denotes the location of $n - 1$ interfaces, and $\mathbf{V_p} = [V_{p1}, V_{p2}, ..., V_{pn}]$ and $\rho = [\rho_1, \rho_2, ..., \rho_n]$ represent P-wave velocities and densities of n layers. In the inversion process, the n is unknown so it is initialized with an arbitrarily chosen number and it is allowed to vary stochastically from the current iteration to the next. Since seismic inversion uses seismic data sampled by 4 ms or 2 ms, the minimum thickness of a layer that can be detected via seismic inversion is a few meters. So we can set an upper limit for n, say, 50 for a model which is 200 m in thickness.

The model space (the allowed ranges of model parameters) for $\mathbf{V_p}$ and ρ is continuous. However the model space for $\mathbf{L}$ and n is discrete since the model has to be spatially discretized in depth or time with a certain given resolution for numerical computation, say, 1 m. If the inversion depth is from 2000 m to 2200 m with resolution of 1 m, then there are $N = 199$ possible values for the depth of an interface L_i, say, 2001, 2002, and so on. However, N should not be confused with n which is the number of layers.

Nevertheless, the inversion product is not only one single optimized model with one parameterization, but is a group of good models with different parameterizations which can fit the data almost equally well regarding the presence of data noise. By statistical analysis in the following sections, we will show that different parameterization schemes will have different probabilities in the posterior probability distribution, that is, there

are more models with proper parameterizations than those with underparameterization and overparameterization because rjMCMC favours proper parameterizations.

2.2.2 Forward Calculation

Forward calculation or the forward modeling is the process to generate data given a model. Disregarding the computation expense, the stochastic rjMCMC approach can adopt forward calculation methods such as Finite Difference Method (FDM), Finite Element Method (FEM), Spectral Element Method (SEM), etc. However, in order to obtain inversion results within a short amount of time for large 3D datasets, it is recommended to use fast forward modeling methods such as the reflectivity method (Kennett, 1983) and seismic convolution method. Due to the fact that our study region has simple geological structures without steep reflectors such as salt diapir, we chose seismic convolution modeling as the forward calculation method in which the seismic data can be generated by the convolution of the source wavelet and seismic reflectivity.

2.2.3 Bayesian Inference

In the earth sciences, inversion is usually implemented in two ways. One is to find a single set of model parameters through optimization of a data misfit function often combined with some regularization term (Parker, 1994). The other way is through sampling of an posterior probability density function (PDF) cast in a Bayesian framework. Standard references for Bayesian inference are by Box and Tiao (1973) and Smith et al. (1992). Its applications in geophysics are given by Tarantola and Valette (1982b), Jackson and Matsu'ura (1985), Duijndam (1988a,b), Mosegaard and Tarantola (1995), Sen and Stoffa (1995, 1996), Malinverno (2000) and Ulrych et al. (2001). The application specifically in seismic inversion is given by Gouveia and Scales (1998) and Buland and Omre (2003).

An inverse problem can be set up in a Bayesian framework which estimates the posterior probability distribution of the model parameters of interests from prior information and a likelihood function, sometimes referred to as a fitness (measure of agreement) or misfit function (measure of disagreement). The misfit function is also called the error function, objective function, cost function, etc. The Bayesian inference in the inverse problem can be formulated as follows:

$$p(\mathbf{m}|\mathbf{d}_{\mathrm{obs}}) = \frac{p(\mathbf{d}_{\mathrm{obs}}|\mathbf{m})p(\mathbf{m})}{p(\mathbf{d}_{\mathrm{obs}})}. \tag{2.1}$$

$p(\mathbf{d}_{\mathrm{obs}}|\mathbf{m})$ is the likelihood function which is the probability of observing the measured data given a model $\mathbf{m}$. $p(\mathbf{m})$ is the prior PDF of $\mathbf{m}$, that is, the prior knowledge of $\mathbf{m}$ before the data $\mathbf{d}_{\mathrm{obs}}$ is considered. $p(\mathbf{d})$ is the probability of the observed data, and it is usually ignored in the inversion process since it is a constant quantity which is not contingent on any model. $p(\mathbf{m}|\mathbf{d}_{\mathrm{obs}})$ is the posterior PDF which indicates how the prior knowledge of $\mathbf{m}$ is updated and constrained after the data information is incorporated. Generally speaking, the posterior distribution of $\mathbf{m}$ is narrower and more constrained than the prior distribution because the data information is added to infer the model.

2.2.4   The Prior Information

The prior knowledge of the model can be comprised of miscellaneous information from different sources. The model priors are the ranges and distributions within which we think the model parameters are reasonable based on the data such as well logs and the knowledge of geophysics, geology and rock physics in the real earth. If there are well logs, we can further constrain these model ranges (or model space). For example, we can set the range of V_p as from V_p^{min}=2.4 km/s to V_p^{max} =4.0 km/s, and the range of ρ as from ρ^{min}=2.1 g/cc to ρ^{max}=2.7 g/cc. Since we are using a transdimensional

approach, the number of layers can vary from an allowed minimum to a maximum, say, from $n^{min}{=}2$ to $n^{max}{=}50$. The prior distribution of model parameters can be set as uniform, Gaussian normal or any other type within these ranges. In this study, we adopted uniform prior distributions for all model parameters because we treated each model parameter has equal prior probability within its own range before the inversion is implemented.

The full prior PDF is separated into four terms:

$$p(\mathbf{m}) = p(\mathbf{V_p}|n, \mathbf{L})p(\rho|n, \mathbf{L})p(\mathbf{L}|n)p(n), \tag{2.2}$$

where $p(n)$ is the prior on the number of layers, $p(\mathbf{L}|n)$ is the prior on the location of $n-1$ interfaces given the number of layers n, and $p(\mathbf{V_p}|n, \mathbf{L})$ and $p(\rho|n, \mathbf{L})$ are the priors on the V_p and ρ models given n and $\mathbf{L}$. These prior PDFs can be formulated as follows:

$$p(\mathbf{V_p}) = \prod_{i=1}^{n} p(V_{pi}|n), \tag{2.3}$$

$$p(V_{pi}|n)) = 1/(V_{pi}^{max} - V_{pi}^{min}), \tag{2.4}$$

$$p(\rho) = \prod_{i=1}^{n} p(\rho_i|n), \tag{2.5}$$

$$p(\rho_i|n)) = 1/(\rho_i^{max} - \rho_i^{min}), \tag{2.6}$$

$$p(n) = 1/(n^{max} - n^{min}), \tag{2.7}$$

$$p(\mathbf{L}|n) = 1/C_{n-1}^{N} = \frac{(n-1)!(N-n+1)!}{N!}, \tag{2.8}$$

where N is total number of possible depths given a certain spatial resolution, and $C_{n-1}^{N} = \frac{N!}{(n-1)!(N-n+1)!}$ is the number of possible combinations for $n-1$ layer interfaces which will occupy $n-1$ depths out of N possible depths in total.

Derived from the above equations, the full prior PDF is written as:

$$p(\mathbf{m}) = \frac{(n-1)!(N-n+1)!}{(n^{max} - n^{min})N! \prod_{i=1}^{n}((V_{pi}^{max} - V_{pi}^{min})(\rho_i^{max} - \rho_i^{min}))}. \tag{2.9}$$

2.2.5 The Likelihood Function

The likelihood function assesses how well a given model can fit the observed data by computing the difference between the observed data and the modeled data from forward modeling. The observed data can be written as a combination of the data produced by the model and data misfit (or data error):

$$\mathbf{d}_{\text{obs}} = \mathbf{d}_{\text{modeled}} + \mathbf{e} = f(\mathbf{m}) + \mathbf{e}. \tag{2.10}$$

The difference of the modeled and observed data can be calculated in many ways, such as the L2-norm error function, a cross correlation (Sen and Stoffa, 1991), and Shannon's entropy (JafarGandomi and Binley, 2013). L2-norm is the square root of the sum of the squares of all the samples (equation (2.11)), whereas the L1-norm is defined as the sum of the absolute values of all the samples (equation (2.12)).

$$\|\mathbf{e}\|_2 = \sqrt{\sum_{i=1}^{N} e_i^2}. \tag{2.11}$$

$$\|\mathbf{e}\|_1 = \sum_{i=1}^{N} |e_i|. \tag{2.12}$$

In this study, our likelihood function adopted the L1-norm misfit instead of the L2-norm for two reasons. One is that the L1-norm favours a "sparse" structure (Oldenburg et al., 1983; Russell, 1988) and this idea is used in the sparse-spike inversion and deconvolution, which means that a model with few layers will be more

favorable if it can fit the data well. The other reason is that the L2-norm may lead to distorted results because it is highly sensitive to data outliers (Claerbout and Muir, 1973).

The L1-norm likelihood function in our inverse problem is written as:

$$p(\mathbf{d}_{\text{obs}}|\mathbf{m}) \propto \exp\left\{-\frac{\Phi^2(\mathbf{m})}{2N_d\sigma_d^2}\right\}, \tag{2.13}$$

$$\Phi(\mathbf{m}) = \|f(\mathbf{m}) - \mathbf{d}_{\text{obs}}\|_1, \tag{2.14}$$

where N_d is the number of data samples and σ_d is a given standard deviation of the data error $\mathbf{e}$ in equation (2.10). σ_d affects likelihood function and acceptance probability, and it serves as the data-fitting criterion in the inversion so that a proposed model with a RMS (root mean square) data-fitting error less than σ_d will have more probability to be accepted and a proposed model with an error larger than σ_d will be less likely to be accepted.

2.2.6   The Transdimensional Method, rjMCMC

A conventional MCMC method based on a Bayesian inference and the Metropolis-Hasting algorithm (Metropolis et al., 1953; Hastings, 1970) is able to generate samples from the posterior probability distribution (PPD) which describes the most likely model parameters that can fit the data, and it estimates the uncertainty based on the ensemble of models. A Markov-chain approach usually adopts a random-walk sampling method that generates a new model $\mathbf{m}'$ stochastically based on the current model $\mathbf{m}$. The random walk is assumed to be stationary and produces an importance sampling of the model space after the beginning part of the chain known as the burn-in period is discarded (Bodin et al., 2012b). The samples from this chain will provide an approximation to the PPD of the model parameters as well as uncertainty

quantification thereof. Also on the basis of the MCMC, the rjMCMC allows inference both on model parameters and model dimensionality. An initial model is selected randomly and an iterative process is implemented in which the current model is randomly perturbed and the new model is accepted or rejected according to the acceptance probability shown by equation (2.15):

$$\alpha(\mathbf{m'}|\mathbf{m}) = min\left[1, \frac{p(\mathbf{m'})}{p(\mathbf{m})} \cdot \frac{p(\mathbf{d}_{\text{obs}}|\mathbf{m'})}{p(\mathbf{d}_{\text{obs}}|\mathbf{m})} \cdot \frac{q(\mathbf{m}|\mathbf{m'})}{q(\mathbf{m'}|\mathbf{m})} \cdot |\mathbf{J}|\right], \qquad (2.15)$$

where $\mathbf{m}$ represents the current model and $\mathbf{m'}$ is the new proposed model. $p(\mathbf{m})$ is the prior probability, $p(\mathbf{d}_{\text{obs}}|\mathbf{m})$ presents the likelihood function, and $q(\mathbf{m'}|\mathbf{m})$ denotes the proposal distribution for model perturbation. The matrix $\mathbf{J}$ is the Jacobian of the transformation from $\mathbf{m}$ to $\mathbf{m'}$, and $|\mathbf{J}|$ proves to be 1 (Bodin et al., 2012b) for our problems. If the acceptance probability $\alpha = 1$, the new proposed model will be accepted. If $\alpha < 1$, the new proposed model will be accepted only if α is larger than a random value generated from a uniform distribution (0, 1), otherwise it will be rejected. If the new proposed model is rejected, the rjMCMC will repeat for the current iteration and propose another new model until it is accepted. This process guarantees that each iteration will have a new model so that it can prevent oversampling in one single model for numerous iterations.

For proposal distribution $q(\mathbf{m'}|\mathbf{m})$, a new model is proposed by drawing from this distribution so that the new model is contingent on the current model $\mathbf{m}$. Our study sets it either as a Gaussian normal distribution or a uniform distribution centered at the current model $\mathbf{m}$. If perturbing V_{pi} or ρ_i and then proposing a new V'_{pi} or ρ'_i, the proposal distribution is a Gaussian normal distribution. The proposal distribution is a uniform distribution if perturbing the location of a interface L_i and proposing a

new L'_i. These distributions are written as:

$$q(V'_{pi}|V_{pi}) = \frac{1}{\sigma_{V_p}\sqrt{2\pi}}\exp\left\{-\frac{(V'_{pi} - V_{pi})^2}{2\sigma_{V_p}^2}\right\}, \tag{2.16}$$

$$q(\rho'_i|\rho_i) = \frac{1}{\sigma_\rho\sqrt{2\pi}}\exp\left\{-\frac{(\rho'_i - \rho_i)^2}{2\sigma_\rho^2}\right\}, \tag{2.17}$$

$$q(L'_i|L_i) = \frac{1}{\Delta h}, \tag{2.18}$$

where $\sigma_{V_p}^2$ and σ_ρ^2 are the given variances of the Gaussian function for the model perturbation. A larger variance means a greater perturbation, and vice versa. Δh is a given perturbation range for moving interface.

Our approach implements the rjMCMC which involves 3 updating strategies during the random walk, and the inversion will randomly pick one updating strategy at each iteration.

1. Move an interface: randomly pick one layer interface and perturb its location, and perturb the geophysical properties (such as V_p and ρ) of the layer either above or below that interface.

2. Add an interface: randomly choose a location in depth and create a new layer interface, and perturb the geophysical properties of the layer either above or below that new interface.

3. Delete an interface: randomly pick one layer interface to remove and perturb the geophysical properties of the new combined layer.

Since the acceptance or rejection of a new proposed model is contingent on the

acceptance probability which is governed by the prior ratio $\frac{p(\mathbf{m'})}{p(\mathbf{m})}$, the likelihood ratio $\frac{p(\mathbf{d}_{\mathrm{obs}}|\mathbf{m'})}{p(\mathbf{d}_{\mathrm{obs}}|\mathbf{m})}$ and the proposal ratio $\frac{q(\mathbf{m}|\mathbf{m'})}{q(\mathbf{m'}|\mathbf{m})}$ all together. Now let's take a look at the formulations of these ratios for different updating strategies respectively.

For the first updating strategy, there is no change of dimension, so the prior ratio $\frac{p(\mathbf{m'})}{p(\mathbf{m})} = 1$, the proposal ratio $\frac{q(\mathbf{m}|\mathbf{m'})}{q(\mathbf{m'}|\mathbf{m})} = 1$, and the likelihood ratio $\frac{p(\mathbf{d}_{\mathrm{obs}}|\mathbf{m'})}{p(\mathbf{d}_{\mathrm{obs}}|\mathbf{m})} = \exp\left\{-\frac{\Phi^2(\mathbf{m'}) - \Phi^2(\mathbf{m})}{2N_d\sigma_d^2}\right\}$.

For the second updating strategy, a new model $\mathbf{m'}$ is proposed with one more layer interface, velocity and density. The prior ratio $\frac{p(\mathbf{m'})}{p(\mathbf{m})} = \frac{n}{N-n+1}$, the proposal ratio $\frac{q(\mathbf{m}|\mathbf{m'})}{q(\mathbf{m'}|\mathbf{m})} = \frac{N-n+1}{nq(V_p'|V_p)q(\rho'|\rho)}$, and the likelihood ratio is the same as that in the first strategy.

For the third updating strategy, a new model $\mathbf{m'}$ is proposed with one fewer layer interface, velocity and density. The prior ratio $\frac{p(\mathbf{m'})}{p(\mathbf{m})} = \frac{N-n+2}{n-1}$, the proposal ratio $\frac{q(\mathbf{m}|\mathbf{m'})}{q(\mathbf{m'}|\mathbf{m})} = \frac{(n-1)q(V_p'|V_p)q(\rho'|\rho)}{N-n+2}$, and the likelihood ratio is the same as that in the first strategy.

Detailed derivations for the proposal ratios are given by Bodin and Sambridge (2009) and Bodin et al. (2012b). But one difference is that we used $n-1$ layers' interfaces to denote n layers' locations, and they used the centers (nuclei) of all k layers, so our $n-1$ is equivalent to their k in the formulations. The other difference is we included terms for density ρ in our equations.

Substituting these ratios into equation (2.15), we will get acceptance probability for 3 updating strategies respectively as follows:

$$\alpha(\mathbf{m'}|\mathbf{m}) = min\left[1, \exp\left\{-\frac{\Phi^2(\mathbf{m}) - \Phi^2(\mathbf{m'})}{2N_d\sigma_d^2}\right\}\right], \tag{2.19}$$

$$\alpha(\mathbf{m}'|\mathbf{m}) = min[1, \frac{\sigma_{V_p}\sqrt{2\pi}}{V_{pi}^{max} - V_{pi}^{min}} \frac{\sigma_\rho\sqrt{2\pi}}{\rho_i^{max} - \rho_i^{min}} \exp\{\frac{(V_{pi}' - V_{pi})^2}{2\sigma_{V_p}^2}$$

$$+ \frac{(\rho_i' - \rho_i)^2}{2\sigma_\rho^2} - \frac{\Phi^2(\mathbf{m}') - \Phi^2(\mathbf{m})}{2N_d\sigma_d^2}\}], \tag{2.20}$$

$$\alpha(\mathbf{m}'|\mathbf{m}) = min[1, \frac{V_{pi}^{max} - V_{pi}^{min}}{\sigma_{V_p}\sqrt{2\pi}} \frac{\rho_i^{max} - \rho_i^{min}}{\sigma_\rho\sqrt{2\pi}} \exp\{-\frac{(V_{pi}' - V_{pi})^2}{2\sigma_{V_p}^2}$$

$$- \frac{(\rho_i' - \rho_i)^2}{2\sigma_\rho^2} - \frac{\Phi^2(\mathbf{m}') - \Phi^2(\mathbf{m})}{2N_d\sigma_d^2}\}]. \tag{2.21}$$

2.2.7 Inversion, Optimization and Sampling

There is a difference between optimization and inversion. Optimization process aims to find the best model with the lowest misfit between the real data and the forwardly modeled data. Due to the data noise, the model with the lowest misfit may not necessarily be the true model for the reasons such as the overfitting of the noise. The noise will also make the global minimum less outstanding on the surface defined by the misfit function, so the good local minima and true global minimum may have almost equal misfits among which it is hard to pick the true global minimum. But statistically, we believe that good local minima are located around the global minimum according to a certain distribution such as Gaussian normal distribution. In most geophysical inverse problems, the goal is not to achieve one single optimized solution, but instead, to find a set of models fitting the data and also assess the uncertainty. So the inversion in our research incorporates two stages. The first stage is the optimization through which an optimized model (or a good local minimum) near the true model (or global minimum) will be found. This stage is termed "burn-in" which means the inversion sampler starts from an initial model of a low likelihood and takes a number of iterations to increase the likelihood until it reaches an equilibrium level that tends to remain constant (Malinverno, 2002; Agostinetti and Malinverno, 2010). In the second stage which is sampling, the

inversion sampler is able to jump out of local minima and sample the entire model space so it can achieve good sampling around the true model. During the sampling stage, the likelihood will fluctuates about its equilibrium value and then a family of good models will be collected. In a statistical sense, the average solution of this ensemble can be regarded as an optimal representation of the true model and the standard deviation of this solution family can be utilized to quantify the uncertainty.

2.2.8 Uncertainty Analysis and Enhancement by Transdimensional Sampling

The model uncertainty results from the non-uniqueness of the inverted model given the data. In most inverse problems a set of models may fit the data within a predefined tolerance through forward calculation. And this set of model solutions is termed the solution space which is a subset of the model space. Because the uncertainty is defined as the range of possible outcomes, the measurement of model uncertainty is a quantification of the size of the solution space in each dimension. However, a direct measurement of model uncertainty is almost impossible for most inverse problems in that it is difficult to find a complete set of all the models that can fit the data especially in a high-dimension model space. Therefore, a stochastic inversion sampler can be utilized to implement the uncertainty estimation for reason that it is able to sample the entire model space in all dimensions and collect good samples which can fit the data. Notwithstanding the group of these samples is not the complete solution space, they still spread over the solution space. Thus, statistically if there are enough samples, the standard deviation of these samples in each dimension is a measurement of the model uncertainty or the size of the solution space in each dimension.

However, for many inverse problems the dimensionality of the model space is unknown. For example, the number of layers is unknown when we try to invert acoustic

impedance in depth for a petroleum reservoir. Hence if we presume a dimensionality which is quite different from the true model's dimensionality prior to inversion, or in another word, if we overparameterize or underparameterize the model, it is very likely that the inversion process will implement a biased sampling because the inversion samples in a different dimensional space than the correct dimensional space where the true model is located. Consequently, the ensemble of inverted model solutions and the average solution may have a bias, and meanwhile the uncertainty estimation cannot be implemented properly. Regarding this issue, we use a transdimensional rjMCMC to enhance inversion and uncertainty estimation on the grounds that the rjMCMC can sample the spaces with different dimensionalities and achieve appropriate parameterizations to depict the true model. The average model can be used as an optimal representation of the true model. To quantify the uncertainty, we need to calculate the standard deviation of the solution ensemble. Since this ensemble includes models with different parameterizations, we have to downscale these models with a uniform finer discretization before we calculate the average and the standard deviation. Statistically this transdimensional implementation introduces less bias than the sampling only in one single space of a possible wrong dimensionality, and therefore it enhances the uncertainty estimation.

2.2.9   Calculation of the Average Model and the Uncertainty

An ensemble of inverted models with lowest data misfit will be selected for the calculation of the average model and the uncertainty. Each model of the ensemble has different parameterizations with different number of layers and their interfaces' locations. Hence, in order to calculate the average model and the uncertainty, we need to downscale all the inverted models in a uniform finer discretization scheme, say, 0.4 m sampling in depth domain or 0.4 ms sampling in time domain. After this

downscaling with the same discretization, all the models will be digitized into vectors or matrices with the same size, so we can easily calculate the mean values of the model ensemble sample by sample for each time or depth, and can also calculate the standard deviations of this ensemble sample by sample for each time or depth for uncertainty quantification. A detailed explanation and the formulations for calculating the average Model and uncertainty are referred to Section 4.2.4.

However, most data contains random noise (data uncertainty) which will inevitably propagate into model parameter and model uncertainty. As previously pointed out, uncertainty includes measurement uncertainty (or data uncertainty) and inference uncertainty (or model uncertainty). Ideally, the inference uncertainty should be independent of measurement uncertainty, whereas in reality the data uncertainty can partially propagate to the model uncertainty. To acquire the average model and model uncertainty without strongly being affected by data uncertainty, we need to eliminate or suppress the effect of the random noise on the model and its uncertainty because we are not expecting a model to explain the unpredictable random noise and we hope the model uncertainty is driven by the inference but not by the random noise. Since a complete elimination of noise effect is almost impossible, our goal here is to suppress it through a lateral moving-average smoothing. The assumption is that the presence of spatial random noise may possibly lead to slight underestimation of model parameter and uncertainty in one location and possibly slight overestimation in its neighboring location, or vice versa. Therefore, this smoothing will assist in neutralization of estimating model parameter and its uncertainty.

2.2.10 Inversion in Depth Domain and Time Domain

Previously we used terms such as the depth of layer interface which implies a model in depth domain. However, this method can be implemented in time domain if

the model is in time domain. And the depth of a layer interface means a certain time in time domain. All the above equations will be the same if used in time domain but the only difference is that **L** has a unit of meter in depth domain, whereas it has a unit of second in time domain. In our study we implemented rjMCMC inversion in time domain and the time is two-way travel time(TWT).

2.2.11   Inversion Parameter Setting

Prior to running rjMCMC for an inverse problem, we need to configure rjMCMC and some parameters.

1. Specify the model priors (including model space and distribution). The model space is defined by the lower/upper limits of each model parameter including V_p, ρ, n and L. For example, the model space for V_p is bounded by a given V_p^{min} and V_p^{max}. Other information such as well logs can be incorporated to design the model inversion limits. And the prior distributions for all model parameters are uniform in this study.

2. Specify the proposal distributions for all model parameters. This study sets Gaussian normal distributions for perturbing V_p and ρ with given σ_{V_p} and σ_ρ. Our research suggests that these values be around 25% of the difference between their corresponding lower and upper limits since a too small perturbation leads to being trapped in the local minima and a too large perturbation leads to slow or none convergence. For example, we can set $\sigma_{V_p} = (V_p^{max} - V_p^{min})/4$ and $\sigma_\rho = (\rho^{max} - \rho^{min})/4$. And we set uniform distributions for the perturbation of **L** and n within given ranges.

3. Specify the standard deviation of data misfit σ_d which will constrain the acceptance probability for a new proposed model. For example, σ_d can be set as 10% of the peak amplitude of the data. A larger σ_d will lead to a higher probability to accept new proposed models and facilitate sampling and jumping out of local minima, and a lower σ_d will enhance local optimization and exploitation instead of global exploration.

2.3   Synthetic Case Study

We created a synthetic model and a corresponding set of synthetic seismograms for the first test of seismic waveform inversion by rjMCMC. The true models for V_p and ρ in time domain are shown by Figure 2.1. This model including a wedge can test the inversion resolution of rjMCMC and how rjMCMC performs when the layer is thin. From V_p and ρ, we calculated the acoustic impedance ($Z_p = V_p\rho$) and then generated zero-offset reflectivities in time domain. A synthetic seismic data with 2 ms sampling interval was generated by the convolution of the reflectivities and a zero-phase Ricker wavelet with central frequency of 25 Hz. The simulated seismic data was also added with zero-mean Gaussian random noise with a standard deviation of 10% of the maximum data value. The noise was added on the amplitude of each sample so the waveform was slighted distorted and also contained spikes. This synthetic seismic data with noise (Figure 2.2) was used as the observed seismic data for the inversion. The synthetic data from this model has 80 traces with a spacing of 12.5 m.

The properties of the overburden rock above 2 s for the true model and the model to be inverted are set to be the same with those of the first layer of the true model. We assumed there was no well log available and we chose constant inversion lower/upper limits for both V_p and ρ, which are (2.4, 4.0) km/s for V_p and (2.1,
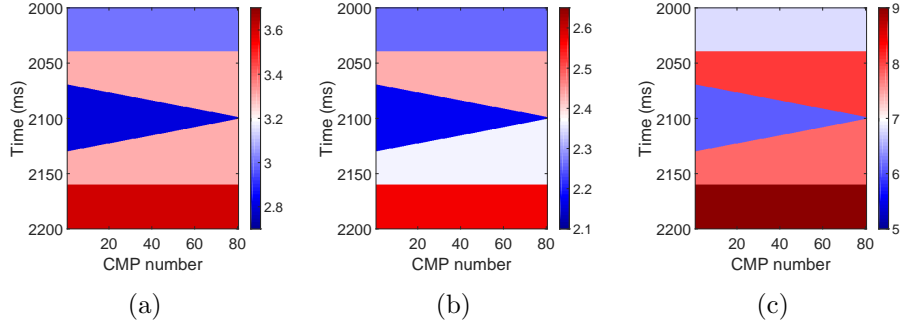
Figure 2.1: Geophysical properties for the wedge model used to test the rjMCMC inversion algorithm. (a) P-wave velocity V_p (km/s). (b) Density ρ (g/cc). (c) Impedance $Z_p = V_p\rho$ (km/s*g/cc).

2.7) g/cc for ρ. Since the number of layers is unknown, we chose a arbitrary model as the initial model which has 10 layers with equal interval in time domain and with the same initial V_p=3.2 km/s and ρ=2.4 g/cc.

The standard deviation of data misfit σ_d in equation (2.13) was set to be 0.03 which is around 20% of the peak of the seismic data. For the standard deviations of the proposal distributions for model perturbation, we set σ_{V_p} and σ_ρ in equation (2.16) and equation (2.17) to be 0.4 km/s and 0.15 g/cc respectively. In this stochastic inversion, we treated V_p and ρ as independent variables and we don't assume a linear or any other type of relationships between them. However, to imitate the properties of rocks in the real case, we set lower/upper limits for the ρ/V_p ratio which is between 0.6 and 0.9. The allowed minimum number of layers is 2 and the allowed maximum is 30. If a new model goes beyond any one of the these bounds, it will be discarded and rjMCMC will repeat the current step and propose another new model until our criterion is met.

The inversion was only based on the synthetic seismic data (eg. Figure 2.2) and was run within the defined model space to recover the true model. We run the
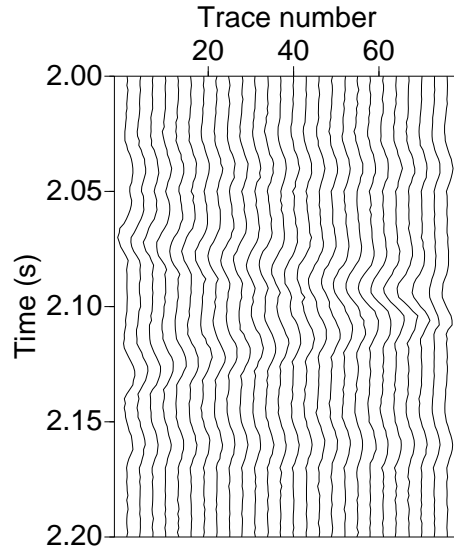
Figure 2.2: Synthetic seismic data generated from the true model and added with 10%random noise. Displayed by every three traces.

inversion trace by trace for 5,000 iterations. Each trace was inverted independently as in the seismic waveform inversion for 1-D earth model (see Section 2.2). We chose the inversion of No.40 trace as an example to illustrate the inversion process. We calculated the RMS error between the synthetic data and the data modeled from the inverted model for all iterations. Figure 2.3 indicates that the misfit decreases rapidly and the rjMCMC finds the low-misfit models after 200 iterations. Since the goal of our stochastic inversion is to sample the entire model space and achieve good sampling around the true model and find a set of good models with low misfits, we kept rjMCMC running for 5,000 iterations so that we would have enough good models in the solution pool through this sampling stage. This would assist us to get a quality average model as well as to quantify the uncertainty.

To demonstrate how the rjMCMC can infer the model dimensionality, we plot
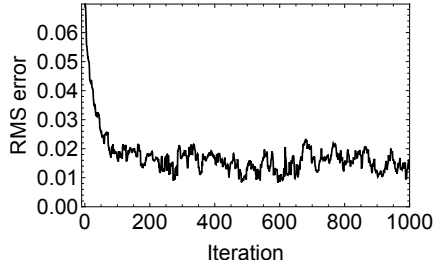
Figure 2.3: RMS error between the data and the modeled data. Displayed for only the first 1000 iterations (Trace No.40).

the number of layers with iterations (Figure 2.4). Out of 5,000 models from 5,000 iterations, we sorted the models by RMS error and chose 2,500 models with relatively less RMS errors. A histogram of the number of layers for these models is shown by Figure 2.5. These figures show that the rjMCMC finds the number of layers n around 5. A minor overparameterization is allowed by rjMCMC but an major overparameterization ($n > 19$) and an underparameterization ($n < 5$) are excluded by rjMCMC.
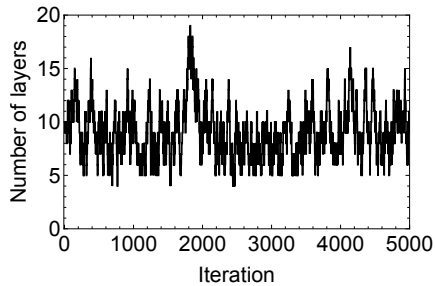
Figure 2.4: The variation of the number of model layers with iterations (Trace No.40).

We downscaled these chosen models with a uniform finer discretization scheme
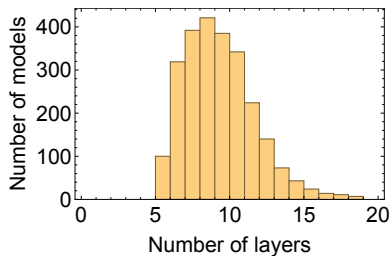
Figure 2.5: Histogram of the number of layers for 2,500 sampled models (Trace No.40).

in time domain (0.4 ms in this case study). As mentioned in Section 2.2.9, after this downscaling with the same discretization, all the models will be digitized into matrices with the same size. Then we computed the average value and the standard deviation sample by sample for all times.

Inverted V_p, rho and Z_p are shown by Figure 2.6. Obviously, the uncertainty (shown by the error bar) of density is larger than that of V_p. The reason is that the density is poorly resolved by P-waves (Debski and Tarantola, 1995; Igel et al., 1996). However, the inverted average density can recover the true density model. Even though most of the 2,500 sampled models have more than 5 layers, the average model exhibits 5 layers that is consistent with the true model, which shows that the rjMCMC is able to infer the model dimensionality.

To illustrate the posterior distribution of the sampled models, we plotted the histogram and show it for one depth (2120 ms) as an example. Figure 2.7 shows an asymmetrical distribution, but the average value approximates the true value (Figure 3.6).

We conducted this inversion process for all traces. As mentioned in Section 2.2.9, since each trace had spatial random noise that would propagate into the inverted results, a lateral moving-average smoothing was applied to suppress the
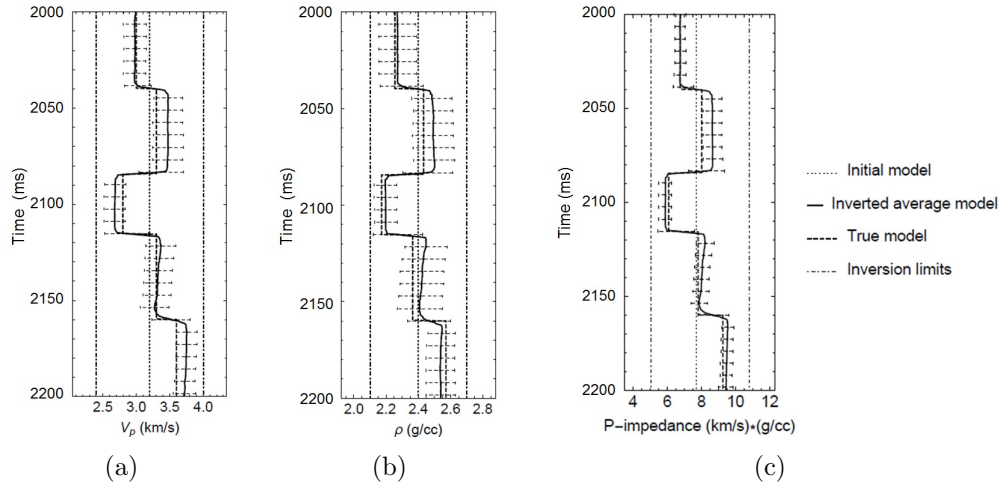
Figure 2.6: Inverted models vs. true models (Trace No.40). (a) V_p (km/s). (b) ρ (g/cc). (c) $Z_p = V_p\rho$ (km/s*g/cc). The inversion uncertainty (standard deviation) is represented by the error bar.

noise effect. Finally, we obtained the inverted average models of V_p, ρ and Z_p (Figure 2.8) and assessed their uncertainty (Figure 2.9). To show the effects of the smoothing, the inverted Z_p without smoothing was chosen (Figure 2.10) to compare with the smoothed results (Figure 2.8(c) and 2.9(c)). Before the smoothing, Z_p and Z_p uncertainty exhibits local underestimation or overestimation. After the lateral moving-average smoothing, the negative effects of the spatial random noise on the inversion results are suppressed to a large extent.

These inversion results indicate that the true model and the layer interfaces for V_p, ρ and Z_p are almost recovered by the rjMCMC. Looking at the wedge tip, we found that the inversion can exactly recover the interfaces if layer thickness is no less than 8 ms (two-way travel time) in time domain which is approximately 12 m in depth domain. If a layer is too thin, such as a few meters in thickness, then the layer interfaces will be unresolvable. This is due to the fact that a thin layer with a few meters in thickness can be added or deleted in a model without obviously changing the

31
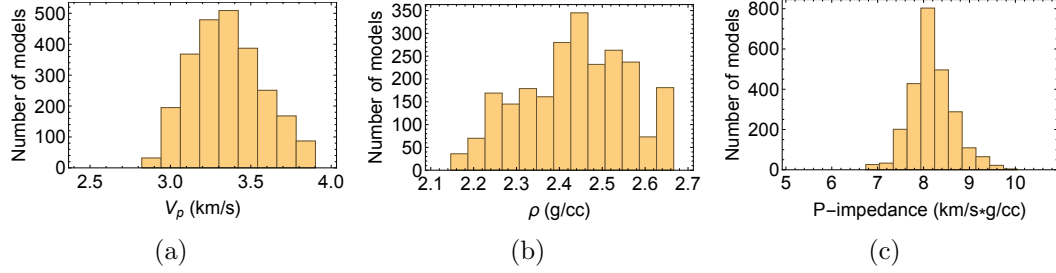
Figure 2.7: Histogram of sampled models (Trace No.40, depth=2120 ms). (a) V_p (km/s). (b) ρ (g/cc). (c) $Z_p = V_p\rho$ (km/s*g/cc).
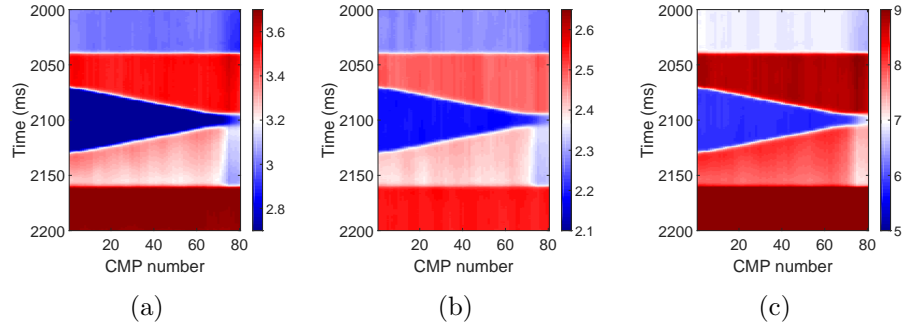
Figure 2.8: Inverted average model by rjMCMC. (a) V_p (km/s). (b) ρ (g/cc). (c) $Z_p = V_p\rho$ (km/s*g/cc).

seismic waveform because of the destructive interference between the two reflections from its two boundaries, a phenomenon called seismic tunning effect. Our seismic wave has a central frequency of 25 Hz which means a wavelength λ of 120 m if V_p is 3 km/s. These results demonstrate an inversion resolution of $\lambda/10$. To validate the inversion quality via data fitting, we computed the modeled seismic data from the inverted average model (Figure 2.11) and also calculated the seismograms generated from all the 2,500 sampled models. The standard deviations for all time samples of the 2,500 seismograms from the 2,500 models are illustrated by the error bars in Figure 2.12 which shows Trace No.40 as an example. Their standard deviations are
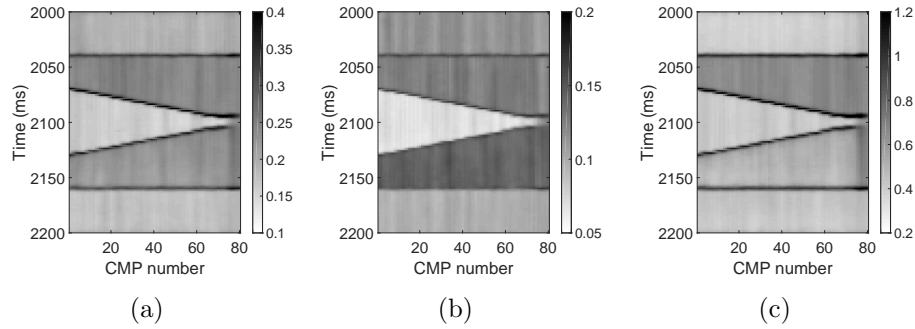
Figure 2.9: rjMCMC Inversion uncertainty. (a) V_p uncertainty (km/s). (b) ρ uncertainty (g/cc). (c) Z_p uncertainty (km/s*g/cc)
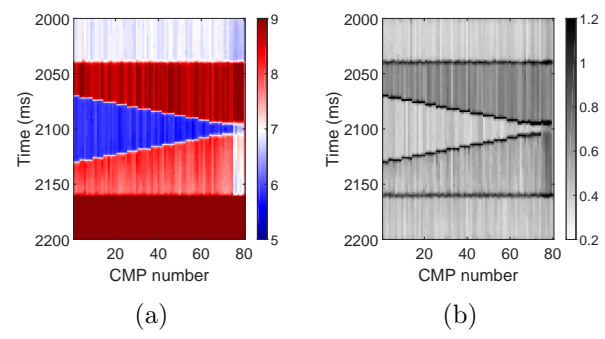
Figure 2.10: Inverted average model for Z_p before smoothing. (a) $Z_p = V_p\rho$ (km/s*g/cc). (b) Z_p uncertainty (km/s*g/cc).

quite small compared to the data, and the average standard deviation is computed to be 0.0098 which is around 7% of the data peak or trough. The data falls into the range of the error bar, which indicates an accurate data fitting for the model ensemble.

By comparing Figures 2.8 and Figure 2.9, another important and surprising phenomenon we discovered is that the high uncertainty of inversion in geophysical properties conforms exactly with layer interfaces which are the surfaces of discontinuity in these properties. Supportive and similar observations were recently published by

33
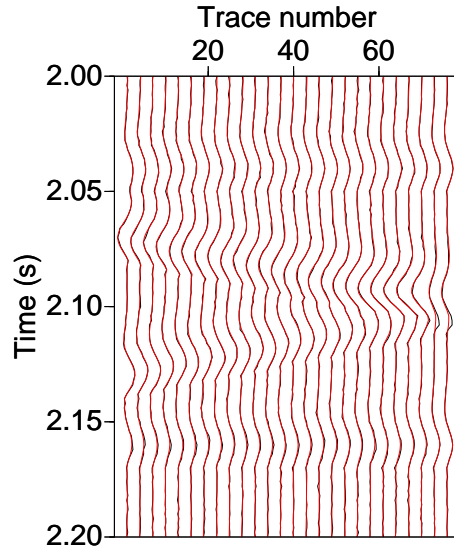
Figure 2.11: Synthetic seismic data generated from the true model and added with noise (black) vs. modeled data generated from the inverted average model (red). Displayed by every three traces.

Reading and Gallagher (2013) and Galetti et al. (2015) who both used rjMCMC for uncertainty analysis. By studying the abrupt changes of borehole geophysical logs, Reading and Gallagher (2013) found that interfaces are sharply defined if there exists a large lithology contrast. By a tomography study using surface wave, Galetti et al. (2015) found out that high uncertainty was observed along a discontinuity in the velocity field and the uncertainty map exhibits some spatial detail of velocity anomaly. Our study reveals that a larger discontinuity will induce a higher property uncertainty at the discontinuity and nevertheless a higher ''certainty'' of the location of that discontinuity. And for continuous region with zero discontinuity, the property uncertainty is much lower. Therefore, we point out that there is a trade-off between the property uncertainty and the location uncertainty in the seismic inversion.

Figure 2.9 shows that the uncertainty trade-off effect for V_p and Z_p is stronger that
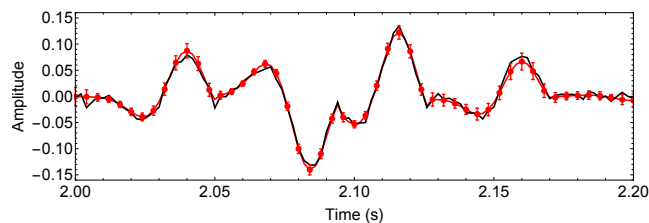
Figure 2.12: Comparison of the modeled data from 2,500 inverted models and the inverted average model with the synthetic data from the true model. Trace No.40 is chosen as an example for display. Black: synthetic seismogram generated from the true model and added with noise. Red: seismogram generated from the inverted average model. Red error bars present the standard deviations for all time samples of the 2,500 seismograms from the 2,500 inverted models (displayed by every two time samples), and the average standard deviation=0.0098.

that for ρ due to the abovementioned reason that ρ is relatively poorly resolved by P-waves seismic data. In the following uncertainty analysis, we will choose acoustic impedance Z_p as a typical example. In our study, the phenomenon of high impedance uncertainty induced by a large discontinuity is due to the fact that if there is a great change of impedance within a short distance across the interface, for example, the Z_p has a sudden jump from 6 to 8 (km/s*g/cc) across the wedge's upper boundary, the inversion therefore has great freedom to choose any value between 6 and 8 in the transition zone to fit the data equally well as we previously pointed out that a perturbation in a very thin layer will not obviously change the seismic wiggles. Our inversion results also indicate that the high impedance uncertainty caused by a large impedance discontinuity is able to delineate the location of this discontinuity. In another word, the impedance uncertainty is larger exactly where the discontinuity is larger. This is due to the fact that a major impedance discontinuity also causes a large seismic event which however will facilitate locating the discontinuity via the inversion, and that is why we see clear interfaces delineated by high impedance

35

uncertainty in this study (Figure 2.9(c)).

In summary, a larger discontinuity of property will induce 1) more uncertainty in model property at the discontinuity and 2) more ''certainty'' of the location of the discontinuity. The layer's impedance Z_p and the layer's location L can be regarded as complementary variables in the seismic inversion since the seismic waveform is governed by the combined effects from both Z_p and L. For example, the impedance of the layers and the locations of layer interfaces can be perturbed in different ways to obtain the same seismic wiggles. We firstly pointed out that the seismic waveform inversion exhibits a trade-off between property uncertainty and location uncertainty in such a way that the property uncertainty and the location uncertainty exert a limitation on each other, which means they cannot be simultaneously certain with high accuracy in one experiment since they are complimentary. To generalize this discovery in any inverse problems in all disciplines, if there are complimentary parameters in the model, the inversion of these parameters may comply with the principle of uncertainty trade-off.

From the above analysis, we can use the uncertainty from a positive perspective and we propose that the inversion uncertainty from our stochastic inversion can be designed as a new attribute to assist in delineating the subsurface reflectors and quantify the magnitude of discontinuities. In section 4 which focuses on uncertainty analysis using rjMCMC, we will talk more about this phenomenon in detail and how to use inversion uncertainty in an optimistic way to better delineate subsurface interfaces and discontinuities and to facilitate drilling planning for petroleum exploration.

Meanwhile, Section 3 will show that the earth model and its layer interfaces such as the challenging wedge tip can be better recovered by using pre-stack seismic waveform inversion. This means that although the property uncertainty and the location uncertainty exert a limitation on one another, by using more data this

limitation can be changeable. We found out that prestack waveform inversion is able to resolve a layer as thin as 5 ms TWT in time domain or 7.5 m in depth domain. This resolution is around $\lambda/16$ which is much finer than a typical seismic resolution of $\lambda/4$. Additionally, using pre-stack or angle-stack seismic data, the rjMCMC can simultaneously invert V_p, V_s and ρ which can be easily converted to acoustic impedance, shear impedance, Poisson's ratio, $\lambda\rho$, $\mu\rho$ and other properties to study the rock physics and DHIs (Direct Hydrocarbon Indicator) and ameliorate reservoir characterization.

2.4 Case Study Using an Oilfield Data, Norne Field, North Sea

In this inversion application to field data, we used a near-offset stacked seismic data and one nearby well in the E-segment of the Norne oilfield to characterize V_p, ρ and acoustic impedance Z_p of the reservoir and estimate their uncertainty.

The Norne field is located in the sourthern part of the Nordland II in the Norwegian Sea. The field size is approximately 9 km by 3 km. The reservoir is sealed by the Melke shale formation and it consists of four sand formations from top to base: Garn, Ile, Tofte and Tilje of Lower to Middle Jurassic age. A gas reservoir is mostly situated in the Garn formation of nearshore facies, the oil reservoir is mainly located in the Ile and Tofte formations which are shallow marine deposits with channelized sandstones, and the Tilje formation is mostly sand with some clay and conglomerates (Rwechungura et al., 2010).

The seismic data of 400 traces is shown by Figure 2.13. The wavelet was extracted from the seismic data and used it for the forward calculation. And we smoothed the V_p and density logs to generate a low-frequency trend and then perturbed the smoothed V_p and density for ± 0.5 km/s and ± 0.3 g/cc respectively to make the inversion lower/upper limits (Figure 2.14). The allowed minimum number of layers is

2 and the allowed maximum is 50. We then upscaled the smoothed logs to blocky logs with equal interval in time domain and used them as our initial model (Figure 2.14). The standard deviation of data misfit σ_d was set to be 10% of the peak amplitude of the seismic data, and σ_{V_p} and σ_ρ in equation (2.16) and equation (2.17) were set to be 0.25 km/s and 0.15 g/cc respectively.
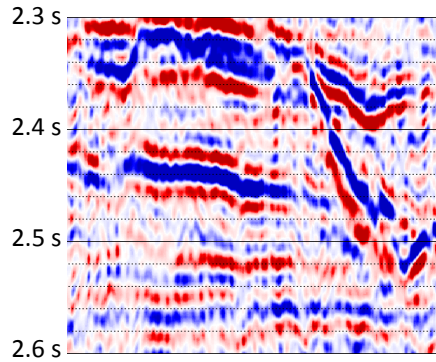
Figure 2.13: Seismic data of Norne field which is used for rjMCMC inversion.

(a)   (b)
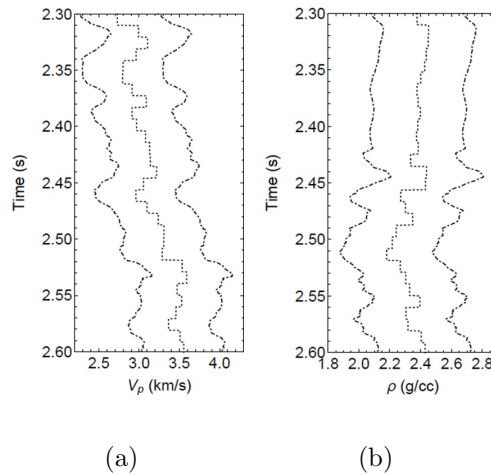
Figure 2.14: Initial model (dotted) and inversion lower/upper limits (dotdashed).

The rjMCMC inversion was run trace by trace for 5,000 iterations and 2,500 inverted models with relatively less data misfits were chosen. The modeled seismic data was calculated by using the inverted average model for validation. Figure 2.15 and Figure 2.16 indicate that the rjMCMC inverted models can fit the data with high accuracy. To show how well all the 2,500 chosen models fit the data, we also computed their seismograms and calculated the standard deviations for each time sample. Here we picked Trace No.200 as an example to display (Figure 2.17). The standard deviations are very small compared to the data, the average standard deviation is 265 (around 5% of the data peak/trough), and the error bar also covers the data. These indicate a successful data fitting for the model ensemble.
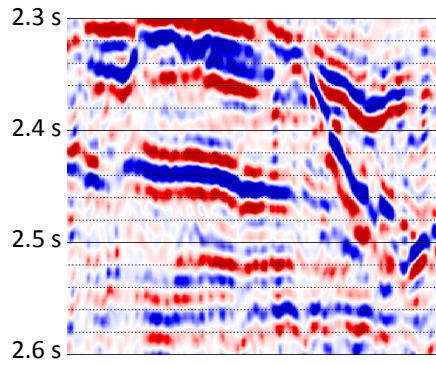
Figure 2.15: Modeled seismic data from rjMCMC inverted average models.
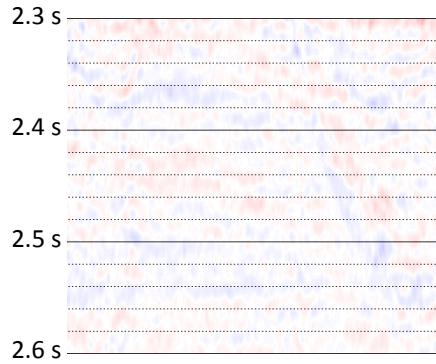
Figure 2.16: The difference between the seismic field data and the modeled seismic data from rjMCMC inverted average models.
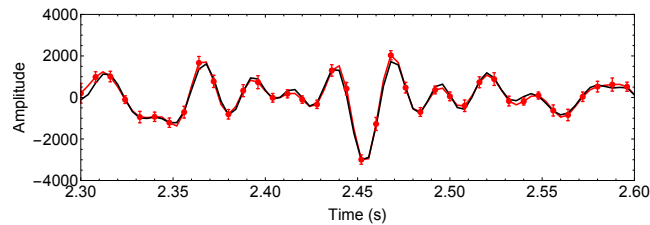
Figure 2.17: Comparison of the modeled data from 2,500 inverted models and the inverted average model with the field data. Trace No.200 is chosen as an example for display. Black: field data. Red: seismogram generated from the inverted average model. Red error bars denote the standard deviations for all time samples of the 2,500 seismograms from the 2,500 inverted models (displayed by every two time samples), and the average standard deviation=265.

To show the distribution of the model ensemble, we plotted the histogram and showed it for the depth at 2500 ms as an example (Figure 2.18). Each histogram

40

for a certain depth and a certain trace provides an average value and a standard deviation. All average values and standard deviations for all depths and all traces constitute the inverted model and its uncertainty shown afterwards.
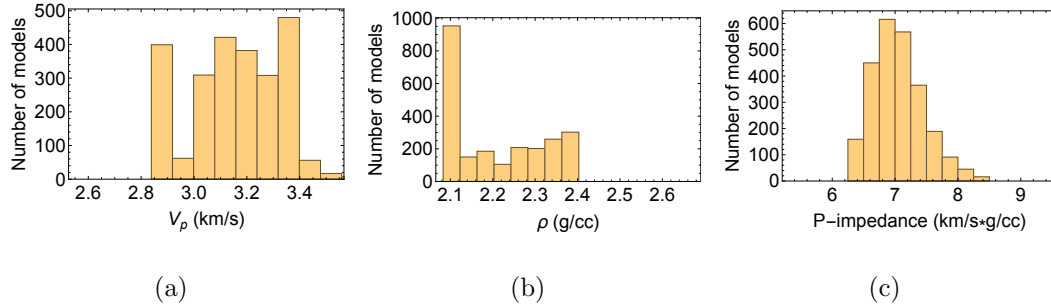
Figure 2.18: Histogram of sampled models (Trace No.200, depth=2500 ms). (a) V_p (km/s). (b) ρ (g/cc). (c) Z_p (km/s*g/cc).

We compared our inverted results with those produced by a commercial software, Hampson-Russell Strata (Version CE8) which uses model-based GLI deterministic inversion. The rjMCMC inversion results are shown by Figure 2.19 and 2.21 and 2.23, and Hampson-Russell's results are shown by Figure 2.20 and 2.22 and 2.24. Our rjMCMC's results and Hampson-Russell's results can validate each other since they are comparable. Both results comply with the published results (Rwechungura et al., 2010). These figures show that the gas reservoir, the Garn sand formation, is located around 2.45 s and is characterized by a relatively lower V_p, density and acoustic impedance (eg. blue in Figure 2.23). Right on the top of the Garn gas sand is the Melke shale formation which is the reservoir seal and characterized by a relatively higher V_p, density and acoustic impedance. Right below the Garn gas sand is the oil zone (brown) which includes the Ile and Tofte formations and has relatively larger

V_p and ρ than those of the overlying gas sand. Below the oil zone is mainly the Tilje sand formation (mixed green and yellow).
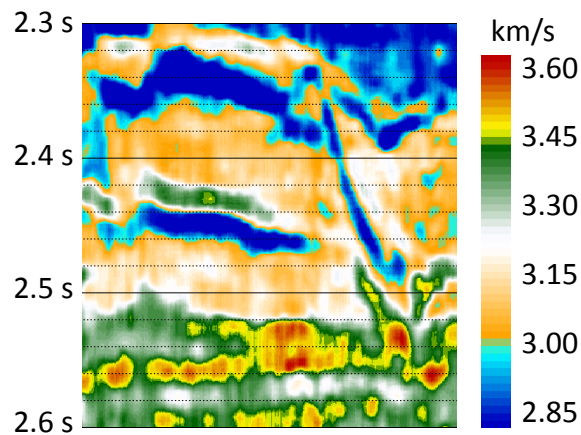
Figure 2.19: Inverted V_p by rjMCMC.
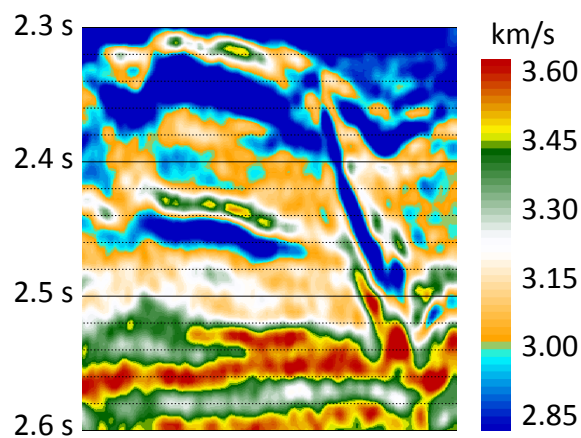
Figure 2.20: Inverted V_p by Hampson-Russell.
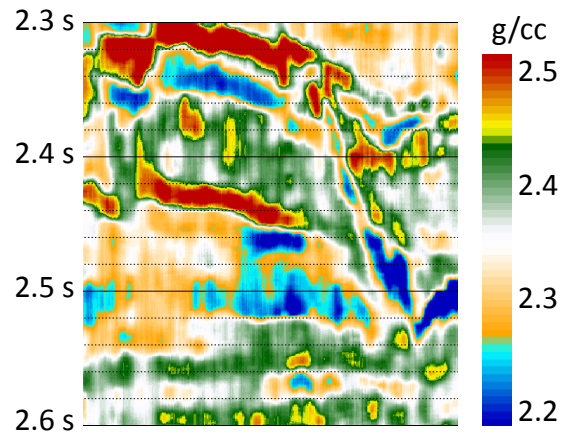
Figure 2.21: Inverted ρ by rjMCMC.
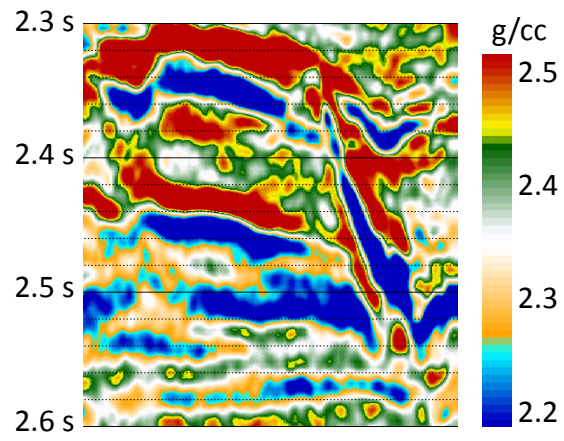
Figure 2.22: Inverted ρ by Hampson-Russell.
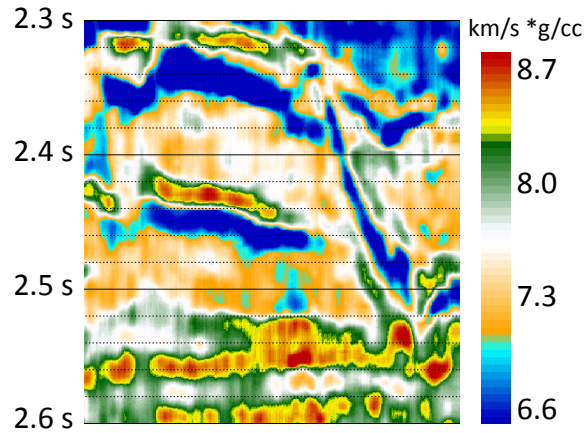
Figure 2.23: Inverted Z_p by rjMCMC.
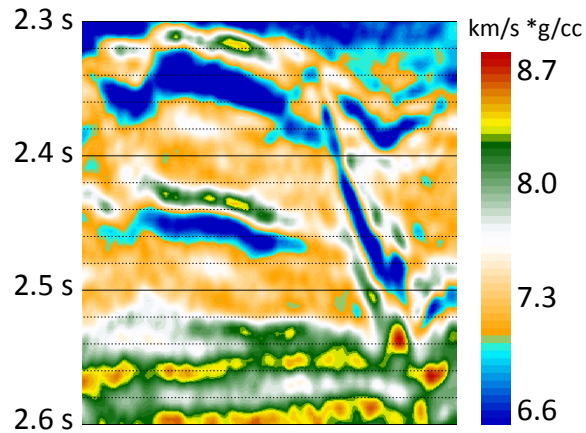
Figure 2.24: Inverted Z_p by Hampson-Russell.

Same as conducted in the previous section, by using rjMCMC we produced uncertainty estimation for V_p, ρ and Z_p models which usually can't be produced by many commercial softwares. Our uncertainty quantification (Figure 2.25, 2.26 and 2.27) demonstrates that the property uncertainty is relatively larger either wherever

the SNR (signal to noise ratio) is lower or wherever major discontinuities of the geophysical properties are encountered. Take acoustic impedance Z_p (Figure 2.27) as an example. A high inversion uncertainty in impedance indicates a large discontinuity of impedance and a low inversion uncertainty indicates a small discontinuity or just continuity. Therefore the uncertainty section is actually indicative of the location (structure) and the magnitude of subsurface discontinuities. As discussed before, although a discontinuity of property may cause a larger uncertainty in property, it also facilitates delineating the discontinuity surface or layer interface in the meanwhile. The high uncertainty in property (thin curves) represents major discontinuities due to changes of lithology or fluids. However, the uncertainty and the discontinuity of each property should be considered individually since different properties may have different discontinuities. For example, the red curve located around 2.44 s indicates a lithology transition from the overlying Melke shale formation to the underlying gas sand formation. At this location, there is a larger V_p discontinuity and V_p uncertainty but a smaller ρ discontinuity and uncertainty. This means V_p has a larger change at this interface whereas the density's change is relatively smaller. These results can help us to understand subsurface geophysical variations from different properties and also further corroborate that we can optimistically use the inversion uncertainty to pinpoint the layer interfaces and transitions of lithology and estimate the magnitude of subsurface discontinuity to facilitate the drilling management.
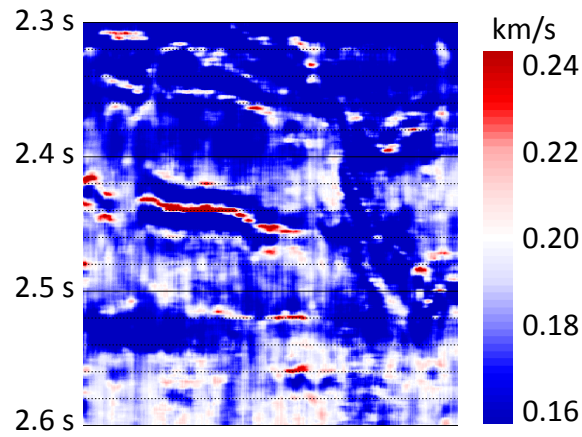
Figure 2.25: V_p inversion uncertainty by rjMCMC.
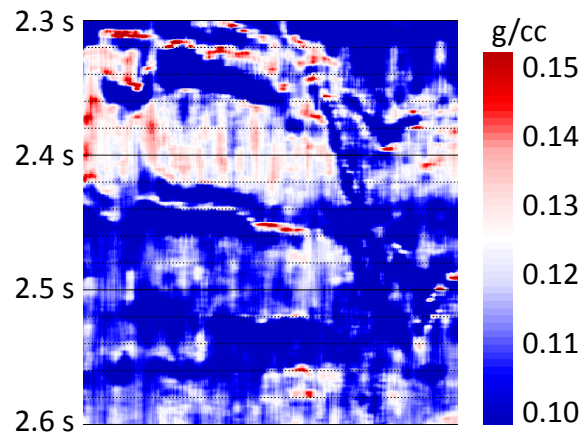
Figure 2.26: ρ inversion uncertainty by rjMCMC.
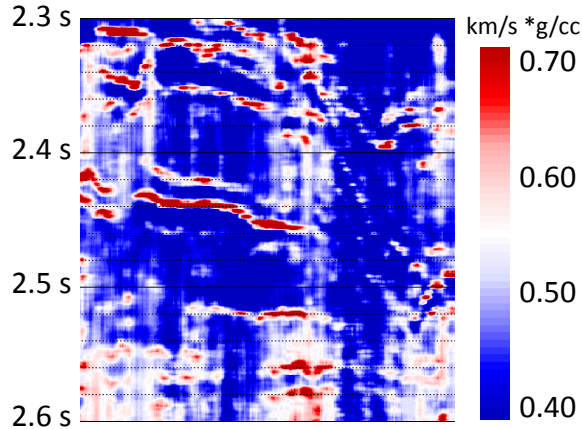
Figure 2.27: Z_p inversion uncertainty by rjMCMC.

2.5   Conclusion and Discussion

We demonstrated that rjMCMC can infer the model dimensionality, converge to proper parameterizations and obtain an ensemble of inverted models with different parameterizations. The rjMCMC enhances uncertainty quantification and prevents a biased sampling in one single space which may have a different dimensionality than that of the true model space. We also validated our results by comparing to those from the commercial software, Hampson-Russell Strata, which uses model-based GLI deterministic inversion. The rjMCMC will be extremely attractive if the model has strong heterogeneity in such a way that some regions have more complexity and need more parameters to depict but the other regions have less complexity and need fewer parameters to characterize.

We found out that there is a strong correlation between the inversion uncertainty and the discontinuity of property. Due to the uncertainty trade-off between property uncertainty and location uncertainty, the discontinuity of property induces a high uncertainty in model property at the discontinuity and a high "certainty" of the

47

location of the discontinuity. Therefore, we propose to utilize inversion uncertainty as a novel attribute to assist in delineation of subsurface reflectors and quantify the magnitude of discontinuities due to the correlation between the uncertainty and discontinuity.

Since most conventional methods may try to adopt a fine parameterization to achieve a better resolution in the inversion results, such an overparameterization will dramatically increase the computation time. The rjMCMC determines a proper parameterization and thus reduce the time for inversion. However, as any stochastic inversion algorithm, rjMCMC may also have high computational cost for a high dimensional problem. In terms of seismic inversion, there is one way to improve the computational efficiency and reduce the "curse of dimensionality". A large model and the corresponding data can be subdivided into several windows or blocks with overlapping tapers, and each window or block can be inverted independently and the inverted results will be combined afterwards to obtain the final model. Also rjMCMC is feasible to be implemented not just with 1-D layers but also with 2-D Voronoi cells (Bodin et al., 2012a) and 3-D Voronoi blocks. To enhance rjMCMC's performance in solving high dimensional problems, we propose another way of using rjMCMC for our future work which involves perturbing, adding and deleting a set of layers, cells or blocks instead of one single layer, cell or block at each iteration. This implementation may require an adaptive spatial grouping of these units in the inversion process. Another scope of using the transdimensional rjMCMC in a flexible way is to integrate with a forward modeling method that can deal with irregular discretization or parameterization, such as finite element method (FEM). Although rjMCMC is an inversion method and FEM is a forward modeling method, the similarity of them is that they work with irregular discretization and the difference is that rjMCMC allows a varying discretization and FEM generally doesn't. Since the

stochastic inversion is an iterative process of forward modeling and data fitting, we propose to integrate rjMCMC and FEM in the following way. Add, delete or perturb a set of cells or blocks in each iteration to generate a new discretization and conduct the forward modeling by FEM based on the new discretization for each iteration. In order to make this idea applicable in 3D earth model which has a large number of parameters, super computing is required.

3. SIMULTANEOUS INVERSION OF ACOUSTIC/SHEAR IMPEDANCE AND DENSITY AND UNCERTAINTY QUANTIFICATION USING TRANSDIMENSIONAL MARKOV CHAIN MONTE CARLO METHOD

3.1 Introduction

Prestack simultaneous inversion of P-wave velocity V_p(or acoustic impedance Z_p), S-wave velocity V_s (or shear impedance Z_s) and density ρ can be useful in lithology and fluid discrimination. These properties can be transformed to other geophysical properties such as Poisson's ratio, $\lambda\mu$ and $\mu\rho$ as well as reservoir properties such as saturation and porosity based on rock physics modeling. All these properties are useful since they can be served as direct hydrocarbon indicators (DHI) and discriminate lithology. To detect the fluid content within reservoirs, both P-wave and S-wave properties of a rock are also required because the P-waves are sensitive to changes in pore fluid and S-waves are mainly affected by the rock matrix and relatively unaffected by the pore fluid. Thus the simultaneous inversion provides more insights to characterize reservoirs than regular impedance (Z_p) inversion. The latter is usually performed using post-stack seismic data, whereas the simultaneous inversion requires prestack or angle-stack data since the shear wave information is contained in the variation of reflection coefficients with source-receiver offsets (AVO).

Prestack seismic inversion can be performed with deterministic methods and stochastic methods. Deterministic methods such as GLI (Generalized Linear Inversion) and Gauss-Newton algorithm have been used for prestack seismic inversion since 1980s (Tarantola, 1986; Mora, 1987; Demirbag et al., 1993; Pan et al., 1994; Sen and Roy, 2003; Hampson et al., 2005; Veire and Landrø, 2006; Russell, 2014). It has also been implemented by a variety of stochastic inversion algorithms, including

Simulated Annealing (SA) (Sen and Stoffa, 1991; Ma, 2001b, 2002; Varela et al., 2006; Srivastava and Sen, 2010), Markov chain Monte Carlo method (MCMC) (Eidsvik et al., 2004; van der Burg et al., 2009; Chen and Glinsky, 2014), Genetic Algorithm (GA) (Mallick, 1995, 1999; Padhi and Mallick, 2013, 2014; Li and Mallick, 2015), Particle Swarm Optimization (PSO) (Zhe and Gu, 2013), Neural Network (NN) (Mohamed et al., 2015). Some of these works are waveform-based inversion and some are amplitude-based. A comparison is reviewed by Mallick and Adhikari (2015).

The application of rjMCMC in prestack seismic inversion is still new. Biswas and Sen (2015) applied it to prestack seismic inversion by using a synthetic model. We firstly applied rjMCMC to a field dataset to simultaneously invert acoustic impedance Z_p, shear impedance Z_s and density ρ and implement uncertainty quantification of these properties. As in Section 2.2.8 we pointed out that the rjMCMC is able to enhance uncertainty quantification, in this section we also conducted uncertainty estimation for Z_p, Z_s and ρ.

In this section, we will illustrate the methodology (Section 3.2), apply rjMCMC using synthetic prestack seismic data (Section 3.3), and then apply it using an oilfield angle-stack seismic data to characterize the petroleum reservoir in Norne field, North Sea (Section 3.4). We will show another scientific contribution in addition to those in Section 2.3 and 2.4, that is, the prestack waveform inversion using rjMCMC is able to achieve an inversion resolution of $\lambda/16$, where λ is the seismic wavelength.

3.2   Methodology

In this section, we conducted seismic waveform inversion of a 2-D prestack to build a 2-D earth model and estimate the uncertainty. The inversion includes these general steps: 1) generate an initial model stochastically based on prior information, 2) update the model using rjMCMC iteratively through a data fitting process that quantifies the

misfit between the observed data with the modeled data and 3) collect an ensemble of all the models with low misfit, obtain the average model and estimate the uncertainty. To generate data given a model, our forward calculation adopts seismic convolution modeling in which seismic traces were generated by the convolution of reflectivities and source wavelet. Reflectivities were computed by the Zoeppritz equation with different incident angles. Each seismic trace is inverted independently based on 1-D layered model, and afterwards all the inverted 1-D models are combined to make the 2-D earth model. The model properties to be inverted are comprised of P-wave velocity V_p, S-wave velocity V_s and density ρ of each layer. The inverted acoustic impedance Z_p are computed by $V_p\rho$, and the inverted shear impedance Z_s by $V_s\rho$. Z_p, Z_s and ρ are the properties of interest in this section. The number of layers is also regarded as an unknown, and it will be inferred from the data through the transdimensional inversion.

3.2.1 Model Parameterization

The model in this study is represented by $\mathbf{m} = [\mathbf{V_p}, \mathbf{V_s}, \rho, \mathbf{L}, n]$, where n is the number of layers, $\mathbf{L} = [L_1, L_2, ..., L_{n-1}]$ indicates the location of $n-1$ interfaces, and $\mathbf{V_p} = [V_{p1}, V_{p2}, ..., V_{pn}]$, $\mathbf{V_s} = [V_{s1}, V_{s2}, ..., V_{sn}]$ and $\rho = [\rho_1, \rho_2, ..., \rho_n]$ denote P-wave velocities, S-wave velocities and densities of n layers. The n is unknown so it is initialized with an arbitrarily given number and it can vary stochastically from the current iteration to the next. Due to the fact that seismic inversion uses seismic data sampled by 4 ms or 2 ms and the minimum thickness of a detectable layer via seismic inversion is a few meters, we can set an upper limit for n, say, 50 for a model which is 200 m in thickness.

The model space for $\mathbf{V_p}$, $\mathbf{V_s}$ and ρ is continuous, but the model space for $\mathbf{L}$ and n is discrete since the model has to be spatially discretized in depth or time with a

certain given resolution (also see Section 2.2.1).

3.2.2 Bayesian Inference, Posterior Distribution, Prior Distribution and Likelihood

Function

The Bayesian inference in the inverse problem can be formulated as follows:

$$p(\mathbf{m}|\mathbf{d}_{\text{obs}}) = \frac{p(\mathbf{d}_{\text{obs}}|\mathbf{m})p(\mathbf{m})}{p(\mathbf{d}_{\text{obs}})}. \tag{3.1}$$

$p(\mathbf{d}_{\text{obs}}|\mathbf{m})$ denotes the likelihood function which is the probability of observing the measured data given a model $\mathbf{m}$. $p(\mathbf{m})$ is the prior PDF of $\mathbf{m}$ which is the prior knowledge of $\mathbf{m}$ before the data $\mathbf{d}_{\text{obs}}$ is taken into consideration. $p(\mathbf{d})$ is the probability of the observed data, and this term is usually ignored in the inversion process for reason that it is a constant quantity which does not rely on any model. $p(\mathbf{m}|\mathbf{d}_{\text{obs}})$ is the PPD which indicates how the prior knowledge of $\mathbf{m}$ is updated and constrained based on the data information through data fitting. Generally speaking, the PPD of $\mathbf{m}$ is narrower and more constrained than the prior distribution.

The prior knowledge of the model can be composed of a variety of different information from different sources. The model priors should be designed with reasonable ranges and distributions based on the data such as well logs and the knowledge of geophysics, geology and rock physics in the real earth. For example, it is well known that the density of a rock in the petroleum reservoir is no less than 1 g/cc and no more than 4 g/cc. When there is well logs available, we can put more constraint on the model space or the ranges of V_p, V_s and ρ. Since we are using a transdimensional approach, the number of layers can vary from an allowed minimum to a maximum, say, from n^{min}=2 to n^{max}=50. The prior distribution of model parameters can be set as uniform, Gaussian normal or any other type within these ranges. In this study, we chose uniform prior distributions for all model parameters in that we treated each

model parameter has equal prior probability within its own range.

The full prior PDF is separated into five prior terms:

$$p(\mathbf{m}) = p(\mathbf{V_p}|n, \mathbf{L})p(\mathbf{V_s}|n, \mathbf{L})p(\rho|n, \mathbf{L})p(\mathbf{L}|n)p(n), \qquad (3.2)$$

where $p(n)$ is the prior on the number of layers, $p(\mathbf{L}|n)$ is the prior on the location of $n - 1$ interfaces given the number of layers n, and $p(\mathbf{V_p}|n, \mathbf{L})$, $p(\mathbf{V_s}|n, \mathbf{L})$ and $p(\rho|n, \mathbf{L})$ are the priors on the V_p, V_s and ρ models given n and $\mathbf{L}$. These prior PDFs can be formulated as follows:

$$p(\mathbf{V_p}) = \prod_{i=1}^{n} p(V_{pi}|n), \qquad (3.3)$$

$$p(V_{pi}|n)) = 1/(V_{pi}^{max} - V_{pi}^{min}), \qquad (3.4)$$

$$p(\mathbf{V_s}) = \prod_{i=1}^{n} p(V_{si}|n), \qquad (3.5)$$

$$p(V_{si}|n)) = 1/(V_{si}^{max} - V_{si}^{min}), \qquad (3.6)$$

$$p(\rho) = \prod_{i=1}^{n} p(\rho_i|n), \qquad (3.7)$$

$$p(\rho_i|n)) = 1/(\rho_i^{max} - \rho_i^{min}), \qquad (3.8)$$

$$p(n) = 1/(n^{max} - n^{min}), \qquad (3.9)$$

$$p(\mathbf{L}|n) = 1/C_{n-1}^{N} = \frac{(n-1)!(N-n+1)!}{N!}, \qquad (3.10)$$

where each model parameter is constrained by given minimum and maximum values, N is the total number of possible depths given a certain spatial resolution, and $C_{n-1}^{N} = \frac{N!}{(n-1)!(N-n+1)!}$ denotes the number of possible combinations for $n - 1$ layer interfaces which will occupy $n - 1$ depths out of N possible depths in total.

The full prior PDF derived from the above equations is written as:

$$p(\mathbf{m}) = \frac{(n-1)!(N-n+1)!}{(n^{max} - n^{min})N! \prod_{i=1}^{n}((V_{pi}^{max} - V_{pi}^{min})(V_{si}^{max} - V_{si}^{min})(\rho_i^{max} - \rho_i^{min}))}. \tag{3.11}$$

As pointed out in Section 2.2.5 for likelihood function, the L1-norm can favor a "sparse" structure and is less sensitive to data outliers, so it is also adopted in this section. The L1-norm likelihood function in our inverse problem is written as:

$$p(\mathbf{d}_{\mathrm{obs}}|\mathbf{m}) \propto \exp\left\{-\frac{\Phi^2(\mathbf{m})}{2N_d\sigma_d^2}\right\}, \tag{3.12}$$

$$\Phi(\mathbf{m}) = \|f(\mathbf{m}) - \mathbf{d}_{\mathrm{obs}}\|_1, \tag{3.13}$$

where N_d is the number of data samples and σ_d is a given standard deviation of the data error. σ_d can be regarded as an estimation of data noise. The effects of σ_d is referred to Section 2.2.5.

3.2.3   The Transdimensional Method, rjMCMC

Same as in Section 2.2.6, the acceptance probability as formulated as follows:

$$\alpha(\mathbf{m}'|\mathbf{m}) = min\left[1, \frac{p(\mathbf{m}')}{p(\mathbf{m})} \cdot \frac{p(\mathbf{d}_{\mathrm{obs}}|\mathbf{m}')}{p(\mathbf{d}_{\mathrm{obs}}|\mathbf{m})} \cdot \frac{q(\mathbf{m}|\mathbf{m}')}{q(\mathbf{m}'|\mathbf{m})} \cdot |\mathbf{J}|\right], \tag{3.14}$$

A new model is proposed by drawing from the given proposal distribution $q(\mathbf{m}'|\mathbf{m})$ so that it is contingent on the current model $\mathbf{m}$. Our study sets it either as a Gaussian normal distribution or a uniform distribution centered at the current model $\mathbf{m}$. The proposal distribution is a Gaussian normal distribution if perturbing V_{pi}, V_{si} or ρ_i and then proposing a new V_{pi}', V_{si}' or ρ_i'. If perturbing the location of a interface L_i and proposing a new L_i', the proposal distribution is a uniform distribution. These

distributions are written as:

$$q(V'_{pi}|V_{pi}) = \frac{1}{\sigma_{V_p}\sqrt{2\pi}}\exp\left\{-\frac{(V'_{pi} - V_{pi})^2}{2\sigma^2_{V_p}}\right\}, \tag{3.15}$$

$$q(V'_{si}|V_{si}) = \frac{1}{\sigma_{V_s}\sqrt{2\pi}}\exp\left\{-\frac{(V'_{si} - V_{si})^2}{2\sigma^2_{V_s}}\right\}, \tag{3.16}$$

$$q(\rho'_i|\rho_i) = \frac{1}{\sigma_\rho\sqrt{2\pi}}\exp\left\{-\frac{(\rho'_i - \rho_i)^2}{2\sigma^2_\rho}\right\}, \tag{3.17}$$

$$q(L'_i|L_i) = \frac{1}{\Delta h}, \tag{3.18}$$

where $\sigma^2_{V_p}$, $\sigma^2_{V_s}$ and σ^2_ρ are the given variances of the Gaussian function for the model perturbation. A larger variance means a greater perturbation, and vice versa. Δh is a given perturbation range for moving interface.

The rjMCMC implements the same three updating strategies during the random walk as mentioned in Section 2.2.6. The prior ratio, the likelihood ratio and the proposal ratio for different updating strategies are formulated as follows.

For the first updating strategy, there is no change of dimension, so the prior ratio $\frac{p(\mathbf{m}')}{p(\mathbf{m})} = 1$, the proposal ratio $\frac{q(\mathbf{m}|\mathbf{m}')}{q(\mathbf{m}'|\mathbf{m})} = 1$, and the likelihood ratio $\frac{p(\mathbf{d}_{\text{obs}}|\mathbf{m}')}{p(\mathbf{d}_{\text{obs}}|\mathbf{m})} = \exp\left\{-\frac{\Phi^2(\mathbf{m}')-\Phi^2(\mathbf{m})}{2N_d\sigma^2_d}\right\}$.

For the second updating strategy, a new model $\mathbf{m}'$ is proposed with one more layer interface, velocity and density. The prior ratio $\frac{p(\mathbf{m}')}{p(\mathbf{m})} = \frac{n}{N-n+1}$, the proposal ratio $\frac{q(\mathbf{m}|\mathbf{m}')}{q(\mathbf{m}'|\mathbf{m})} = \frac{N-n+1}{nq(V'_p|V_p)q(V'_s|V_s)q(\rho'|\rho)}$, and the likelihood ratio is the same as that in the first strategy.

For the third updating strategy, a new model $\mathbf{m}'$ is proposed with one fewer layer interface, velocity and density. The prior ratio $\frac{p(\mathbf{m}')}{p(\mathbf{m})} = \frac{N-n+2}{n-1}$, the proposal ratio $\frac{q(\mathbf{m}|\mathbf{m}')}{q(\mathbf{m}'|\mathbf{m})} = \frac{(n-1)q(V'_p|V_p)q(V'_s|V_s)q(\rho'|\rho)}{N-n+2}$, and the likelihood ratio is the same as that in the first strategy.

Substituting these ratios into equation (3.14), we will get acceptance probability for 3 updating strategies respectively as follows:

$$\alpha(\mathbf{m'}|\mathbf{m}) = min\left[1, \exp\left\{-\frac{\Phi^2(\mathbf{m}) - \Phi^2(\mathbf{m'})}{2N_d\sigma_d^2}\right\}\right], \tag{3.19}$$

$$\begin{aligned}
\alpha(\mathbf{m'}|\mathbf{m}) = min[1, &\frac{\sigma_{V_p}\sqrt{2\pi}}{V_{pi}^{max} - V_{pi}^{min}} \frac{\sigma_{V_s}\sqrt{2\pi}}{V_{si}^{max} - V_{si}^{min}} \frac{\sigma_\rho\sqrt{2\pi}}{\rho_i^{max} - \rho_i^{min}} \cdot \\
&\exp\{\frac{(V_{pi}' - V_{pi})^2}{2\sigma_{V_p}^2} + \frac{(V_{si}' - V_{si})^2}{2\sigma_{V_s}^2} + \frac{(\rho_i' - \rho_i)^2}{2\sigma_\rho^2} \\
&- \frac{\Phi^2(\mathbf{m'}) - \Phi^2(\mathbf{m})}{2N_d\sigma_d^2}\}],
\end{aligned} \tag{3.20}$$

$$\begin{aligned}
\alpha(\mathbf{m'}|\mathbf{m}) = min[1, &\frac{V_{pi}^{max} - V_{pi}^{min}}{\sigma_{V_p}\sqrt{2\pi}} \frac{V_{si}^{max} - V_{si}^{min}}{\sigma_{V_s}\sqrt{2\pi}} \frac{\rho_i^{max} - \rho_i^{min}}{\sigma_\rho\sqrt{2\pi}} \cdot \\
&\exp\{-\frac{(V_{pi}' - V_{pi})^2}{2\sigma_{V_p}^2} - \frac{(V_{si}' - V_{si})^2}{2\sigma_{V_s}^2} - \frac{(\rho_i' - \rho_i)^2}{2\sigma_\rho^2} \\
&- \frac{\Phi^2(\mathbf{m'}) - \Phi^2(\mathbf{m})}{2N_d\sigma_d^2}\}].
\end{aligned} \tag{3.21}$$

3.2.4   Calculation of the Average Model and the Uncertainty

Similar as mentioned in Section 2.2.9, firstly, we select an ensemble of inverted models with lowest data misfit. Each model of the ensemble has different parameterizations (different the number of layers and different layer interfaces). For the calculation of the average model and the uncertainty, we have to downscale all the inverted models in a uniform finer discretization scheme in time or depth domain. The method to calculate the average model and the uncertainty is referred to Section 2.2.9, and the detailed formulations are referred to Section 4.2.4.

3.3   Synthetic Case Study

We designed a synthetic model for V_p, V_s, and ρ in time domain, and calculated acoustic impedance ($Z_p = V_p\rho$) and shear impedance ($Z_s = V_s\rho$). V_p, V_s, and ρ

are independent variables and our final goal is to characterize Z_p, Z_s and ρ. True model of Z_p, Z_s and ρ are shown by Figure 3.1. This model including a wedge can test the inversion resolution of rjMCMC and how rjMCMC performs if the layer is thin. Using the true model, we calculated the reflectivities based on the Zoeppritz equation in time domain. A prestack synthetic seismic data sampled by 2 ms was generated by the convolution of the reflectivities and a zero-phase Ricker wavelet with central frequency of 25 Hz. To mimic angle gathers that consists of near, mid and far offsets, each CMP (common midpoint) gather has 3 traces with incident angles of 5, 15 and 25 degrees. Same as conducted in Section 2.3, the simulated seismic data was also added with zero-mean Gaussian random noise with a standard deviation of 10% of the maximum data value. The noise was added on the amplitude of each sample, and therefore the waveform was slighted distorted and also contained spikes. This synthetic seismic data with noise was used as the observed seismic data for the inversion. The model is composed of 80 CMPs with an interval of 12.5 m. We calculated the synthetic seismic data for each CMP, and here we chose one CMP in the middle of the model and display the synthetic seismic data (Figure 3.2).
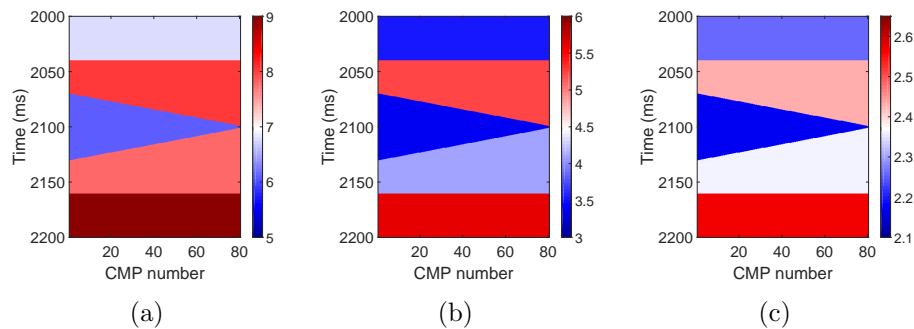
Figure 3.1: Geophysical properties for the wedge model used to test the rjMCMC inversion algorithm. (a) Acoustic impedance Z_p (km/s*g/cc). (b) Shear impedance Z_s (km/s*g/cc). (c) Density ρ (g/cc).
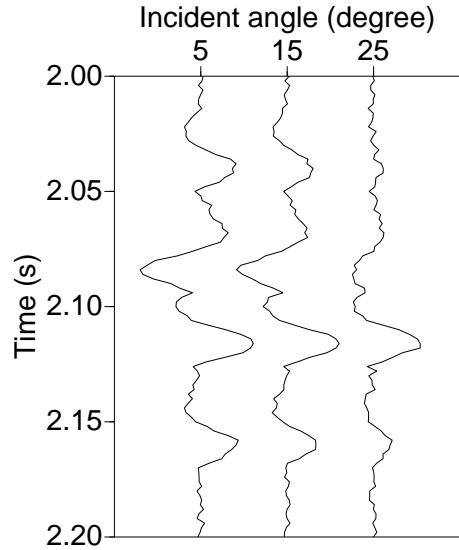
Figure 3.2: Synthetic prestack seismic data generated from the true model and added with 10%random noise. No.40 CMP is chosen for display.

We set the properties of the overburden rock above 2 s for the true model and the model to be inverted to be the same with those of the first layer of the true model. The lower/upper inversion limits of the uniform prior distributions for both V_p, V_s and ρ are set as constants because there was no well log in this case study. These limits for V_p, V_s and ρ are (2.4, 4.0) km/s, (1.2, 2.4) km/s and (2.1, 2.7) g/cc respectively. Since the number of layers is assumed to be unknown and the initial model is arbitrarily chosen which has 10 layers with equal interval in time domain as well as with the same initial V_p=3.2 km/s, V_s=1.8 km/s and ρ=2.4 g/cc.

The standard deviation of data misfit σ_d in equation (3.12) was set to be 0.03 which is around 20% of the peak of the seismic data. Regarding the standard deviations of the proposal distributions for model perturbation, we set σ_{V_p}, σ_{V_s} and σ_ρ in equation (3.15), (3.16) and (3.17) to be 0.4 km/s, 0.3 km/s and 0.15 g/cc respectively (see

Section 2.2.11). In this stochastic inversion, V_p, V_s and ρ are independent variables so we don't assume a linear or any other type of relationships between them. However, to imitate the properties of rocks in the real case, we set lower/upper limits for the V_s/V_p ratio as (0.5, 0.66) and ρ/V_p ratio as (0.6, 0.9). The allowed minimum number of layers is 2 and the allowed maximum is 30. If a new model goes beyond any one of the abovementioned bounds, it will be discarded and rjMCMC will repeat the current step and propose another new model until our criterion is satisfied.

The synthetic seismic data (eg. Figure 3.2) plus the above model priors were used to conduct the inversion to recover the true model. We ran the inversion CMP by CMP for 5,000 iterations and each CMP is inverted independently as in the seismic waveform inversion for 1-D earth model (see Section 3.2). To assess the inversion process, we chose one CMP as a demonstration example. We calculated the RMS (root mean square) error between the synthetic data and the modeled data for all iterations, which is shown by Figure 3.3. The rjMCMC finds the low-misfit models in the first few hundred of iterations. Since the purpose is to sample the entire model space, achieve good sampling around the true model and find a set of good models with low misfits, we kept rjMCMC running for 5,000 iterations. So there would be enough good models in the solution pool through the sampling stage for us to get a quality average model and conduct uncertainty quantification.

To illustrate that the rjMCMC is able to infer the model dimensionality, the number of layers with iterations was plotted (Figure 3.4). Same as we did in Section 2.3, we sorted 5,000 models from 5,000 iterations by RMS error and chose 2,500 models with relatively less RMS errors. A histogram of the number of layers for these models is shown by Figure 3.5. These figures indicate that the rjMCMC finds the number of layers n around 5. A minor overparameterization is allowed by rjMCMC but an major overparameterization ($n > 15$) and an underparameterization ($n < 5$)
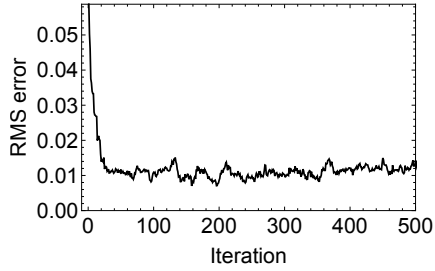
Figure 3.3: RMS error between the data and the modeled data. Displayed for only the first 500 iterations (No.40 CMP).

are ruled out by rjMCMC.
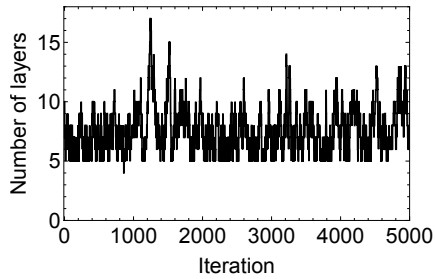
Figure 3.4: The variation of the number of model layers with iterations (No.40 CMP).

We downscaled these chosen models with a uniform finer discretization scheme (0.4 ms in time domain) to make a solution set. As mentioned in Section 3.2, all the models will be digitized into matrices with the same size after this downscaling with the same discretization. Then we calculated the average model of this set sample by sample in time domain and used it as the final inverted model, and computed the standard deviations of this set sample by sample in time domain to estimate the uncertainty.
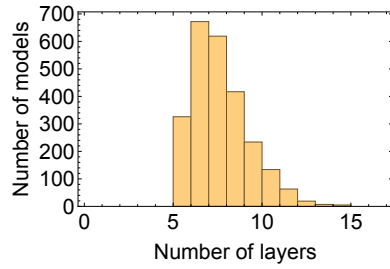
Figure 3.5: Histogram of the number of layers for 2,500 sampled models (No.40 CMP).

Inverted Z_p, Z_s and *rho* are shown as an example (Figure 3.6). Obviously, the uncertainty (shown by the error bar) of Z_p or Z_s is less than that of density. The reason is that the density is poorly resolved by P-waves seismic data (Debski and Tarantola, 1995; Igel et al., 1996). However, the inverted average density statistically approximates the true density model.
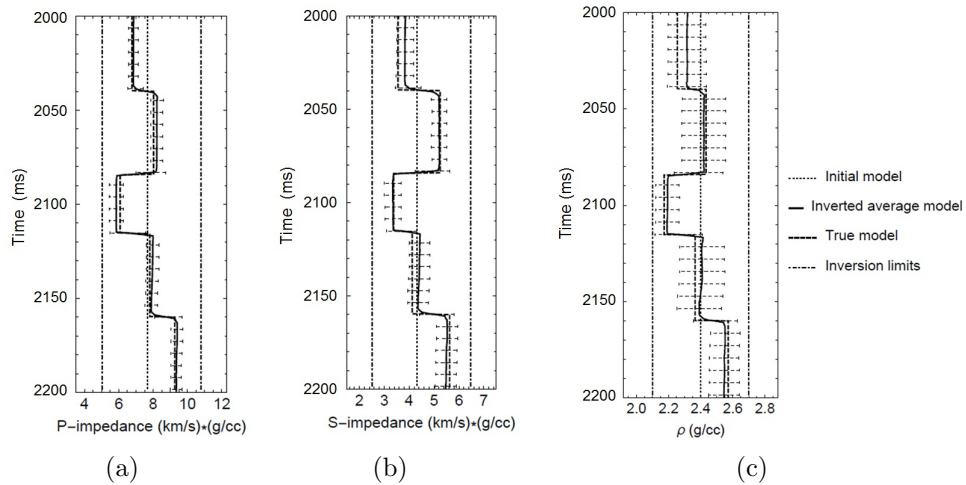
Figure 3.6: Inverted models vs. true models (Trace No.40). (a) Z_p (km/s*g/cc). (b) Z_s (km/s*g/cc). (c) ρ (g/cc). The inversion uncertainty (standard deviation) is represented by the error bar.

As we found in Section 2.3 for post-stack seismic inversion, the prestack inversion also substantiates that although most of the 2,500 sampled models have more than 5 layers, the average model presents 5 layers that is accordant with the true model, which means that the rjMCMC is capable of inferring the model dimensionality. To show the posterior distribution of the sampled models, we plotted the histogram and show it for one depth (2120 ms) as an example. Figure 3.7 indicates an asymmetrical distribution, but the average value is close to the true value (Figure 3.6).
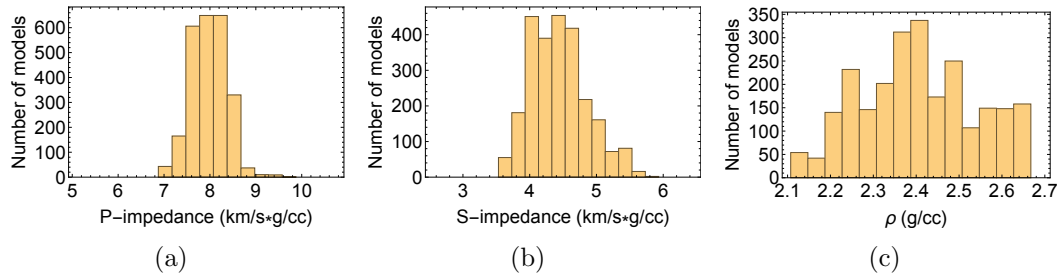
Figure 3.7: Histogram of sampled models (Trace No.40, depth=2120 ms). (a) Z_p (km/s*g/cc). (b) Z_s (km/s*g/cc). (c) ρ (g/cc).

This procedure was conducted for all CMPs. Because each CMP gather had spatial random noise that would propagate into the inverted results as mentioned in Section 2.2.9, a lateral moving-average smoothing was applied to reduce the noise effect. Finally, we acquired the inverted average models of Z_p, Z_s and ρ (Figure 3.8) and appraised their uncertainty (Figure 3.9).

These inversion results indicate that the true model and the layer interfaces for V_p, ρ and Z_p are almost recovered by the rjMCMC. Looking at the wedge tip, we found that the inversion can exactly recover the interfaces if layer thickness is no less than 5 ms (two-way travel time) in time domain which is approximately 7.5 m
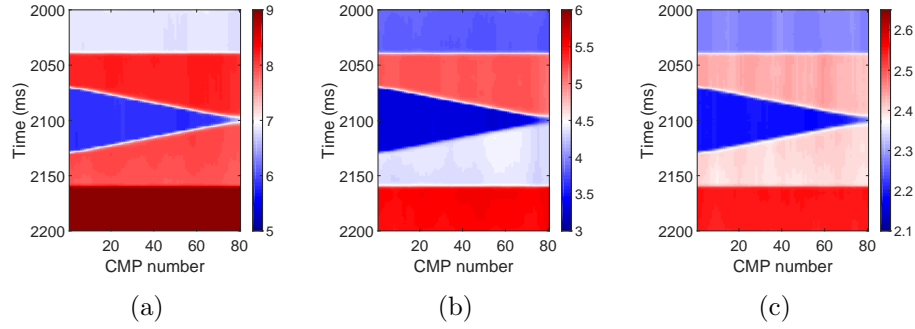
Figure 3.8: Inverted average models by rjMCMC. (a) Z_p (km/s*g/cc). (b) Z_s (km/s*g/cc). (c) ρ (g/cc).
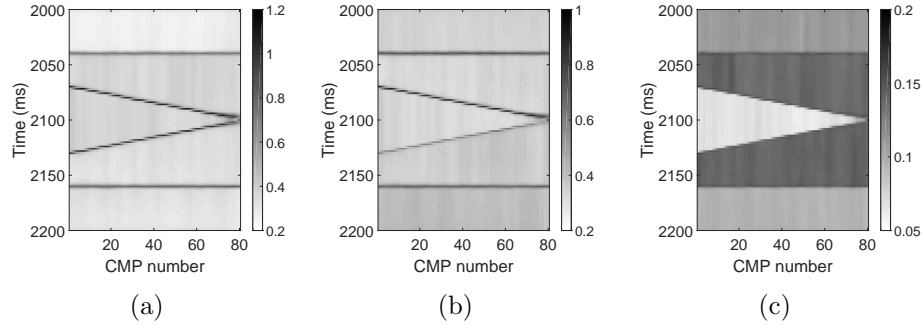
Figure 3.9: rjMCMC Inversion uncertainty. (a) Z_p uncertainty (km/s*g/cc). (b) Z_s uncertainty (km/s*g/cc). (c) ρ uncertainty (g/cc).

in depth domain. Our seismic wave has a central frequency of 25 Hz which means a wavelength λ of 120 m if V_p is 3 km/s. These results demonstrate an inversion resolution of $\lambda/16$. To validate inverted results, we computed the modeled seismic data from the inverted average model and here we chose one CMP to display (Figure 3.10). To show how well all the 2,500 sampled models fit the synthetic data, we also computed their seismograms and calculated the standard deviations for each time sample. Here we picked the mid-offset seismogram of No.40 CMP as an example to display (Figure 3.11). The standard deviations are very small compared to the data,

the average standard deviation is 0.0061 (around 5% of the data peak/trough), and the error bar also covers the data. These indicate a successful data fitting for the model ensemble.
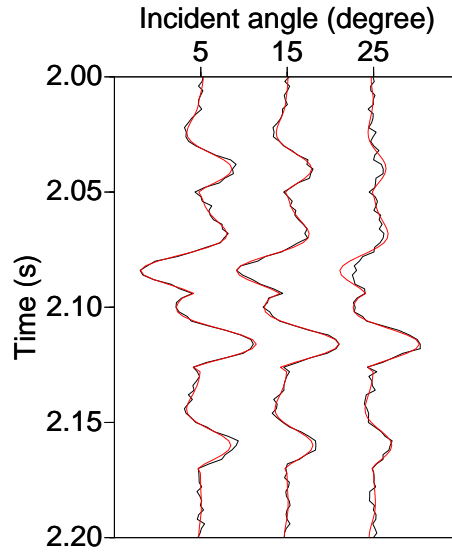
Figure 3.10: Synthetic seismic data generated from the true model and added with noise (black) vs. modeled data generated from the inverted average model (red). No.40 CMP is chosen for display.

Similar as the post-stack inversion results in Section 2.3, the prestack inversion study also reveals that a larger discontinuity will induce a higher property uncertainty at the discontinuity and nevertheless a higher "certainty" of the location of that discontinuity. And for continuous region with zero discontinuity, the property uncertainty is much lower. Therefore, we further corroborate that there is a trade-off between the property uncertainty and the location uncertainty in the seismic inversion either using post-stack or prestack data. Figure 3.9 shows that the uncertainty trade-
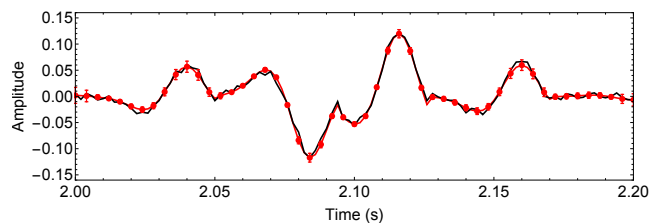
Figure 3.11: Comparison of the modeled data from 2,500 inverted models and the inverted average model with the synthetic data from the true model. The mid-offset (angle=15°) trace of No.40 CMP is chosen as an example for display. Black: synthetic seismogram generated from the true model and added with noise. Red: seismogram generated from the inverted average model. Red error bars denote the standard deviations for all time samples of the 2,500 seismograms from the 2,500 inverted models (displayed by every two time samples), and the average standard deviation=0.0061.

off effect for Z_p and Z_s is stronger that that for ρ due to the abovementioned reason that ρ is relatively poorly resolved by P-waves.

In Section 2.3, we found that post-stack seismic waveform inversion obeys a trade-off between property uncertainty and location uncertainty in such a way that the property uncertainty and the location uncertainty exert a limitation. However, this limitation can be changed by using prestack seismic waveform inversion, which means that the trade-off relationship can be altered if there are more data used. Comparing the inverted acoustic impedance Z_p in Section 2.3 and 3.3, prestack inversion produce lower Z_p uncertainty (Figure 3.9(a)) than that by post-stack inversion (Figure 2.9(c)). Meanwhile, the model boundaries are better delineated and the inversion resolution is upgraded from $\lambda/10$ to $\lambda/16$ if using prestack inversion (compare Figure 3.8(a) with Figure 2.8(c)).

Therefore, prestack seismic inversion makes further enhancements and assists us to use the uncertainty in an optimistic perspective and to facilitate delineating the subsurface reflectors and quantify the magnitude of discontinuities.

3.4 Case Study Using an Oilfield Data, Norne Field, North Sea

In this inversion application to field data, we characterized Z_p, Z_s and ρ of a petroleum reservoir in the E-segment of the Norne oilfield and estimate their uncertainty by using one nearby well and three angle stacks which are near-offset stacked $(5 - 15°)$, mid-offset stacked $(15 - 30°)$ and far-offset stacked $(30 - 40°)$ seismic data which has been corrected for geometrical spreading and time migrated by the data provider. The average angles for the three angle stacks are $10°$, $22.5°$ and $35°$ respectively. Since these seismic stacks have been time migrated, their traces for the same CMP are corresponding to the same reflection point. We created an angle gather from these three stacks, and each CMP consists of three traces from the three stacks respectively. The geological information about the Norne field is referred to Section 2.4.

The wavelet was extracted from the seismic data and used it for the forward calculation. The V_p, V_s and density logs were smoothed to generate a low-frequency trend and then were perturbed for ± 0.5 km/s, ± 0.4 km/s and ± 0.3 g/cc respectively to make the inversion lower/upper limits (Figure 3.12). The initial model was generated by upscaling the smoothed logs to blocky logs with equal interval in time domain (Figure 3.12). The standard deviation of data misfit σ_d were set to be 12.5% of the peak amplitude of the seismic data, and σ_{V_p}, σ_{V_s} and σ_ρ in equation (3.15, 3.16 and 3.17) were set to be 0.25 km/s, 0.2 km/s and 0.15 g/cc respectively (see Section 2.2.11).
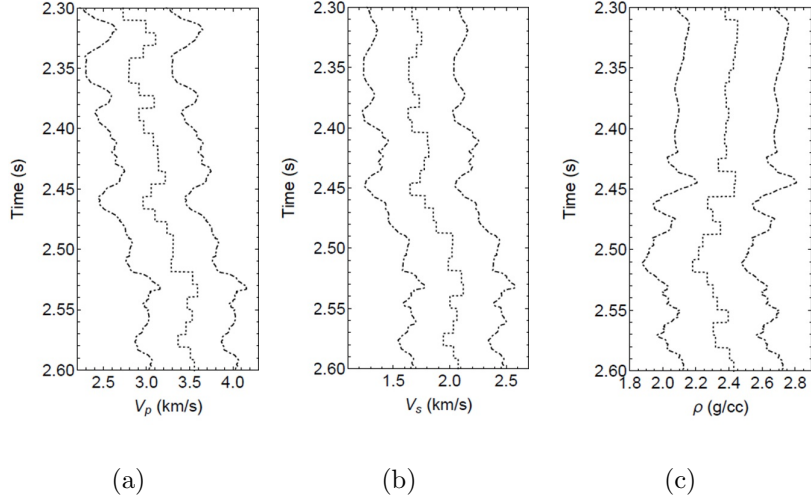
Figure 3.12: Initial model (dotted) and inversion lower/upper limits (dotdashed).

The studied region has 400 CMPs. The rjMCMC inversion was run CMP by CMP for 5,000 iterations and 2,500 models with relatively lower data misfit were selected. The modeled seismic data was computed by using the inverted average model for validation. Here we chose No.200 CMP as an example to display (Figure 3.13). The standard deviations for all time samples of the 2,500 seismograms from the 2,500 sampled models are illustrated by the error bars in Figure 3.14 which shows the mid-offset trace of No.200 CMP as an example. Their standard deviations are quite small compared to the data, and the average standard deviation is calculated to be 194 which is around 5% of the data peak or trough. The data falls into the range of the error bar. These figures indicate that the rjMCMC inverted models can fit the data with high accuracy.

68
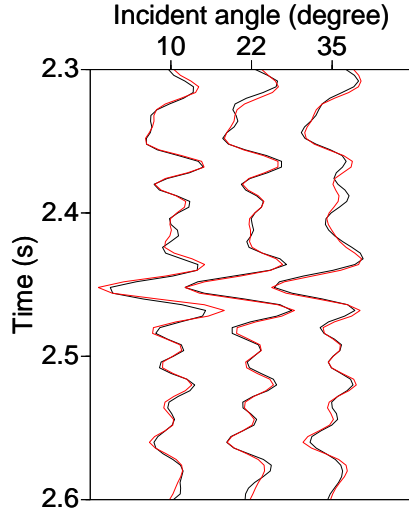
Figure 3.13: Modeled prestack seismic data from rjMCMC inverted average models (red) vs. seismic field data (black). No.200 CMP is chosen for display.
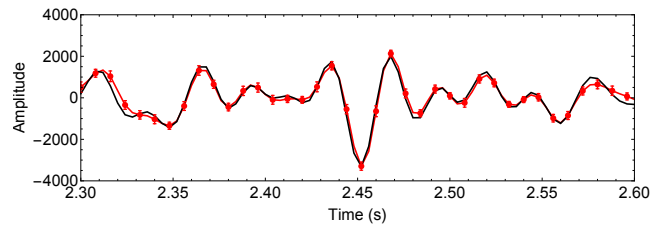
Figure 3.14: Comparison of the modeled data from 2,500 inverted models and the inverted average model with the field data. The mid-offset (angle=22.5°) trace of No.200 CMP is chosen as an example for display. Black: field data. Red: seismogram generated from the inverted average model. Red error bars represent the standard deviations for all time samples of the 2,500 seismograms from the 2,500 inverted models (displayed by every two time samples), and the average standard deviation=194.

To show the distribution of the model ensemble, we plotted the histogram and showed it for the depth at 2500 ms as an example (Figure 3.15). Each histogram for a certain depth and a certain trace provides an average value and a standard deviation. All average values and standard deviations for all depths and all traces constitute the inverted model and its uncertainty shown afterwards.
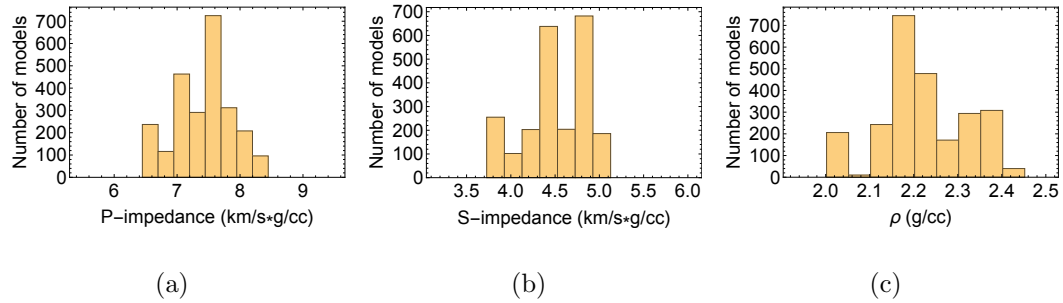
Figure 3.15: Histogram of sampled models (No.200 CMP, depth=2500 ms). (a) Z_p (km/s*g/cc). (b) Z_s (km/s*g/cc). (c) ρ (g/cc).

We compared our inverted results with those produced by the commercial software, Hampson-Russell Strata (Version CE8) which uses model-based GLI deterministic inversion. The rjMCMC inversion results are shown by Figure 3.16, 3.18 and 3.20, and Hampson-Russell's results are shown by Figure 3.17, 3.19 and 3.21. Results from our rjMCMC are comparable with those from Hampson-Russell, which means they can validate each other. Both results are in accordance with the published results (Rwechungura et al., 2010). The gas reservoir, the Garn sand formation, is located around 2.45 s and is characterized by a relatively lower Z_p, Z_s, and density (eg. blue in Figure 3.16). The Melke shale formation, right on the top of the Garn gas sand, is the reservoir seal and characterized by a relatively higher Z_p, Z_s, and density.

The oil reservoir (brown) right below the Garn gas sand incorporates the Ile and Tofte formations and has relatively larger impedance and density than those of the overlying Garn. Below the oil zone is mainly the Tilje sand formation (mixed green and yellow). These results are consistent with those in Section 2.4.
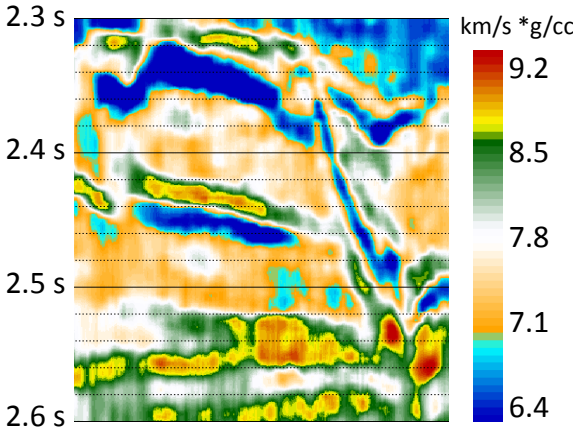
Figure 3.16: Inverted Z_p by rjMCMC.
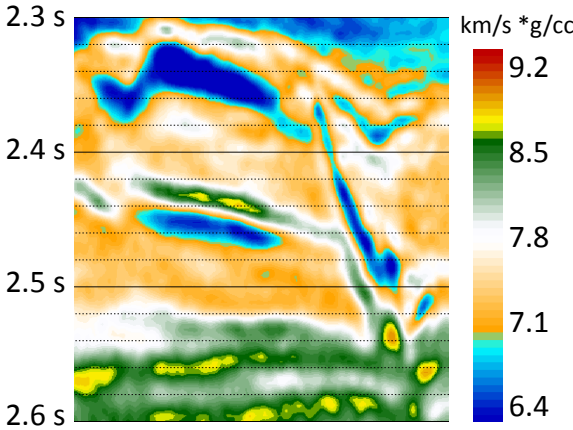
Figure 3.17: Inverted Z_p by Hampson-Russell.

71
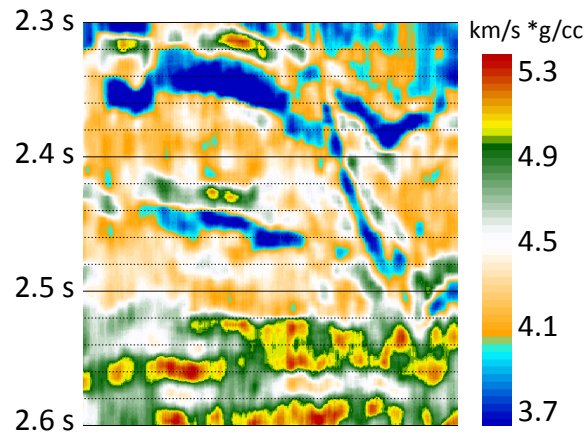
Figure 3.18: Inverted Z_s by rjMCMC.
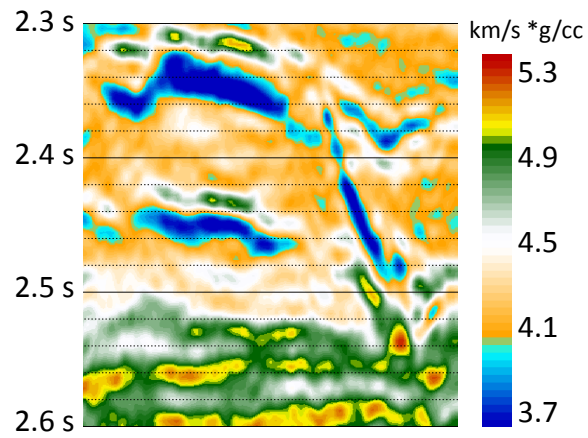
Figure 3.19: Inverted Z_s by Hampson-Russell.
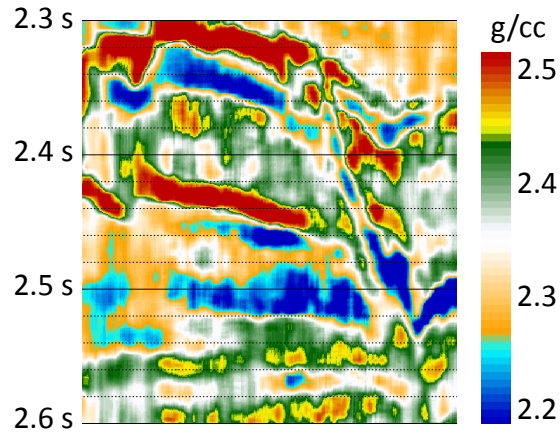
Figure 3.20: Inverted ρ by rjMCMC.
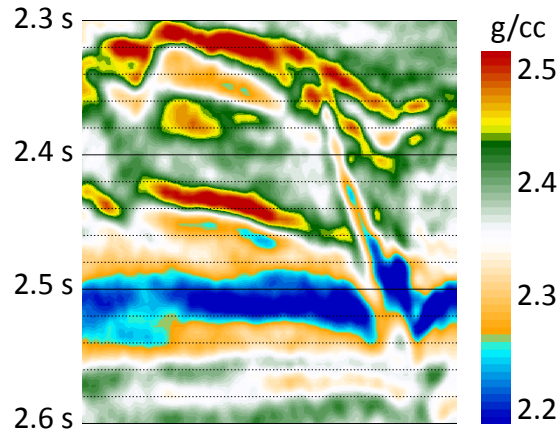
Figure 3.21: Inverted ρ by Hampson-Russell.

Same as conducted in the previous section, by using rjMCMC we produced uncertainty estimation for Z_p, Z_s and ρ models which usually can't be produced by many commercial softwares. Our uncertainty quantification (Figure 3.22, 3.23 and 3.24) demonstrates that the property uncertainty is relatively larger either wherever

73

the SNR (signal to noise ratio) is lower or wherever major discontinuities of the geophysical properties are encountered. Take acoustic impedance Z_p (Figure 2.27) as an example. A larger Z_p discontinuity induces a higher inversion uncertainty in Z_p, and a continuity or a smaller discontinuity yields a lower inversion uncertainty. Therefore the Z_p uncertainty is actually indicative of the location (structure) and the magnitude of subsurface Z_p discontinuities. This applies for Z_s and ρ as well. The high uncertainty in property (thin curves) caused by major discontinuities to assist in delineating the discontinuity surfaces or layer interfaces which usually indicate changes of lithology or fluids. For example in Figure 3.22, the red curve located around 2.44 s indicates a lithology transition from the overlying Melke shale formation to the underlying gas sand formation. At this location, we have a large Z_p discontinuity and Z_s uncertainty, whereas we have a small Z_s discontinuity and Z_s uncertainty (Figure 3.23). As previously pointed out, S-waves are relatively unaffected by the pore fluid. These results assist us to understand the reservoir from different properties and further substantiate that the inversion uncertainty can be used optimistically as an attribute to accurately locate the layer interfaces (transitions of lithology or fluids) and estimate the magnitude of discontinuity to enhance the drilling management.
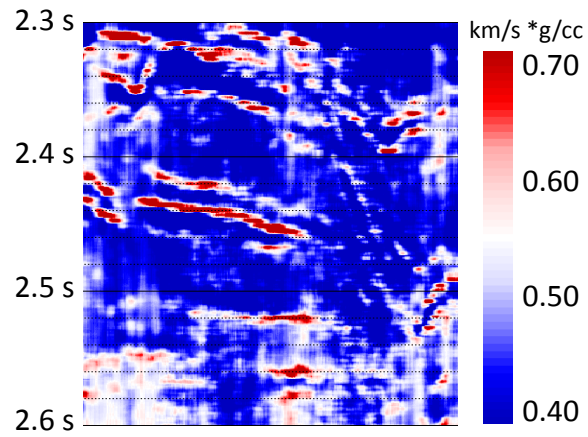
Figure 3.22: Z_p inversion uncertainty by rjMCMC.
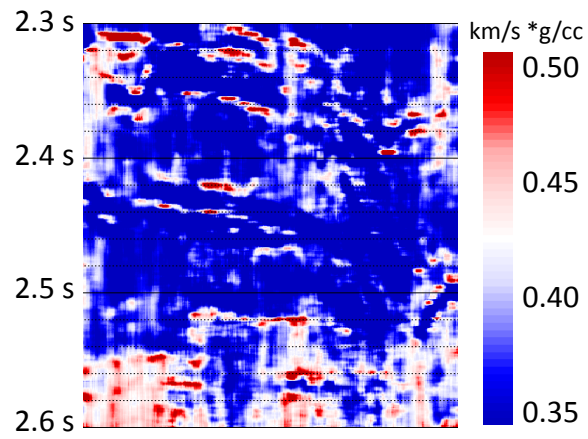
Figure 3.23: Z_s inversion uncertainty by rjMCMC.
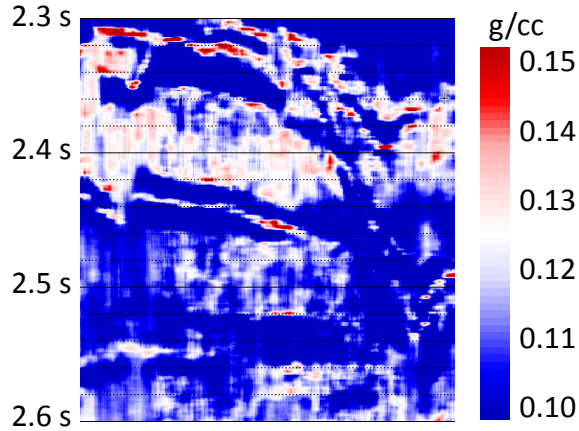
Figure 3.24: ρ inversion uncertainty by rjMCMC.

3.5   Conclusion

Via synthetic study and comparison with a commercial software, we have shown that prestack seismic waveform using rjMCMC is able to invert acoustic/shear impedance and density with high accuracy and achieve a high inversion resolution of $\lambda/16$ in terms of locating layer interfaces. From the prestack seismic inversion, we also found out that the inversion uncertainty is strongly correlated with the discontinuity of property in a way that the former is able to depict the location (structure) and the magnitude of the discontinuity. Due to the uncertainty trade-off between property uncertainty and location uncertainty in prestack inversion, a larger discontinuity of property will induce a higher uncertainty in property at the discontinuity but also a more ''certainty'' of the location of the discontinuity. These prestack inversion results are in accordance with those post-stack inversion results in Section 2.4.

4. UNCERTAINTY ANALYSIS USING TRANSDIMENSIONAL MARKOV CHAIN MONTE CARLO METHOD

4.1   Introduction

Uncertainty is inherent in every stage of the quantitative inference of subsurface properties via geophysical data. Uncertainty estimation facilitates decision-making in the oil and gas exploration and production business. Since uncertainty is defined as the range of the ensemble of possible outcomes, the uncertainty estimation should be able to quantify how each outcome is deviated from the ensemble. In geophysics, uncertainty is comprised of measurement uncertainty (or data uncertainty) and inference uncertainty (or model uncertainty). Data uncertainty includes systematic and random errors in measurements and is essentially a characterization of the dispersion of a measurement (Ma, 2011). Inference uncertainty is caused by a variety of errors or inaccuracy in methodology, interpretation, modeling, etc. Both uncertainties can be estimated through statistical analysis of the probability distribution of possible outcomes. In this section, our uncertainty analysis concentrates on the model uncertainty.

Since an ensemble of an infinite number of models may explain the data within a predefined tolerance in most inverse problems, our uncertainty estimation is a measurement of the ranges of this model ensemble, which requires enough inverted models to be collected from this ensemble for statistical analysis. Our uncertainty analysis using rjMCMC is cast in a Bayesian framework since the posterior probability distribution (PPD) is quantifiable, and the standard deviation of the PPD is a direct measurement of uncertainty.

The uncertainty estimation in geophysical inverse problems has been conducted by

various stochastic inversion algorithms, such as Markov chain Monte Carlo method (MCMC) (Liu and Stock, 1993; Malinverno and Briggs, 2004; Chen and Dickens, 2009; Gunning et al., 2010; Kwon and Snieder, 2011), Simulated Annealing (SA) (Dosso, 2002; Dosso and Nielsen, 2002; Bhattacharya et al., 2003; Roy et al., 2005; Varela et al., 2006), Particle Swarm Optimization (PSO) (Fernández-Martínez et al., 2012; Rumpf and Tronicke, 2015), and reversible jump Markov chain Monte Carlo method (rjMCMC) (Dettmer et al., 2013; Reading and Gallagher, 2013; Dadi, 2014; Galetti et al., 2015; Dadi et al., 2015). Particularly in seismic inversion, Dadi (2014) and Dadi et al. (2015) applied rjMCMC in seismic impedance inversion, uncertainty estimation and well log upscaling. Biswas and Sen (2015) used it for prestack seismic inversion by using a synthetic model. The applications of rjMCMC in data uncertainty estimation were conducted by Bodin et al. (2012a,b). Methods such as SA and PSO are classified as optimization methods which aim to converge to the global minimum but possibly get trapped in local minima due to data noise. And their convergence is controlled by the parameters set by the workers. Therefore, the inherent nature of optimization methods may lead to underestimation of uncertainty. Furthermore, the conventional inversion methods such as MCMC, SA, and PSO presume and fix the number of model parameters and may lead to a bias sampling in one model space, whereas the rjMCMC can transdimensionally search different spaces and look for models with different parameterization to prevent a bias sampling a single space.

We conducted the uncertainty analysis via a prestack seismic inversion problem using rjMCMC and revealed that the inversion uncertainty is correlated with discontinuities in material properties and it follows a trade-off between property uncertainty and location uncertainty. Compared to the previous sections, we will here carry out an uncertainty analysis to study the trade-off effects more completely. Sections 2.3, 2.4, 3.3 and 3.4 have shown that a larger discontinuity will induce a larger uncertainty

in model property but also a larger "certainty" in location. In addition to the above point, this section will adopt a different synthetic model to also substantiate that a smaller discontinuity will induce a less uncertainty in model property but also a larger uncertainty in location. We will illustrate the methodology (Section 4.2), apply rjMCMC for uncertainty analysis using a synthetic model (Section 4.3), and then discuss more on the uncertainty from the inversion study of the petroleum reservoir in Norne field, North Sea (Section 4.4).

4.2 Methodology

In this section, we implemented seismic waveform inversion of a 2-D prestack data to build a 2-D earth model and quantify the uncertainty in the same way shown by Section 3.2. The illustration of the inverse problem is also referred to Section 3.2.

4.2.1 Model Parameterization

The earth model incorporates geophysical properties such as P-wave velocity V_p, S-wave velocity V_s and density ρ of each layer and also the number of layers, which can be written as $\mathbf{m} = [\mathbf{P}, \mathbf{L}, n]$. Here n is the number of layers, $\mathbf{L} = [L_1, L_2, ..., L_{n-1}]$ represents the location of $n - 1$ interfaces, and $\mathbf{P} = [P_1, P_2, ..., P_n]$ denotes the geophysical properties such as V_p, V_s and ρ of n layers. Since n is unknown, it is initialized with an arbitrarily chosen number and allowed to vary stochastically from the current iteration to the next. Seismic data is usually sampled by 4 ms or 2 ms, so the minimum thickness of a detectable layer via seismic inversion is a few meters. So we can set an upper limit for n, say, 50 for a model which is 200 m in thickness.

The model space for $\mathbf{P}$ is continuous. However for $\mathbf{L}$ and n, the model space is discrete since the model has to be spatially discretized in depth or time with a given sampling (also see Section 2.2.1).

As in the previous sections, the Bayesian inference in the inverse problem can be formulated as follows:

$$p(\mathbf{m}|\mathbf{d}_{\text{obs}}) = \frac{p(\mathbf{d}_{\text{obs}}|\mathbf{m})p(\mathbf{m})}{p(\mathbf{d}_{\text{obs}})}. \tag{4.1}$$

The full prior PDF is separated into four terms:

$$p(\mathbf{m}) = p(\mathbf{P}|n, \mathbf{L})p(\rho|n, \mathbf{L})p(\mathbf{L}|n)p(n), \tag{4.2}$$

where $p(n)$ is the prior on the number of layers, $p(\mathbf{L}|n)$ on the location of $n-1$ interfaces given the number of layers n, and $p(\mathbf{P}|n, \mathbf{L})$ on the geophysical properties given n and $\mathbf{L}$. These prior PDFs can be formulated as follows:

$$p(\mathbf{P}) = \prod_{i=1}^{n} p(P_i|n), \tag{4.3}$$

$$p(P_i|n)) = 1/(P_i^{max} - P_i^{min}), \tag{4.4}$$

$$p(n) = 1/(n^{max} - n^{min}), \tag{4.5}$$

$$p(\mathbf{L}|n) = 1/C_{n-1}^{N} = \frac{(n-1)!(N-n+1)!}{N!}, \tag{4.6}$$

where each model parameter is constrained by given minimum and maximum values, N is total number of possible depths given a certain spatial resolution, and $C_{n-1}^{N} = \frac{N!}{(n-1)!(N-n+1)!}$ is the number of possible combinations for $n-1$ layer interfaces which will occupy $n-1$ depths out of N possible depths in total.

The full prior PDF is written as:

$$p(\mathbf{m}) = \frac{(n-1)!(N-n+1)!}{(n^{max} - n^{min})N! \prod_{i=1}^{n}(P_i^{max} - P_i^{min})}. \tag{4.7}$$

For our problems, the likelihood function based on the L1-norm is written as:

$$p(\mathbf{d}_{\text{obs}}|\mathbf{m}) \propto \exp\left\{-\frac{\Phi^2(\mathbf{m})}{2N_d\sigma_d^2}\right\}, \tag{4.8}$$

$$\Phi(\mathbf{m}) = \|f(\mathbf{m}) - \mathbf{d}_{\text{obs}}\|_1, \tag{4.9}$$

where N_d is the number of data samples and σ_d is a given standard deviation of the data misfit and can be regarded as an estimation of data noise. The effects of $sigma_d$ is referred to Section 2.2.5.

4.2.3 The Transdimensional Method, rjMCMC

A new model is proposed by drawing from the predefined proposal distribution $q(\mathbf{m}'|\mathbf{m})$ so that it is contingent on the current model $\mathbf{m}$. Our study sets it either as a Gaussian normal distribution or a uniform distribution centered at the current model $\mathbf{m}$. If perturbing P_i and then proposing a new P_i', the proposal distribution is a Gaussian normal distribution $N(P_i, \sigma_P)$. If perturbing the location of a interface L_i and proposing a new L_i', the proposal distribution is a uniform distribution. These distributions are written as:

$$q(P_i'|P_i) = \frac{1}{\sigma_P\sqrt{2\pi}}\exp\left\{-\frac{(P_i' - P_i)^2}{2\sigma_P^2}\right\}, \tag{4.10}$$

$$q(L_i'|L_i) = \frac{1}{\Delta h}, \tag{4.11}$$

where σ_P^2 is the given variance of the Gaussian function for the perturbation of the geophysical properties. A larger variance means a greater perturbation, and vice versa. Δh is a given perturbation range for moving interface.

The prior ratio, the likelihood ratio and the proposal ratio for different updating strategies are formulated as follows (refer to Section 3.2.3).

For the first updating strategy, there is no change of dimension, so the prior ratio $\frac{p(\mathbf{m}')}{p(\mathbf{m})} = 1$, the proposal ratio $\frac{q(\mathbf{m}|\mathbf{m}')}{q(\mathbf{m}'|\mathbf{m})} = 1$, and the likelihood ratio $\frac{p(\mathbf{d}_{\mathrm{obs}}|\mathbf{m}')}{p(\mathbf{d}_{\mathrm{obs}}|\mathbf{m})} = \exp\left\{-\frac{\Phi^2(\mathbf{m}')-\Phi^2(\mathbf{m})}{2N_d\sigma_d^2}\right\}$.

For the second updating strategy, a new model $\mathbf{m}'$ is proposed with one more layer interface, velocity and density. The prior ratio $\frac{p(\mathbf{m}')}{p(\mathbf{m})} = \frac{n}{N-n+1}$, the proposal ratio $\frac{q(\mathbf{m}|\mathbf{m}')}{q(\mathbf{m}'|\mathbf{m})} = \frac{N-n+1}{nq(P'|P)}$, and the likelihood ratio is the same as that in the first strategy.

For the third updating strategy, a new model $\mathbf{m}'$ is proposed with one fewer layer interface, velocity and density. The prior ratio $\frac{p(\mathbf{m}')}{p(\mathbf{m})} = \frac{N-n+2}{n-1}$, the proposal ratio $\frac{q(\mathbf{m}|\mathbf{m}')}{q(\mathbf{m}'|\mathbf{m})} = \frac{(n-1)q(P'|P)}{N-n+2}$, and the likelihood ratio is the same as that in the first strategy.

Substituting these ratios into equation (2.15), we will get acceptance probability for 3 updating strategies respectively as follows:

$$\alpha(\mathbf{m}'|\mathbf{m}) = min\left[1, \exp\left\{-\frac{\Phi^2(\mathbf{m})-\Phi^2(\mathbf{m}')}{2N_d\sigma_d^2}\right\}\right], \tag{4.12}$$

$$\alpha(\mathbf{m}'|\mathbf{m}) = min[1, \frac{\sigma_P\sqrt{2\pi}}{P_i^{max}-P_i^{min}}\exp\{\frac{(P_i'-P_i)^2}{2\sigma_P^2} - \frac{\Phi^2(\mathbf{m}')-\Phi^2(\mathbf{m})}{2N_d\sigma_d^2}\}], \tag{4.13}$$

$$\alpha(\mathbf{m}'|\mathbf{m}) = min[1, \frac{P_i^{max}-P_i^{min}}{\sigma_{V_p}\sqrt{2\pi}}\exp\{-\frac{(P_i'-P_i)^2}{2\sigma_P^2} - \frac{\Phi^2(\mathbf{m}')-\Phi^2(\mathbf{m})}{2N_d\sigma_d^2}\}]. \tag{4.14}$$

4.2.4 Calculation of the Uncertainty

An ensemble of inverted models with lowest data misfit are selected in the first stage. Each model of the ensemble has different parameterizations (different number of layers and different layer interfaces). To calculate the uncertainty, we have to downscale all the inverted models in a uniform finer discretization scheme in time or depth domain. Then all the models will be digitized into vectors or matrices with the same size, so we can easily calculate the standard deviations of this ensemble sample by sample for each time or depth for uncertainty quantification.

Take a 1-D layered model as the example for uncertainty quantification. Suppose we collect M inverted models with good data fitness. Each model is denoted by $\mathbf{m}^j = [\mathbf{P}^j, \mathbf{L}^j, n^j]$, where $j = 1, 2, ..., M$, n^j is the number of layers for the model $\mathbf{m}^j$, $\mathbf{L}^j = [L_1^j, L_2^j, ..., L_{n^j-1}^j]$ represents the locations (depths) of all layer interfaces and $\mathbf{P}^j = [P_1^j, P_2^j, ..., P_{n^j}^j]$ denotes the property of all layers. Since each model has different parameterizations with a different n^j and $\mathbf{L}^j$, they need to be downscaled with a uniform finer discretization as follows. $\mathbf{m}^j = [\mathbf{P}_d^j, \mathbf{L}_d, N_d]$, the subscript "d" means "downscaled", N_d is the total number of finer layers after downscaling, $\mathbf{L}_d = [L_{d(1)}, L_{d(2)}, ..., L_{d(N_d-1)}]$ and $\mathbf{P}_d^j = [P_{d(1)}^j, P_{d(2)}^j, ..., P_{d(N_d)}^j]$ represent the interface locations and the property of all layers for model $\mathbf{m}^j$. Now that N_d is the same for all M models, and since the inversion "window" is fixed, that is, every model has the same depth of the top and bottom, so $\mathbf{L}_d = [L_{d(1)}, L_{d(2)}, ..., L_{d(N_d-1)}]$ is the same for all M models as well. Obviously, before downscaling the size of $\mathbf{P}^j = [P_1^j, P_2^j, ..., P_{n^j}^j]$ is n^j which varies for different models, but after downscaling the size of $\mathbf{P}_d^j = [P_{d(1)}^j, P_{d(2)}^j, ..., P_{d(N_d)}^j]$ is N_d which is the same for all models.

For example, consider a subsurface 2-layer model and a 5-layer velocity model in time domain, $\mathbf{P}^1 = [3.2, 3.8]$ km/s and $\mathbf{P}^2 = [2.8, 3.1, 3.4, 3.7, 4.3]$ km/s. The

top and bottom for these two model is (2, 3) s, so interface location $\mathbf{L}^1 = [2.5]$ s, $\mathbf{L}^2 = [2.2, 2.4, 2.6, 2.8]$ s. If both of them are downscaled by, say, 0.1 km as a new depth interval, they will both have 10 layers and the same interfaces $\mathbf{L} = [2.1, 2.2, 2.3, \ldots, 2.8, 2.9]$ s. The new velocity model $\mathbf{P}_{\mathrm{d}}^1 = [3.2, 3.2, 3.2, 3.2, 3.2, 3.8, 3.8, 3.8, 3.8, 3.8]$ and $\mathbf{P}_{\mathrm{d}}^2 = [2.8, 2.8, 3.1, 3.1, 3.4, 3.4, 3.7, 3.7, 4.3, 4.3]$. The average model is $\overline{\mathbf{P}_{\mathrm{d}}} = [3.0, 3.0, 3.15, 3.15, 3.3, 3.6, 3.75, 3.75, 4.05, 4.05]$ km/s and the standard deviation is $\sigma = [0.28, 0.28, 0.07, 0.07, 0.14, 0.28, 0.07, 0.07, 0.35, 0.35]$ km/s which characterizes the velocity uncertainty. We can see that only till downscaling will we able to compute the average and the standard deviation for all M models. In this section, we choose a very fine sampling interval for downscaling, say, 0.4 ms.

The average model is represented by $\overline{\mathbf{m}} = [\overline{\mathbf{P}_{\mathrm{d}}}, \mathbf{L}_{\mathrm{d}}, N_{\mathrm{d}}]$. The formulations for the average model property are written as:

$$\overline{\mathbf{P}_{\mathrm{d}}} = [\overline{P_{\mathrm{d}(1)}}, \overline{P_{\mathrm{d}(2)}}, ..., \overline{P_{\mathrm{d}(N_{\mathrm{d}})}}], \tag{4.15}$$

$$\overline{P_{\mathrm{d}(k)}} = \frac{1}{M} \sum_{j=1}^{M} P_{\mathrm{d}(k)}^j, \tag{4.16}$$

where $k = 1, 2, ..., N_{\mathrm{d}}$. And the property uncertainty, or the standard deviation of M models, is calculated as follows:

$$\sigma = [\sigma_{(1)}, \sigma_{(2)}, ..., \sigma_{(N_{\mathrm{d}})}], \tag{4.17}$$

$$\sigma_{(k)} = \frac{1}{M} \sum_{j=1}^{M} (P_{\mathrm{d}(k)}^j - \overline{P_{\mathrm{d}(k)}})^2. \tag{4.18}$$

4.3   Synthetic Case Study

The synthetic studies in previous sections point out a high uncertainty is caused by a large discontinuity, the following study is going to show if there is a small discontinuity, how it would affect the uncertainty differently from a large discontinuity. Then we will be able to understand quantitatively how the magnitude of discontinuity influence the uncertainty.

We made a synthetic wedge model for V_p, V_s, and ρ in time domain, and calculated acoustic impedance ($Z_p = V_p\rho$) and shear impedance ($Z_s = V_s\rho$). This model has 5 layers with $V_p = (3.2, 2.8, 3.2, 3.35, 3.7)$ km/s, $V_s = (1.9, 1.65, 1.9, 2.0, 2.2)$ km/s and $\rho = (2.35, 2.2, 2.35, 2.45, 2.6)$ g/cc from the top down. The wedge has a relatively lower Z_p, Z_s and ρ which represents a gas reservoir. The synthetic true model implies interface discontinuities as follows: $V_p = (-0.4, +0.4, +0.15, +0.35)$ km/s, $V_s = (-0.25, +0.25, +0.1, +0.2)$ km/s and $\rho = (-0.15, +0.15, +0.1, +0.15)$ g/cc, which means a relatively larger discontinuity at the first, second and fourth interfaces, and a relatively smaller discontinuity at the third interface. V_p, V_s, and ρ are independent variables and our final goal is to characterize Z_p, Z_s and ρ. True model of Z_p, Z_s and ρ are shown by Figure 4.1. Using the true model, we calculated the reflectivities with different incident angles based on the Zoeppritz equation in time domain. We convolved the reflectivities with a zero-phase Ricker wavelet with central frequency of 25 Hz to generate synthetic seismic data with 2 ms sampling interval. To mimic angle gathers comprised of near, mid and far offsets, each CMP (common midpoint) gather has 3 traces with incident angles of 5, 15 and 25 degrees. Same as implemented in previous sections, the simulated seismic data was also added with zero-mean Gaussian random noise with a standard deviation of 10% of the maximum data value. The noise was added on the amplitude of each sample, so the waveform

was slighted distorted and also contained spikes. This synthetic seismic data with noise was used as the observed seismic data for the inversion. The wedge model is comprised of 80 CMPs with an interval of 12.5 m. We generated synthetic seismic data for each CMP, and here we chose one CMP to display the seismic data (Figure 4.2).
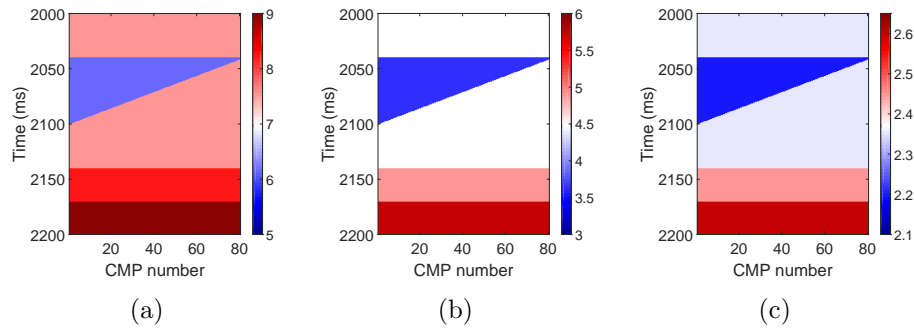
Figure 4.1: Geophysical properties for the wedge model used to test the rjMCMC inversion algorithm. (a) Acoustic impedance Z_p (km/s*g/cc). (b) Shear impedance Z_s (km/s*g/cc). (c) Density ρ (g/cc).

The properties of the overburden rock above 2 s for the true model and the model to be inverted are set to be the same with those of the first layer of the true model. Constant inversion lower/upper limits for V_p, V_s and ρ are (2.5, 4.1) km/s, (1.3, 2.5) km/s and (2.1, 2.7) g/cc respectively. Since the number of layers is unknown, the initial model is arbitrarily chosen which has 10 layers with equal interval in time domain as well as with the same initial V_p=3.3 km/s, V_s=1.9 km/s and ρ=2.4 g/cc. To imitate the properties of rocks in the real case, we set lower/upper limits for the V_s/V_p ratio as (0.5, 0.66) and ρ/V_p ratio as (0.6, 0.9). The allowed minimum number of layers is 2 and the allowed maximum is 30. If a new model goes beyond any one of these bounds, it will be discarded and rjMCMC will repeat the current step and
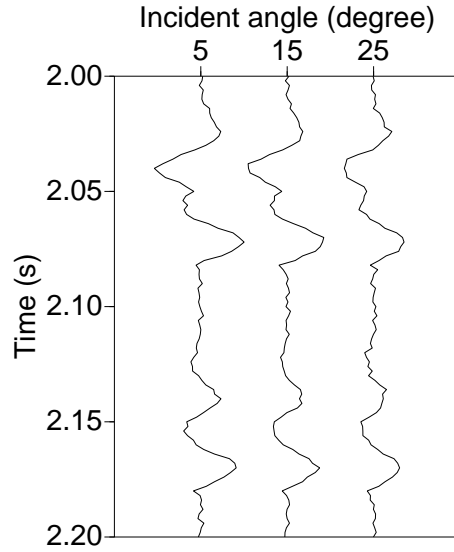
Figure 4.2: Synthetic prestack seismic data generated from the true model and added with 10%random noise. No.40 CMP is chosen for display.

propose another new model until all these criteria are satisfied.

The standard deviation of data misfit σ_d in equation (4.8) was set to be 0.03 which is around 20% of the peak of the seismic data. For the standard deviations of the proposal distributions for model perturbation, we set σ_{V_p}, σ_{V_s} and σ_ρ in equation (4.10) to be 0.4 km/s, 0.3 km/s and 0.15 g/cc respectively (see Section 2.2.11).

We ran the inversion CMP by CMP for 5,000 iterations and each CMP is inverted independently as in the seismic waveform inversion for 1-D earth model (see Section 3.2). To assess the inversion process, we chose one CMP as a demonstration example. Figure 4.3 shows the RMS (root mean square) error between the synthetic data and the modeled data for all iterations, and it illustrates that the rjMCMC finds the low-misfit models in the first few hundred of iterations.

Similar as the studies in previous sections, we kept rjMCMC running for 5,000
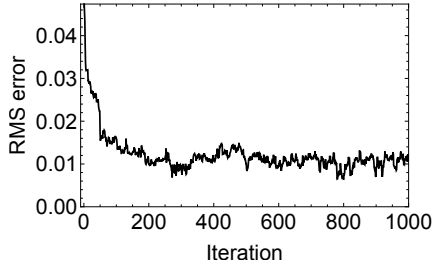
Figure 4.3: RMS error between the data and the modeled data. Displayed for only the first 1000 iterations (No.40 CMP).

iterations so that we would have enough good models in the solution pool through the sampling stage, which assisted us in getting a quality average model as well as in uncertainty quantification. The number of layers versus iteration number was plotted to illustrate that the rjMCMC is able to infer the model dimensionality (Figure 4.4). Out of 5,000 models from 5,000 iterations, we sorted the models by RMS error and chose 2,500 models with relatively lower data RMS errors. A histogram of the number of layers for these sampled models is shown by Figure 4.5. These figures show that the rjMCMC infers the number of layers n to be around 5. A minor overparameterization is allowed by rjMCMC whereas an major overparameterization $(n > 15)$ and an underparameterization $(n < 5)$ are abandoned by rjMCMC.

We downscaled these chosen models with a uniform finer discretization scheme in time domain (0.4 ms in this study) to make a solution set. As mentioned in Section 4.2.4, after this downscaling with the same discretization, all the models will be digitized into matrices with the same size. Then we calculated the average model of this set sample by sample in time domain and used it as the final solution, and computed the standard deviations of this set sample by sample in time domain to appraise the uncertainty.
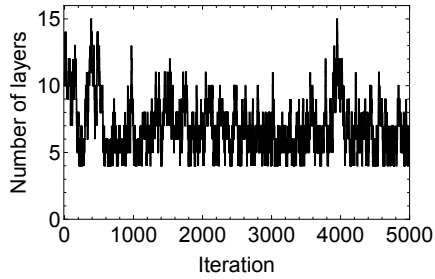
Figure 4.4: The variation of the number of model layers with iterations (No.40 CMP).
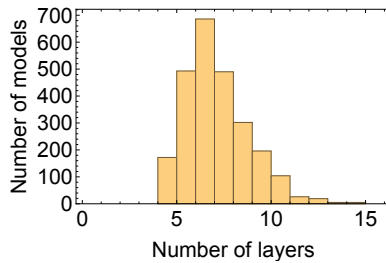
Figure 4.5: Histogram of the number of layers for 2,500 sampled models with low misfit (No.40 CMP).

Inverted Z_p, Z_s and rho are shown as an example (Figure 4.6). As previously pointed out in Section 2.3 and 3.3, the uncertainty (shown by the error bar) of Z_p or Z_s is less than that of density. The reason is that the density is poorly resolved by P-waves seismic data (Debski and Tarantola, 1995; Igel et al., 1996), but the inverted average density statistically approximates the true density model.

To show the posterior distribution of the sampled models, we plotted the histogram and show it for one depth (2080 ms) as an example. Figure 4.7 indicates an asymmetrical distribution, but the average value is almost the same as the true value (Figure 4.6).

We implemented this process for all CMPs. Due to the reason that each CMP

89
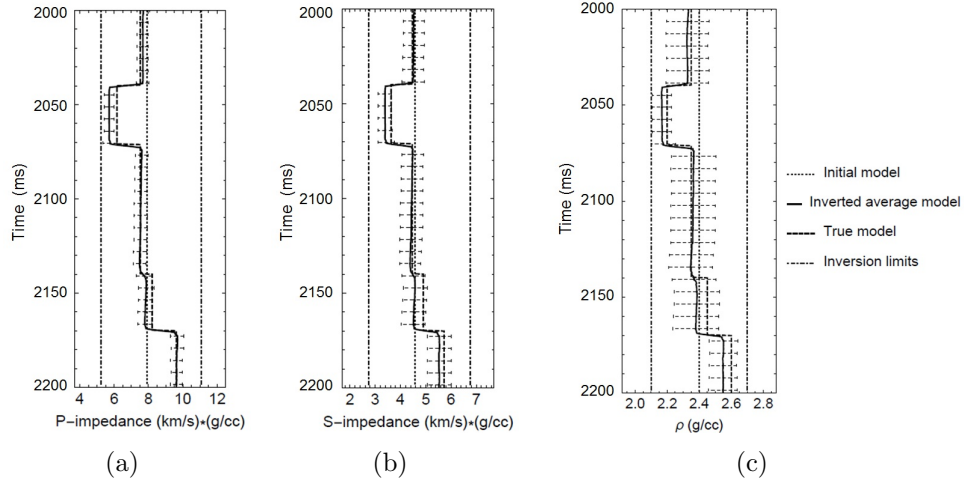
Figure 4.6: Inverted models vs. true models (Trace No.40). (a) Z_p (km/s*g/cc). (b) Z_s (km/s*g/cc). (c) ρ (g/cc). The inversion uncertainty (standard deviation) is represented by the error bar.
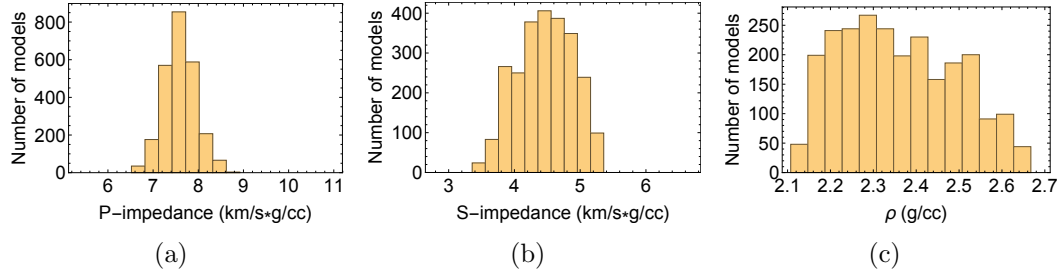
Figure 4.7: Histogram of sampled models (Trace No.40, depth=2080 ms). (a) Z_p (km/s*g/cc). (b) Z_s (km/s*g/cc). (c) ρ (g/cc).

gather had spatial random noise that would propagate into the inverted models as mentioned in Section 2.2.9, a lateral moving-average smoothing was applied to suppress the noise effect. Finally, we obtained the inverted average models of Z_p, Z_s and ρ (Figure 4.8) and quantified their uncertainty (Figure 4.9).

These inversion results obtained from the 2,500 inverted models show that the true model and the layer interfaces for V_p, ρ and Z_p are almost recovered by the
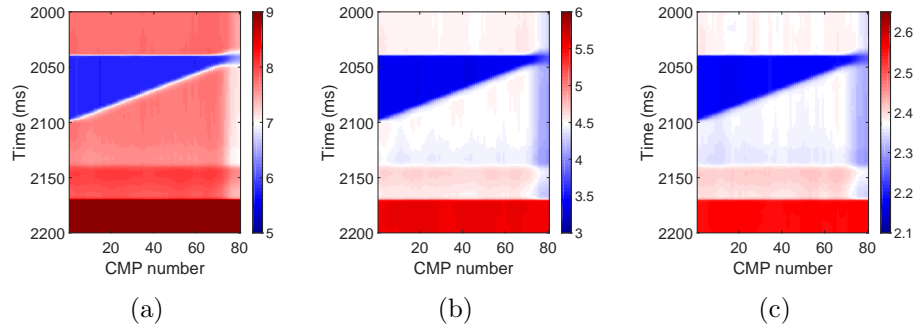
Figure 4.8: Inverted average models by rjMCMC. (a) Z_p (km/s*g/cc). (b) Z_s (km/s*g/cc). (c) ρ (g/cc).
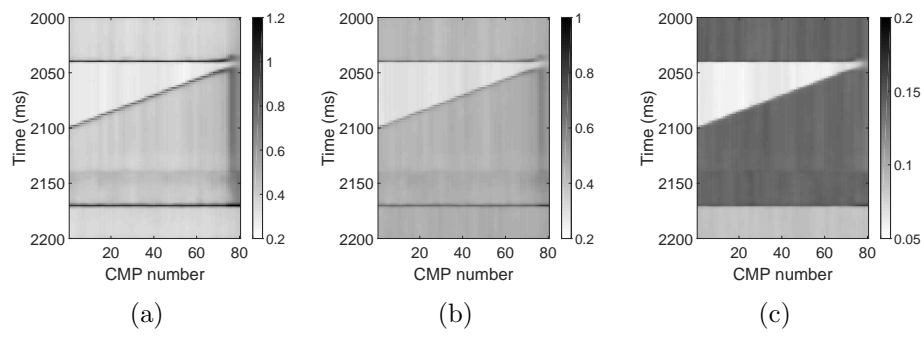
Figure 4.9: rjMCMC Inversion uncertainty. (a) Z_p uncertainty (km/s*g/cc). (b) Z_s uncertainty (km/s*g/cc). (c) ρ uncertainty (g/cc).

rjMCMC.

To assess the data fitting for inversion results, we computed the modeled seismic data from the inverted average model and here we chose one CMP to display (Figure 4.10). To show how well all the 2,500 sampled models fit the synthetic data, we also computed their seismograms and calculated the standard deviations for each time sample. Here we picked the mid-offset seismogram of No.40 CMP as an example to display (Figure 4.11). The standard deviations are quite small compared to the synthetic data, the average standard deviation is 0.0062 (around 7% of the data

peak/trough), and the data falls into the range of the error bar. These indicate a successful data fitting for the model ensemble.
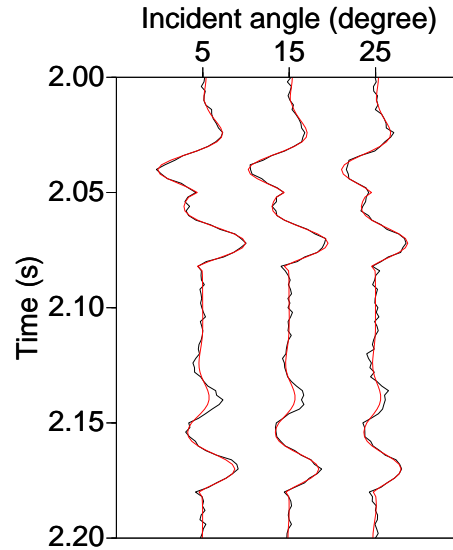
Figure 4.10: Synthetic seismic data generated from the true model and added with noise (black) vs. modeled data generated from the inverted average model (red). No.40 CMP is chosen for display.

Since the true model was designed with three interfaces (first, second and fourth) of relatively larger discontinuity and one interface (third) of smaller discontinuity, the inversion uncertainty in impedance (Figure 4.9(a)) shows that the third interface has a smaller uncertainty in impedance than those of the other three interfaces. However, the third interface is less sharply defined than the other interfaces as well. This shows that a smaller discontinuity will induce a less uncertainty in impedance around the interface but also give rise to more uncertainty of the interface's location.

To sum up, a larger discontinuity of property will induce 1) more uncertainty
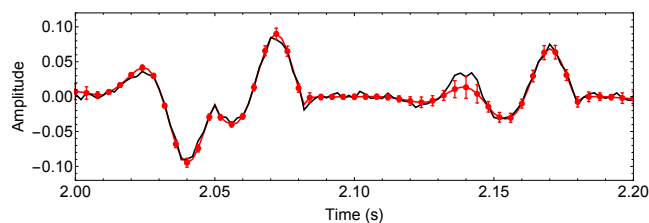
Figure 4.11: Comparison of the modeled data from 2,500 inverted models and the inverted average model with the synthetic data from the true model. The mid-offset (angle=15°) trace of No.40 CMP is chosen as an example for display. Black: synthetic seismogram generated from the true model and added with noise. Red: seismogram generated from the inverted average model. Red error bar represent the standard deviations for all time samples of the 2,500 seismograms from the 2,500 inverted models (displayed by every two time samples), and the average standard deviation=0.0062.

in model property at the discontinuity but also 2) more "certainty" of the location of the discontinuity. And a smaller discontinuity will induce 1) less uncertainty in model property at the discontinuity but also 2) more uncertainty of the location of the discontinuity. This synthetic study shows the trade-off effects from two opposite cases while the studies in previous sections only focuses the first case. It shows that the property uncertainty and the location uncertainty exert a limitation on each other so they cannot be simultaneously certain with high accuracy.

4.4   Case Study Using an Oilfield Data, Norne Field, North Sea

Here we use the inversion results from Section 3.4 for a more detailed uncertainty analysis as follows. Previously in the synthetic study, we have pointed out a large property discontinuity results in a large property uncertainty and a small location (or structural) uncertainty and a small discontinuity has an opposite effect. The inversion of this field data substantiates this statement furthermore. Disregarding the negative effects from the low SNR (signal to noise ratio) in the deeper region, we

found out the uncertainty results (Figure 4.15, 4.16 and 4.17) generally delineate the geological structure shown by Figure 4.12, 4.13 and 4.14. The higher uncertainty in a property (red) indicates a larger discontinuity of that property. The lower uncertainty (white) indicates a smaller discontinuity. Even there exists no discontinuity, there is still some uncertainty since the uncertainty does always exist, but non-discontinuity (continuous) regions exhibit the lowest uncertainty. So we can interpret the lowest uncertainty in a property as the indicator of continuity of that property.
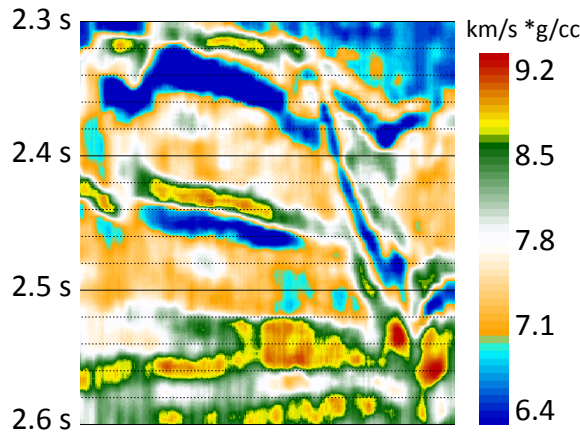
Figure 4.12: Inverted Z_p by rjMCMC. The inversion procedure is described in Section 3.4.

Next, let's focus on the discontinuity of this reservoir. For example, at time around 2.44s where there is a transition from shale to gas sand, the Z_p uncertainty is very large at the interface (Figure 4.15), which shows there is major Z_p discontinuity. However, at the same location, the Z_s uncertainty (Figure 4.16) is much lower than that in the surrounding regions, which indicates the Z_s discontinuity is small there. These results honor the fact that P-waves are sensitive to changes in pore fluid and S-waves are relatively unaffected by the pore fluid. Furthermore, the ρ uncertainty

94
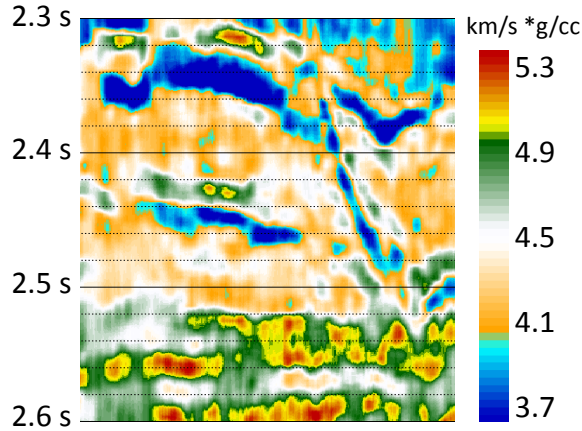
Figure 4.13: Inverted Z_s by rjMCMC. The inversion procedure is described in Section 3.4.

(Figure 4.17) shows fewer sharp discontinuity surfaces which means the density is relatively more continuous than Z_p. This is consistent with the fact that the density for the whole region has small variations and the most values are in the range of (2.2, 2.5) g/cc, and also the variation over the average for density is around 15%, while that for Z_p is around 35%. This is why Z_p discontinuity (uncertainty) presents more discontinuity interfaces than those for ρ in this reservoir.

All the above studies in this dissertation inspired us to use the uncertainty as a novel attribute optimistically to assist in pinpointing the location of the subsurface reflectors and quantify the magnitude of discontinuities. And when the uncertainty and the discontinuity of different properties are analyzed together, the Z_p, Z_s and ρ uncertainties can give us comprehensive insights to better understand the subsurface characteristics from different ways.
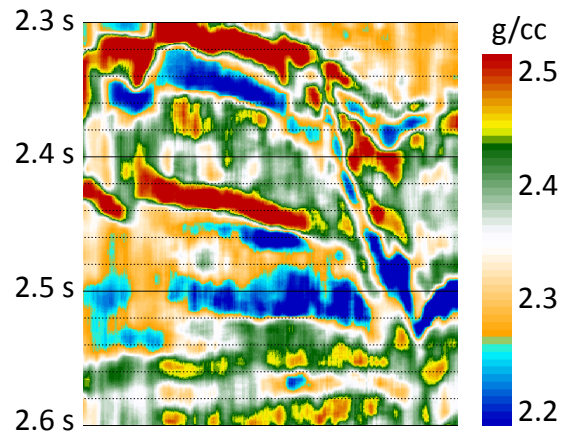
Figure 4.14: Inverted ρ by rjMCMC. The inversion procedure is described in Section 3.4.
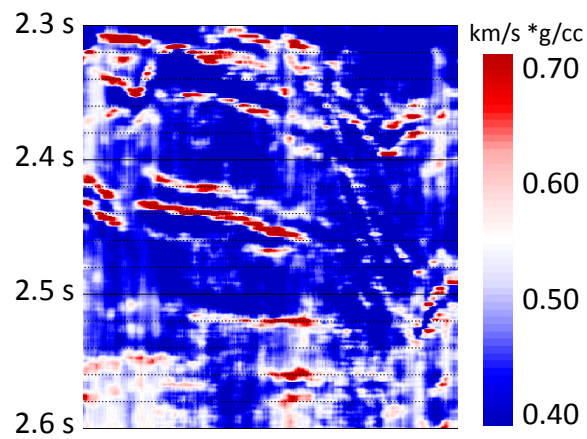
Figure 4.15: Z_p inversion uncertainty by rjMCMC. The inversion procedure is described in Section 3.4.
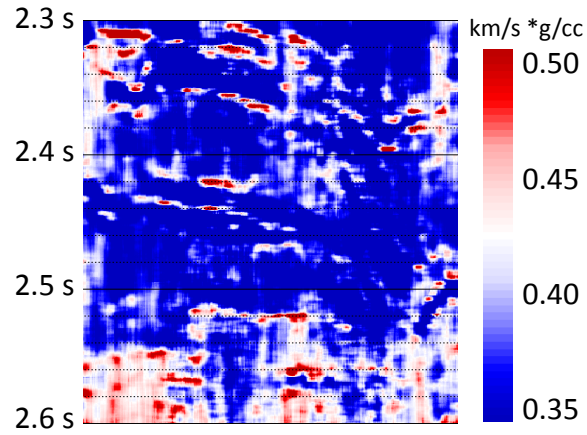
Figure 4.16: Z_s inversion uncertainty by rjMCMC. The inversion procedure is described in Section 3.4.
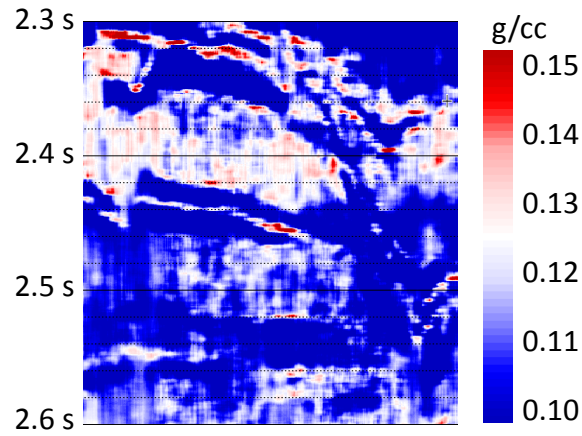
Figure 4.17: ρ inversion uncertainty by rjMCMC. The inversion procedure is described in Section 3.4.

4.5 Conclusion and Discussion

From different studies with synthetic or field and post-stack or prestack data in this dissertation, our uncertainty analysis shows that the inversion uncertainty is correlated with the discontinuity of property and complies the uncertainty trade-off between property uncertainty and location uncertainty. On one other, a smaller discontinuity of property induces less uncertainty in property at the discontinuity and nevertheless more uncertainty of the location of the discontinuity. On the other, a larger discontinuity leads to more uncertainty in property at the discontinuity and nevertheless more ''certainty'' of the location of the discontinuity. Therefore, we propose to utilize inversion uncertainty as a new attribute to depict the magnitude and the location (structure) of subsurface discontinuities and reflectors that normally are related to a transition of lithology or fluid content. This discovery may be generalized in any inverse problem in all disciplines because the uncertainty trade-off can be a general principle in any inverse problem as long as there are complementary parameters to be inverted.

The word ''uncertainty'' sounds scary since we tend to think it is something negative and we are trying to avoid. However, this may not be true because when we have more uncertainty in something, we may have more certainty in its complementary partner according to the uncertainty trade-off. This also means we can not have certainty with high accuracy in both complementary partners (such as A and B) in the same experiment by the same method. If we want to have certainty in both A and B, we can conduct two independent experiments and use different approaches. One experiment focuses on constraining A with higher certainty, whereas the other experiment with a different method focuses on constraining B. The combined results may give certainty on both. Since there are lots of surprising hidden information in

98

the uncertainty for us to understand the research target in different perspectives, a geophysicist or any inversion scientist may not necessarily treat the uncertainty as a negative result because we may also have more certainty on the other side of the coin even if we have uncertainty on one side.

5. CONCLUSION AND DISCUSSION

5.1 Conclusion

This dissertation demonstrates that the transdimensional rjMCMC can answer together these three critical questions that arise in addressing inverse problems, that is, how to parameterize the earth model with appropriate parameters, how to estimate these parameters from the data available and how to assess the uncertainty. The main focus of this research is to put more emphasis on discussing the first and the third questions through seismic waveform inversion using post-stack and prestack data. This is a relatively new topic, and relevant recent literature includes Dadi (2014) and Biswas and Sen (2015).

We have shown that the rjMCMC is able to infer the model dimensionality from the data itself and achieve proper parameterizations so that it can prevent under-parameterization and overparameterization. We have also demonstrated that this method can facilitate uncertainty estimation on the grounds that the transdimensional sampler searches different spaces of different dimensionalities which are close to that of the true model. Statistically, the average and the standard deviation of the solution ensemble can yield a less bias compared to the scenario that the inversion is implemented in only a predefined single space whose dimensionality may be distinct from that of the true model space. Additionally, by using this algorithm in prestack seismic waveform inversion, we obtained a high resolution of inversion results which is $\lambda/16$, where λ is the seismic wavelength.

A critical scientific contribution of this research is that we discovered that the uncertainty in an inverse problem may conform with a trade-off between property uncertainty and location uncertainty if there are complementary parameters in the

model. This is due to the reason that geophysical properties and the location are complementary in the inversion. This discovery along with our research results reveals that we can utilize the inversion uncertainty as an attribute that is able to depict the model discontinuity. A larger discontinuity of property will induce a higher uncertainty in model property and a less uncertainty in location. A smaller discontinuity will induce a lower uncertainty in model property and a higher uncertainty in location. In the seismic exploration, we can use the inversion uncertainty to understand the location and the magnitude of subsurface discontinuities and reflectors which usually represent a transition of lithology and fluids.

5.2   Discussion

The transdimensional inversion method, rjMCMC, is not only feasible for the geophysical inverse problems in which the model parameterization is usually unknown, but also for any inverse problem that has the same issue. This tool will be extremely attractive if the model has strong heterogeneity and complexity in such a way that some regions are more complicated and need more parameters to depict but the other regions are less complicated and need fewer parameters to characterize. Due to the flexibility of the transdimensional MCMC, it infers the model dimensionality and converges to proper parameterizations which may depict the model in a more optimized way than using a uniform discretization for the whole model as implemented in most traditional inversion methods. Therefore, it is able to prevent overparameterization in more complicated region and prevent underparameterization in a less complicated region. For instance, as for a reservoir upscaling problem whose goal is to find an optimal upscaled model that can be handled by computer efficiently and can also fit the data via reservoir simulation, it can be treated as an inverse problem and a transdimensional implementation can facilitate building a upscaled reservoir

model with a proper discretization and use more parameters to characterize the more complex part and fewer parameters to depict the less complex part.

The research examples in this dissertation conducted rjMCMC inversion based on 1-D layered earth model. However, this method is able to be implemented in 2-D and 3-D earth model using Voronoi cells (Bodin et al., 2012a) and 3D Voronoi blocks. To solve problems in these settings, we propose to use rjMCMC in another way which involves adding, deleting and perturbing a set of cells or blocks in stead of one single cell or block at each iteration. This approach may require adaptive grouping of these units. Another scope of using the transdimensional rjMCMC is to integrate with a forward modeling method that can handle irregular discretization or parameterization, such as finite element method (FEM). The similarity of rjMCMC and FEM is that they work with irregular discretization. The differences are that 1) rjMCMC is an inversion method whereas FEM is a forward modeling method and 2) rjMCMC allows a varying discretization but FEM generally doesn't. Since the stochastic inversion is an iterative process of forward modeling and data fitting, we propose to integrate rjMCMC and FEM in the following way. Add, delete or perturb a set of cells or blocks in each iteration and conduct the forward modeling based on the new discretization using FEM for each iteration. In order to make this idea feasible with 3D earth model which has a large number of parameters, super computing is required.

To generalize our discovery that the seismic inversion complies with the trade-off between property uncertainty and location uncertainty, we put forward that an inverse problem may conform with the principle of uncertainty trade-off as long as there are complementary parameters to be inverted in one experiment and we may not have ''certainty'' with high accuracy in both complementary partners in one experiment. However, if we want to have certainty in both, we may need to

have two independent experiments which might require different approaches so that one experiment with one certain approach can constrain one parameter and the other experiment with a different approach can constrain the complementary partner. Conceptually, we do need a refreshment of the philosophical view of uncertainty. A geophysicist or any inversion scientist may not necessarily treat the uncertainty as a negative result because whenever we have more uncertainty on something, we may also have more certainty on the others, which means that there are lots of hidden information in the uncertainty which can be taken advantage of to understand the research target in different perspectives.

REFERENCES

Aarts, E., and J. Korst, 1988, Simulated annealing and Boltzmann machines: John Wiley and Sons Inc., New York.

Agostinetti, N. P., and A. Malinverno, 2010, Receiver function inversion by trans-dimensional Monte Carlo sampling: Geophysical Journal International, **181**, 858--872.

Ahmadi, M. A., S. Zendehboudi, A. Lohi, A. Elkamel, and I. Chatzis, 2013, Reservoir permeability prediction by neural networks combined with hybrid genetic algorithm and particle swarm optimization: Geophysical Prospecting, **61**, 582--598.

An, P., W. M. Moon, and F. Kalantzis, 2001, Reservoir characterization using seismic waveform and feedforword neural networks: Geophysics, **66**, 1450--1456.

Anily, S., and A. Federgruen, 1987a, Ergodicity in parametric nonstationary Markov chains: an application to simulated annealing methods: Operations Research, **35**, 867--874.

--------, 1987b, Simulated annealing methods with general acceptance probabilities: Journal of Applied Probability, **24**, 657--667.

Baddari, K., N. Djarfour, T. Afa, and J. Ferahtia, 2010, Acoustic impedance inversion by feedback artificial neural network: Journal of Petroleum Science and Engineering, **71**, 106--111.

Basu, A., and L. N. Frazer, 1990, Rapid determination of the critical temperature in simulated annealing inversion: Science, **249**, 1409--1412.

Bhattacharya, B. B., Shalivahan, and M. K. Sen, 2003, Use of VFSA for resolution, sensitivity and uncertainty analysis in 1D DC resistivity and IP inversion: Geophysical Prospecting, **51**, 393--408.

Biswas, R., and M. K. Sen, 2015, Pre-stack trans-dimensional seismic inversion: 85th SEG Meeting, Expanded Abstracts, 3492--3496.

Bodin, T., and M. Sambridge, 2009, Seismic tomography with the reversible jump algorithm: Geophysical Journal International, **178**, 1411--1436.

Bodin, T., M. Sambridge, and K. Gallagher, 2009, A self-parametrizing partition model approach to tomographic inverse problems: Inverse Problems, **25**, 055009.

Bodin, T., M. Sambridge, N. Rawlinson, and P. Arroucau, 2012a, Transdimensional tomography with unknown data noise: Geophysical Journal International, **189**, 1536--1556.

Bodin, T., M. Sambridge, H. Tkalcic, P. Arroucau, K. Gallagher, and N. Rawlinson, 2012b, Transdimensional inversion of receiver functions and surface wave dispersion: Journal of Geophysical Research: Solid Research, **117**, B02301.

Boschetti, F., M. Dentith, and R. List, 1995, A staged genetic algorithm for tomographic inversion of seismic refraction data: Exploration Geophysics, **26**, 331--335.

Boschetti, F., M. C. Dentith, and R. D. List, 1996, Inversion of seismic refraction data using genetic algorithms: Geophysics, **61**, 1715--1727.

Box, G. E., and G. C. Tiao, 1973, Bayesian inference in statistical analysis: Addison-Wesley Publishing Company.

Brodie, R. C., and M. Sambridge, 2012, Transdimensional Monte Carlo inversion of AEM data: ASEG Extended Abstracts: 22nd Geophysical Conference, 1--4.

Buckles, B., and F. Petry, 1992, Genetic algorithms: IEEE Computer Society Press.

Buland, A., and H. Omre, 2003, Bayesian linearized AVO inversion: Geophysics, **68**, 185--198.

Calderón-Macías, C., M. K. Sen, and P. L. Stoffa, 2000, Artificial neural networks for parameter estimation in geophysics: Geophysical Prospecting, **48**, 21--47.

Chen, J., and T. A. Dickens, 2009, Effects of uncertainty in rock-physics models on

reservoir parameter estimation using seismic amplitude variation with angle and controlled-source electromagnetics data: Geophysical Prospecting, **57**, 61--74.

Chen, J., and M. E. Glinsky, 2014, Stochastic inversion of seismic PP and PS data for reservoir parameter estimation: Geophysics, **79**, R233--R246.

Claerbout, J. F., and F. Muir, 1973, Robust modeling with erratic data: Geophysics, **38**, 826--844.

Cooke, D. A., and W. A. Schneider, 1983, Generalized linear inversion of reflection seismic data: Geophysics, **48**, 665--676.

Curtis, A., and A. Lomax, 2001, Prior information, sampling distributions, and the curse of dimensionality: Geophysics, **66**, 372--378.

Dadi, S., 2014, Estimation of impedance using seismic reflection data based on transdimensional inversion: PhD thesis, Texas A&M University.

Dadi, S., R. L. Gibson, and K. Wang, 2015, Quantification of uncertainty in velocity log upscaling using reversible jump MCMC: 85th SEG Meeting, Expanded Abstracts, 3476--3481.

Davis, L., 1987, Genetic algorithms and simulated annealing: Morgan Kaufman Publishers, Inc., Los Altos, CA.

Debski, W., and A. Tarantola, 1995, Information on elastic parameters obtained from the amplitudes of reflected waves: Geophysics, **60**, 1426--1436.

Demirbag, E., C. Coruh, and J. Costain, 1993, Inversion of P-wave AVO, *in* Offset-dependent reflectivity-theory and practice of AVO analysis: Society of Exploration Geophysicists, 287--302.

Dettmer, J., and S. E. Dosso, 2012, Trans-dimensional matched-field geoacoustic inversion with hierarchical error models and interacting Markov chains: Journal of the Acoustical Society of America, **132**, 2239--2250.

Dettmer, J., S. E. Dosso, and C. W. Holland, 2010, Trans-dimensional geoacoustic

inversion: Journal of the Acoustical Society of America, **128**, 3393--3405.

Dettmer, J., C. W. Holland, and S. E. Dosso, 2013, Transdimensional uncertainty estimation for dispersive seabed sediments: Geophysics, **78**, WB63--WB76.

Dosso, S. E., 2002, Quantifying uncertainty in geoacoustic inversion. I. A fast Gibbs sampler approach: The Journal of the Acoustical Society of America, **111**, 129--142.

Dosso, S. E., J. Dettmer, G. Steininger, and C. W. Holland, 2014, Efficient transdimensional Bayesian inversion for geoacoustic profile estimation: Inverse Problems, **30**, 114018.

Dosso, S. E., and P. L. Nielsen, 2002, Quantifying uncertainty in geoacoustic inversion. II. Application to broadband, shallow-water data: The Journal of the Acoustical Society of America, **111**, 143--159.

Duijndam, A. J. W., 1988a, Bayesian estimation in seismic inversion, part I: Principles: Geophysical Prospecting, **36**, 878--898.

--------, 1988b, Bayesian estimation in seismic inversion, part II: Uncertainty analysis: Geophysical Prospecting, **36**, 899--918.

Eidsvik, J., P. Avseth, H. Omre, T. Mukerji, and G. Mavko, 2004, Stochastic reservoir characterization using prestack seismic data: Geophysics, **69**, 978--993.

Fang, Z., and D. Yang, 2015, Inversion of reservoir porosity, saturation, and permeability based on a robust hybrid genetic algorithm: Geophysics, **80**, R265--R280.

Fernández-Martínez, J. L., J. P. FernándezAlvarez, M. E. GarcíaGonzalo, C. O. M. Pérez, and H. A. Kuzma, 2008, Particle swarm optimization (PSO): a simple and powerful algorithm family for geophysical inversion: 78th SEG Meeting, Expanded Abstracts, 3568--3571.

Fernández-Martínez, J. L., T. Mukerji, E. García-Gonzalo, and A. Suman, 2012, Reservoir characterization and inversion uncertainty via a family of particle swarm optimizers: Geophysics, **77**, M1--M16.

Fliedner, M. M., S. Treitel, and L. MacGregor, 2012, Full-waveform inversion of seismic data with the Neighborhood Algorithm: The Leading Edge, **31**, 570--579.

Forrest, S., 1993, Genetic algorithms: principles of natural selection applied to computation: Science, **261**, 872--878.

Galetti, E., A. Curtis, G. A. Meles, and B. Baptie, 2015, Uncertainty loops in travel-time tomography from nonlinear wave physics: Phys. Rev. Lett., **114**, no. 14, 148501.

Gallagher, K., K. Charvin, S. Nielsen, M. Sambridge, and J. Stephenson, 2009, Markov chain Monte Carlo (MCMC) sampling methods to determine optimal models, model resolution and model choice for Earth science problems: Marine and Petroleum Geology, **26**, 525--535.

Gallagher, K., and M. Sambridge, 1994, Genetic algorithms: a powerful tool for large-scale nonlinear optimization problems: Computers & Geosciences, **20**, 1229--1236.

Gallagher, K., M. Sambridge, and G. Drijkoningen, 1991, Genetic algorithms: an evolution from Monte Carlo methods for strongly non-linear geophysical optimization problems: Geophysical Research Letters, **18**, 2177--2180.

Gehrmann, R. A. S., J. Dettmer, K. Schwalenberg, M. Engels, S. E. Dosso, and A. zmaral, 2015, Trans-dimensional Bayesian inversion of controlled-source electromagnetic data in the German North Sea: Geophysical Prospecting, **63**, 1314--1333.

Geman, S., and D. Geman, 1984, Stochastic relaxation, Gibbs distributions, and the Bayesian restoration of images: IEEE Transactions on Pattern Analysis and Machine Intelligence, **6**, 721--741.

Geyer, C., and J. Moller, 1994, Simulation procedures and likelihood inference for spatial point-process: Scandinavian Journal of Statistics, **21**, 359--373.

Godfrey, R., F. Muir, and F. Rocca, 1980, Modeling seismic impedance with Markov chains: Geophysics, **45**, 1351--1372.

Goldberg, D. E., 1989, Genetic algorithms in search, optimization, and machine learning: Addison Wesley.

Gouveia, W. P., and J. A. Scales, 1998, Bayesian seismic waveform inversion: parameter estimation and uncertainty analysis: Journal of Geophysical Research: Solid Earth, **103**, 2759--2779.

Green, P., 1995, Reversible jump Markov chain Monte Carlo computation and Bayesian model determination: Biometrika, **82**, 711--732.

Green, P. J., 2003, Trans-dimensional Markov chain Monte Carlo: Oxford Statistical Science Series, 179--198.

Gunning, J., M. E. Glinsky, and J. Hedditch, 2010, Resolution and uncertainty in 1D CSEM inversion: a Bayesian approach and open-source implementation: Geophysics, **75**, F151--F171.

Hampson, D., B. Russell, et al., 1984, First-break interpretation using generalized linear inversion: J. Can. Soc. Expl. Geophys, **20**, 40--50.

Hampson, D. P., B. H. Russell, and B. Bankhead, 2005, Simultaneous inversion of pre-stack seismic data: 75th SEG Meeting, Expanded Abstracts, 1633--1637.

Hastings, W., 1970, Monte-Carlo sampling methods using Markov chains and their applications: Biometrika, **57**, 97--109.

Holland, J. H., 1975, Adaptation in natural and artificial systems: an introductory analysis with applications to biology, control, and artificial intelligence: University of Michigan Press.

Hong, T., and M. K. Sen, 2009, A new MCMC algorithm for seismic waveform inversion and corresponding uncertainty analysis: Geophysical Journal International, **177**, 14--32.

Igel, H., H. Djikpéssé, and A. Tarantola, 1996, Waveform inversion of marine reflection seismograms for P impedance and Poisson's ratio: Geophysical Journal

International, **124**, 363--371.

Jackson, D., and M. Matsu'ura, 1985, A Bayesian-approach to nonlinear inversion: Journal of Geophysical Research: Solid Earth and Planets, **90**, 581--591.

JafarGandomi, A., and A. Binley, 2013, A Bayesian trans-dimensional approach for the fusion of multiple geophysical datasets: Journal of Applied Geophysics, **96**, 38--54.

Kennedy, J., and R. Eberhart, 1995, Particle swarm optimization: Proceedings of IEEE International Conference on Neural Networks, 1995, 1942--1948.

Kennett, B., 1983, Seismic wave propagation in stratified media: Cambridge University Press.

Kirkpatrick, S., C. D. Gelatt, and M. P. Vecchi, 1983, Optimization by simulated annealing: Science, **220**, 671--680.

Kolb, J. M., and V. Lekić, 2014, Receiver function deconvolution using transdimensional hierarchical Bayesian inference: Geophysical Journal International, **197**, 1719--1735.

Kwon, M. J., and R. Snieder, 2011, Uncertainty analysis for the integration of seismic and controlled source electro-magnetic data: Geophysical Prospecting, **59**, 609--626.

Langer, H., G. Nunnari, and L. Occhipinti, 1996, Estimation of seismic waveform governing parameters with neural networks: Journal of Geophysical Research: Solid Earth, **101**, 20109--20118.

Leite, E. P., and A. C. Vidal, 2011, 3D porosity prediction from seismic inversion and neural networks: Computers & Geosciences, **37**, 1174--1180.

Li, T., and S. Mallick, 2015, Multicomponent, multi-azimuth pre-stack seismic waveform inversion for azimuthally anisotropic media using a parallel and computationally efficient non-dominated sorting genetic algorithm: Geophysical Journal

International, **200**, 1134--1152.

Liu, C., and J. M. Stock, 1993, Quantitative determination of uncertainties in seismic refraction prospecting: Geophysics, **58**, 553--563.

Ma, X.-Q., 2001a, A constrained global inversion method using an overparameterized scheme: application to poststack seismic data: Geophysics, **66**, 613--626.

--------, 2001b, Global joint inversion for the estimation of acoustic and shear impedances from AVO derived P-and S-wave reflectivity data: First Break, **19**, 557--566.

--------, 2002, Simultaneous inversion of prestack seismic data for rock properties using simulated annealing: Geophysics, **67**, 1877--1885.

Ma, Y. Z., 2011, Uncertainty analysis in reservoir characterization and management: How much should we know about what we don't know?: AAPG Memoir, **96**, 1--15.

Malinverno, A., 2000, A Bayesian criterion for simplicity in inverse problem parametrization: Geophysical Journal International, **140**, 267--285.

--------, 2002, Parsimonious Bayesian Markov chain Monte Carlo inversion in a nonlinear geophysical problem: Geophysical Journal International, **151**, 675--688.

Malinverno, A., and V. A. Briggs, 2004, Expanded uncertainty quantification in inverse problems: hierarchical Bayes and empirical Bayes: Geophysics, **69**, 1005--1016.

Malinverno, A., and S. Leaney, 2000, A Monte Carlo method to quantify uncertainty in the inversion of zero-offset VSP data: 70th SEG Meeting, Expanded Abstracts, 2393--2396.

Malinverno, A., and W. S. Leaney, 2005, Monte-Carlo Bayesian look-ahead inversion of walkaway vertical seismic profiles: Geophysical Prospecting, **53**, 689--703.

Mallick, S., 1995, Model-based inversion of amplitude-variations-with-offset data using a genetic algorithm: Geophysics, **60**, 939--954.

--------, 1999, Some practical aspects of prestack waveform inversion using a genetic algorithm: an example from the east Texas Woodbine gas sand: Geophysics, **64**, 326--336.

Mallick, S., and S. Adhikari, 2015, Amplitude-variation-with-offset and prestack-waveform inversion: a direct comparison using a real data example from the Rock Springs Uplift, Wyoming, USA: Geophysics, **80**, B45--B59.

Martin, J., L. C. Wilcox, C. Burstedde, and O. Ghattas, 2012, A stochastic Newton MCMC method for large-scale statistical inverse problems with Application to Seismic Inversion: SIAM Journal on Scientific Computing, **34**, A1460--A1487.

Metropolis, N., A. W. Rosenbluth, M. N. Rosenbluth, A. H. Teller, and E. Teller, 1953, Equation of state calculations by fast computing machines: The Journal of Chemical Physics, **21**, 1087--1092.

Minsley, B. J., 2011, A trans-dimensional Bayesian Markov chain Monte Carlo algorithm for model assessment using frequency-domain electromagnetic data: Geophysical Journal International, **187**, 252--272.

Mitra, D., F. Romeo, and Sangiovannivincentelli, 1986, Convergence and finite-time behavior of simulated annealing: Advances in Applied Probability, **18**, 747--771.

Mohamed, I. A., H. Z. El-Mowafy, and M. Fathy, 2015, Prediction of elastic properties using seismic prestack inversion and neural network analysis: Interpretation, **3**, T57--T68.

Mora, P., 1987, Nonlinear two-dimensional elastic inversion of multioffset seismic data: Geophysics, **52**, 1211--1228.

Morgan, E. C., M. Vanneste, I. Lecomte, L. G. Baise, O. Longva, and B. McAdoo, 2012, Estimation of free gas saturation from seismic reflection surveys by the genetic algorithm inversion of a P-wave attenuation model: Geophysics, **77**, R175--R187.

Mosegaard, K., and M. Sambridge, 2002, Monte Carlo analysis of inverse problems:

Inverse Problems, **18**, R29--R54.

Mosegaard, K., S. Singh, D. Snyder, and H. Wagner, 1997, Monte Carlo analysis of seismic reflections from Moho and the W reflector: Journal of Geophysical Research: Solid Earth, **102**, 2969--2981.

Mosegaard, K., and A. Tarantola, 1995, Monte-Carlo sampling of solutions to inverse problems: Journal of Geophysical Research: Solid Earth, **100**, 12431--12447.

Oldenburg, D. W., T. Scheuer, and S. Levy, 1983, Recovery of the acoustic impedance from reflection seismograms: Geophysics, **48**, 1318--1337.

Osypov, K., Y. Yang, A. Fournier, N. Ivanova, R. Bachrach, C. E. Yarman, Y. You, D. Nichols, and M. Woodward, 2013, Model-uncertainty quantification in seismic tomography: method and applications: Geophysical Prospecting, **61**, 1114--1134.

Padhi, A., and S. Mallick, 2013, Accurate estimation of density from the inversion of multicomponent prestack seismic waveform data using a nondominated sorting genetic algorithm: The Leading Edge, **32**, 94--98.

--------, 2014, Multicomponent pre-stack seismic waveform inversion in transversely isotropic media using a non-dominated sorting genetic algorithm: Geophysical Journal International, **196**, 1600--1618.

Pan, G. S., C. Y. Young, and J. P. Castagna, 1994, An integrated target-oriented prestack elastic waveform inversion: sensitivity, calibration, and application: Geophysics, **59**, 1392--1404.

Parker, R. L., 1994, Geophysical inverse theory: Princeton University Press.

Poulton, M. M., 2002, Neural networks as an intelligence amplification tool: a review of applications: Geophysics, **67**, 979--993.

Ray, A., and K. Key, 2012, Bayesian inversion of marine CSEM data with a transdimensional self parametrizing algorithm: Geophysical Journal International, **191**, 1135--1151.

Ray, A., K. Key, T. Bodin, D. Myer, and S. Constable, 2014, Bayesian inversion of marine CSEM data from the Scarborough gas field using a transdimensional 2-D parametrization: Geophysical Journal International, **199**, 1847--1860.

Reading, A. M., and K. Gallagher, 2013, Transdimensional change-point modeling as a tool to investigate uncertainty in applied geophysical inference: an example using borehole geophysical logs: Geophysics, **78**, WB89--WB99.

Röth, G., and A. Tarantola, 1994, Neural networks and inversion of seismic data: Journal of Geophysical Research: Solid Earth, **99**, 6753--6768.

Rothman, D. H., 1985, Nonlinear inversion, statistical mechanics, and residual statics estimation: Geophysics, **50**, 2784--2796.

--------, 1986, Automatic estimation of large residual statics corrections: Geophysics, **51**, 332--346.

Roy, L., M. K. Sen, D. D. Blankenship, P. L. Stoffa, and T. G. Richter, 2005, Inversion and uncertainty estimation of gravity data using simulated annealing: an application over Lake Vostok, East Antarctica: Geophysics, **70**, J1--J12.

Rumpf, M., and J. Tronicke, 2015, Assessing uncertainty in refraction seismic traveltime inversion using a global inversion strategy: Geophysical Prospecting, **63**, 1188--1197.

Russell, B. H., 1988, Introduction to seismic inversion methods: Society of Exploration Geophysicists, **2**.

--------, 2014, Prestack seismic amplitude analysis: an integrated overview: Interpretation - A Journal of Subsurface Characterization, **2**, SC19--SC36.

Rwechungura, R., E. Suwartadi, M. Dadashpour, J. Kleppe, B. Foss, et al., 2010, The Norne field case - A unique comparative case study: Paper SPE, **127538**.

Saggaf, M. M., M. N. Toksz, and H. M. Mustafa, 2003, Estimation of reservoir properties from seismic data by smooth neural networks: Geophysics, **68**, 1969--

1983.

Sambridge, M., 1999a, Geophysical inversion with a neighbourhood algorithm I. Searching a parameter space: Geophysical Journal International, **138**, 479--494.

--------, 1999b, Geophysical inversion with a neighbourhood algorithm II. Appraising the ensemble: Geophysical Journal International, **138**, 727--746.

Sambridge, M., and G. Drijkoningen, 1992, Genetic algorithms in seismic waveform inversion: Geophysical Journal International, **109**, 323--342.

Sambridge, M., K. Gallagher, A. Jackson, and P. Rickwood, 2006, Trans-dimensional inverse problems, model comparison and the evidence: Geophysical Journal International, **167**, 528--542.

Sambridge, M., and K. Mosegaard, 2002, Monte Carlo methods in geophysical inverse problems: Reviews of Geophysics, **40**, 3--1 -- 3--29.

Scales, J., M. Smith, and T. Fischer, 1991, Global optimization methods for highly nonlinear inverse problems: Mathematical and Numerical Aspects of Wave Propagation Phenomena, 434--444.

Scales, J. A., M. L. Smith, and T. L. Fischer, 1992, Global optimization methods for multimodal inverse problems: Journal of Computational Physics, **103**, 258--268.

Scales, J. A., and L. Tenorio, 2001, Prior information and uncertainty in inverse problems: Geophysics, **66**, 389--397.

Sen, M. K., and I. G. Roy, 2003, Computation of differential seismograms and iteration adaptive regularization in prestack waveform inversion: Geophysics, **68**, 2026--2039.

Sen, M. K., and P. L. Stoffa, 1991, Nonlinear one-dimensional seismic waveform inversion using simulated annealing: Geophysics, **56**, 1624--1638.

--------, 1992, Rapid sampling of model space using genetic algorithms: examples from seismic waveform inversion: Geophysical Journal International, **108**, 281--292.

--------, 1995, Global optimization methods in geophysical inversion: Elsevier.

--------, 1996, Bayesian inference, Gibbs' sampler and uncertainty estimation in geophysical inversion: Geophysical Prospecting, **44**, 313--350.

--------, 2013, Global optimization methods in geophysical inversion: Cambridge University Press.

Shaw, R., and S. Srivastava, 2007, Particle swarm optimization: a new tool to invert geophysical data: Geophysics, **72**, F75--F83.

Sisson, S., 2005, Transdimensional Markov chains: a decade of progress and future perspectives: Journal of the American Statistical Association, **100**, 1077--1089.

Smith, M. L., J. A. Scales, and T. L. Fischer, 1992, Global search and genetic algorithms: The Leading Edge, **11**, 22--26.

Srivastava, R. P., and M. K. Sen, 2009, Fractal-based stochastic inversion of poststack seismic data using very fast simulated annealing: Journal of Geophysics and Engineering, **6**, 412--425.

--------, 2010, Stochastic inversion of prestack seismic data using fractal-based initial models: Geophysics, **75**, R47--R59.

Steininger, G., J. Dettmer, S. E. Dosso, and C. W. Holland, 2013, Trans-dimensional joint inversion of seabed scattering and reflection data: The Journal of the Acoustical Society of America, **133**, 1347--1357.

Stoffa, P. L., and M. K. Sen, 1991, Nonlinear multiparameter optimization using genetic algorithms: inversion of planewave seismograms: Geophysics, **56**, 1794--1810.

Tarantola, A., 1986, A strategy for nonlinear elastic inversion of seismic reflection data: Geophysics, **51**, 1893--1903.

Tarantola, A., and B. Valette, 1982a, Generalized nonlinear inverse problems solved using the least squares criterion: Reviews of Geophysics and Space Physics, **20**,

219--232.

--------, 1982b, Inverse problems= quest for information: Journal of Geophysics, **50**, 150--170.

Tran, K. T., and D. R. Hiltunen, 2012a, One-Dimensional Inversion of Full Waveforms using a Genetic Algorithm: Journal of Environmental and Engineering Geophysics, **17**, 197--213.

--------, 2012b, Two-dimensional inversion of full waveforms using simulated annealing.: Journal of Geotechnical & Geoenvironmental Engineering, **138**, 1075--1090.

Ulrych, T. J., M. D. Sacchi, and A. Woodbury, 2001, A Bayes tour of inversion: a tutorial: Geophysics, **66**, 55--69.

van der Baan, M., and C. Jutten, 2000, Neural networks in geophysical applications: Geophysics, **65**, 1032--1047.

van der Burg, D., A. Verdel, and K. Wapenaar, 2009, Ray-based stochastic inversion of prestack seismic data for improved reservoir characterization: Geophysics, **74**, R85--R97.

van Laarhoven, P. J., and E. H. Aarts, 1987, Simulated annealing: theory and applications: Springer Netherlands, volume **37** *of* Mathematics and Its Applications.

Varela, O. J., C. Torres-Verdín, and M. K. Sen, 2006, Enforcing smoothness and assessing uncertainty in non-linear one-dimensional prestack seismic inversion: Geophysical Prospecting, **54**, 239--259.

Veire, H. H., and M. Landrø, 2006, Simultaneous inversion of PP and PS seismic data: Geophysics, **71**, R1--R10.

Vestergaard, P. D., and K. Mosegaard, 1991, Inversion of post-stack seismic data using simulated annealing: Geophysical Prospecting, **39**, 613--624.

Young, M. K., N. Rawlinson, and T. Bodin, 2013, Transdimensional inversion of ambient seismic noise for 3D shear velocity structure of the Tasmanian crust:

Geophysics, **78**, WB49--WB62.

Zhe, Y., and H. Gu, 2013, Non-linear prestack seismic inversion with global optimization using an edge-preserving smoothing filter: Geophysical Prospecting, **61**, 747--760.

Zulfakriza, Z., E. Saygin, P. R. Cummins, S. Widiyantoro, A. D. Nugraha, B.-G. Lühr, and T. Bodin, 2014, Upper crustal structure of central Java, Indonesia, from transdimensional seismic ambient noise tomography: Geophysical Journal International, **197**, 630--635.